UNIVERSITY OF SOUTHAMPTON

FACULTY OF ENGINEERING, SCIENCE AND MATHEMATICS

School of Chemistry

Rapid and definitive identification of pharmaceutical drug metabolites using mass spectrometry

---

by

Stephen William Holman BSc (Hons) AMRSC

A thesis submitted in partial fulfilment of the requirements for the

degree of Doctor of Philosophy

January 2010

University of Southampton

Abstract

Faculty of Science, Engineering and Mathematics

Doctor of Philosophy

Rapid and definitive identification of pharmaceutical drug metabolites using mass spectrometry

by Stephen William Holman

Low-energy collision-induced dissociation-tandem mass spectrometry (CID-MS/MS) is a well-established approach for identifying pharmaceutical drug metabolites. The technique fulfils many necessary requirements for this task, such as a low limit of detection, simple interfacing to chromatographic techniques, capability of fast analyses and automation, and high sensitivity, selectivity and accuracy. However, one of the main limitations of low-energy CID-MS/MS is that unambiguous assignment of the site of metabolism is often not possible, particularly for oxidised metabolites. Further, data interpretation can be time-consuming, thus producing a bottleneck to high-throughput analyses. The aim of the presented study was to identify structurally dependent dissociation pathways using low-energy CID-MS/MS that could facilitate rapid and definitive assignment of the sites of metabolism of new chemical entities. Chapter 4 details a specific loss of 50 *m/z* units in a model *S*-oxide that arises due to an *ortho*-effect. This loss could be used to definitively assign the site of oxidation and discriminate between multiple sulfur atoms in a parent compound. The 50 *m/z* unit loss was also shown to be a two-step process involving sequential radical losses; a rare observation for even-electron precursor ions under low-energy CID conditions. Chapter 5 discusses the experimental investigation of two unexpected rearrangements during the dissociation of a model *S*-oxide that could prevent correct assignment of the site of metabolism. Chapter 6 presents a rapid and definitive approach to the characterisation of dialkyl tertiary amine-*N*-oxides. The work also elucidated generic dissociation behaviour under low-energy CID conditions. Finally, chapter 7 considers an observation of site-specific intra-ionic hydrogen/deuterium exchange in the gas phase. Seven sets of compounds were analysed to investigate the substructures that facilitate the exchange. The work demonstrates a method by which a deuterium label can be inserted into the carbon skeleton of a small molecule without having to synthetically produce the compound, which could be useful in performing timely and cost-effective structural elucidation studies. In summary, the presented study provides two potentially useful approaches for the rapid and definitive identification of oxidised metabolites, as well as increasing the body of knowledge relating to ion-chemistry under low-energy CID conditions.

For Dad

I hope that you would be proud

"We shine in the light of others."

Fred W. McLafferty

Table of contents

Table of figures

Table of tables

Declaration of authorship

I, Stephen William Holman, declare that the thesis entitled

Rapid and definitive identification of pharmaceutical drug metabolites using mass spectrometry

and the work presented in the thesis are both my own, and have been generated by me as the result of my own original research. I confirm that

- this work was done wholly or mainly while in candidature for a research degree at this University;

- where any part of this thesis has previously been submitted for a degree of any other qualification at this university or any other institution, this has been clearly stated;

- where I have consulted the published work of others, this is always clearly attributed;

- where I have quoted from the work of others, the source is always given. With the exception of such quotations, this thesis is entirely is my own work;

- I have acknowledged all main sources of help;

- where the thesis is based on work done by myself jointly with others, I have made clear exactly what was done by others and what I have contributed myself;

o   All work has been conducted wholly by myself with the exception of the following experiments;

-   Generation of tetracaine metabolites *in vitro* and subsequent QqTOF-MS experiments were performed by Pat Wright;
-   Molecular modelling calculations were performed under the guidance of Doctor Alexander Alex.

•   parts of this work have been published as
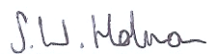
S. W. Holman, P. Wright and G. J. Langley, "High-throughput approaches towards the definitive identification of pharmaceutical drug metabolites. 1. Evidence for an *ortho* effect on the fragmentation of 4-benzenesulfinyl-3-methylphenylamine using electrospray ionisation mass spectrometry", *Rapid Commun. Mass Spectrom.*, 2008; **22**; 2355-2365.

S. W. Holman, P. Wright and G. J. Langley, "High-throughput approaches towards the definitive identification of pharmaceutical drug metabolites. 2. An example of how unexpected dissociation behaviour could preclude correct assignment of sites of metabolism", *Rapid Commun. Mass Spectrom.*, 2009; **23**; 2017-2025.

S. W. Holman, P. Wright, N. J. Wells and G. J. Langley, "Evidence for site-specific intra-ionic hydrogen/deuterium exchange in the low-energy collision-induced dissociation product ion spectra of protonated small molecules generated by electrospray ionisation", *J. Mass Spectrom., In press*.

S. W. Holman, P. Wright and G. J. Langley, "High-throughput approaches towards the definitive identification of pharmaceutical drug metabolites. 3. A rapid methodology for the characterisation of dialkyl tertiary amine-*N*-oxides metabolites using structurally dependent dissociation pathways and reconstructed ion current chromatograms", *Anal. Chem.*, *Submitted*.

Signed:

Date: 10/01/2010

Acknowledgements

I would like to begin by acknowledging my academic supervisor, Doctor John Langley. His positive attitude has been infectious and his guidance and trust has enabled me to develop as an analytical scientist. A compassionate ear throughout my three years has also ensured that I've stayed the course. I would not have swapped the Langley group with any other laboratory for my PhD.

My industrial supervisor, Pat Wright, has provided me with excellent support, without which this work would not have been completed. The difficult task of supervising a student from afar is one that she has achieved with ease. I am also indebted for her willingness to perform some experiments at Pfizer on my behalf.

The mass spectrometry community is a tight-knit one and I have many friends and colleagues who I would like to thank. At the University of Southampton, the Langley group members past and present; Doctor Amaury Cazenave Gassiot, Doctor Louisa Wronska, Angie Galezowska, Julie Herniman, Mohini Thite and Chrissie Wicking, generated a fantastic environment in which to work. In the wider community, I would like to recognise the contributions of Professor John Monaghan, Professor Frank Pullen, Doctor Perdita Barran, Doctor Tony Bristow, Doctor Eddie Clayton, Doctor Helen Cooper, Doctor Sally-Ann Fancy, Doctor Mark Harrison, Doctor Katerina Klagkou, Doctor Jackie Mosely, Doctor Gavin O'Connor, Doctor Steve Pleasance and George Perkins for helpful discussions about everything from dissociation mechanisms to post-doctoral work to moisturising cream and Joy Division (you know who you are!). Further, the reviewers of our publications are thanked for their helpful comments and suggestions, which improved the manuscripts greatly. Outside of mass spectrometry, those scientists in the areas of metabolite identification (Doctor Heather Chassaing, Doctor Russell Jones, Doctor Angus Nedderman, Drew Gibson and Michelle Gleave) and molecular modelling (Doctor Alexander Alex) are thanked for their expertise. Finally, I am grateful to Doctor Neil Wells in the

School of Chemistry, whose benevolence towards my lack of NMR spectroscopy knowledge was most appreciated.

Moving to Southampton was a daunting prospect but happily I have made so many friends that they are almost too numerous to mention. One particular individual deserves special mention; Doctor Rohan Ranasinghe. I don't believe it's possible for a man to find a better gig-going companion, Drummond drinking buddy, Lennon's dancing partner or organic chemistry tutor (although I wasn't much good at the latter). Rohan, I salute you. Other people who I have great fondness for in Southampton are also thanked; Doctor Sam Birtwell, Doctor Mark Dixon, Doctor Adeline Durand, Graham Broder, Martin Challand, Wendy King, Joey Merrett and Mike Merrett. I would also like to thank the Cole family of Chandler's Ford; Chris, Judith, David and Peter, for their warm hospitality and always making me feel so welcome in their home. In addition, a mention goes those friends who made the effort to visit me in Southampton; John Butcher, Gavin Foad, Moina Macaskill and Ben Starling.

Special thanks go to those closest to me. Mum has constantly strived to support me in every endeavour, especially in these last few years which have been terribly difficult for her, and I can not convey enough how much I appreciate her. The Blackwell branch of the Holman family; Andrew, Debbie, Eleanor, Harry, Freya and Joseph, have also been incredibly supportive and have provided a retreat from work (not that you can even try to work with that many kids about!).

And finally, a message for Laura. From the moment that we met, I have thought the world of you, and I am grateful that you think something of me too. If I were a more lyrical and elegant wordsmith I would be able to express myself much more poetically. *In lieu* of a greater command of the English language, I shall stick with this; I love you.

Abbreviations

AGC	Automatic gain control
AMM	Accurate mass measurement
APCI	Atmospheric pressure chemical ionisation
API	Atmospheric pressure ionisation
APPI	Atmospheric pressure photoionisation
ASAP	Atmospheric pressure solids analysis probe
CF-FAB	Continuous-flow-fast atom bombardment
CI	Chemical ionisation
CID	Collision-induced dissociation
CYP450	Cytochrome P450
DART	Direct analysis in real time
Da	Daltons
dB	Decibels
DC	Direct current
DDA	Data-dependent acquisition
DE	Delayed extraction
DESI	Desorption electrospray ionisation
DFT	Density functional theory
ECD	Electron capture dissociation
EI	Electron ionisation
eV	Electron volts
ESI	Electrospray ionisation
FAB	Fast atom bombardment
FD	Field desorption
FDA	Food and Drug Administration
FI	Field ionisation
FT-ICR	Fourier transform-ion cyclotron resonance
FWHM	Full width at half maximum
H/D	Hydrogen/deuterium
HPLC	High performance liquid chromatography

hr	Hour
Hz	Hertz
i.d.	Internal diameter
IMS	Ion mobility spectrometry
K	Kelvin
Kcal	Kilocalories
kV	Kilovolts
L	Litre
LMCO	Low mass cut-off
M	Molar
MALDI	Matrix-assisted laser desorption/ionisation
min	Minute
MIST	Metabolites in Safety Testing
mM	Millimolar
mm	Millimetres
MME	Mass measurement error
mol	Moles
mL	Millilitres
$[M + D]^+$	Fully exchanged, deuterated molecule
$[M + H]^+$	Protonated molecule
MS	Mass spectrometry
MS/MS	Tandem mass spectrometry
MS^n	Mass spectrometry to the nth degree
ms	Milliseconds
m/z	Mass-to-charge
$NADP^+$	Nicotinamide adenine dinucleotide phosphate
NADPH	Reduced nicotinamide adenine dinucleotide phosphate
NCE	New chemical entity
ng	Nanogram
ns	Nanoseconds
NMR	Nuclear magnetic resonance
oa-TOF	Orthogonal acceleration-time-of-flight

PCA	Principal component analysis
PIE	Pulsed-ion extraction
ppm	Parts-per-million
psi	Pounds-per-square-inch
QIT	Quadrupole ion trap
QqQ	Triple quadrupole
QqTOF	Quadrupole time-of-flight
RA	Relative abundance
RF	Radio frequency
RICC	Reconstructed ion current chromatogram
RP-HPLC	Reversed phase-high performance liquid chromatography
rpm	Revolutions per minute
s	Seconds
SORI	Sustained off-resonance excitation
SWIFT	Stored-waveform inverse Fourier transform
TICC	Total ion current chromatogram
TLF	Time-lag focussing
TOF	Time-of-flight
TSP	Thermospray
UDP	Uridine diphosphate
UDPGA	Uridine diphosphate glucuronic acid
UPLC	Ultra performance liquid chromatography
UV	Ultra-violet
V	Volts
v/v	Volume by volume
Δ	Change
µg	Micrograms
µL	Microlitres
µM	Micromolar
µs	Microseconds
^{o}C	Degree Celsius

Chapter 1

Introduction to mass spectrometry

1.1 Synopsis

Mass spectrometry (MS) is an analytical technique that measures the mass-to-charge (m/z) ratio of gas-phase ions. It is capable of providing qualitative and quantitative information with high sensitivity, selectivity, speed, accuracy and precision, and at low limits of detection.[1] In this study, structural elucidation of pharmaceutically relevant compounds, including model oxidised drug metabolites, was performed using MS. The aim was to identify structurally dependent dissociation pathways that were indicative of sites of oxidation of pharmaceutical compounds, thus facilitating rapid and definitive characterisation. Additionally, an increased understanding of ion-chemistry under low-energy collision-induced dissociation (CID) conditions was sought.

1.2 Construction of a mass spectrometer

A mass spectrometer is made up of six key components; an inlet, an ion source, a mass analyser, a detector, a data analysis system and a vacuum system. These components are shown schematically in **Figure 1.1**. Various technologies are available for each of these components. Those that vary most, and also have the greatest impact on the analysis of compounds by MS, are the ion source and the mass analyser. This is because the selections of these components are dictated by the chemistry of the analyte(s) of interest and the information that is required. Detailed discussions of the ionisation technique and the mass analysers utilised in this study are given below.
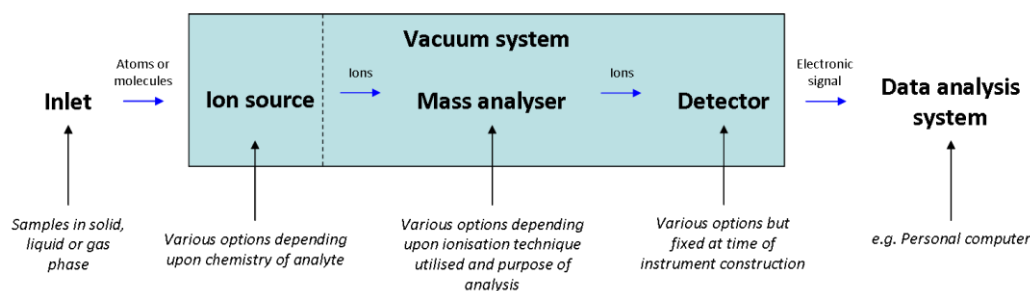
Figure 1.1   Schematic of the key components of a mass spectrometer

1.3   Ionisation techniques

A fundamental requirement for an atom or compound to be analysed by MS is that it must exist as a gas-phase ion. Many techniques have been developed to ionise analytes from the solid, liquid and gas phases. These techniques can be broadly separated into two categories, the second of which being subdivided into a further two groupings; those performed under vacuum and those undertaken at atmospheric pressure with samples either in the solution or solid phases. **Table 1.1** gives commercially available examples from each of these categories.   The   ionisation   technique   used   throughout   this   study   was electrospray ionisation (ESI).

Table 1.1   Commercially available ionisation techniques defined by the conditions under which ionisation takes place

In vacuo ionisation techniques	Atmospheric pressure ionisation (API) techniques	
	Solution phase	**Solid phase**
Electron ionisation (EI)[2]	Electrospray ionisation (ESI)[3]	Desorption electrospray ionisation (DESI)[4]
Chemical ionisation (CI)[5]	Atmospheric pressure chemical ionisation (APCI)[6]	Direct analysis in real time (DART)[7]
Matrix-assisted laser desorption/ionisation (MALDI)[8]	Atmospheric pressure photoionisation (APPI)[9]	Atmospheric pressure solids analysis probe (ASAP)[10]

1.3.1 Electrospray ionisation (ESI)

Electrospray was first demonstrated as a method for generating gas-phase ions by Malcolm Dole and co-workers.[11] This work provided the inspiration for the group of John Fenn to use MS as a method for detecting both positive and negative ions generated by electrospray, leading to the development of what is referred to today as ESI-MS.[3, 12] The pioneering work performed by Fenn led to him sharing the Nobel Prize in Chemistry in 2002.[13]

A number of reviews focussing on the principles,[14] fundamentals,[15] and applications[16] of ESI have appeared in the literature. ESI was selected for this study because it is the established ionisation technique in the pharmaceutical industry, being utilised in both discovery and development for the identification, characterisation and quantification of new chemical entities (NCEs),[17] metabolites,[18] degradants[19] and impurities.[20] The wide application stems from the many strengths of the technique. Firstly, compounds can be analysed directly from solution at atmospheric pressure. This is advantageous in a pharmaceutical setting because the analytes of interest are frequently within the liquid phase *e.g.* a plasma or urine matrix or stored dissolved in dimethylsulfoxide.[14, 21] A further benefit of directly sampling from solution is that non-volatile and/or thermally unstable species are amenable to analysis by MS. This property broadened the range of compounds that could be easily analysed by MS to include biological macromolecules, such as peptides,[22] nucleotides,[23] saccharides[24] and protein complexes.[25] These types of compound were difficult or impossible to ionise by techniques such as EI and CI because they would thermally degrade before volatilising due to their high boiling points. A number of ionisation techniques, including fast atom bombardment (FAB),[26] field desorption (FD),[27] field ionisation (FI)[28] and thermospray (TSP),[29] did allow the ionisation of thermally unstable compounds of low volatility. However, either limitations in the analytical performance or the requirement for highly skilled analysts to conduct the experiments meant that routine application was difficult to realise. ESI alleviates the need to transfer analytes

to the gas phase prior to ionisation, thus allowing compounds not amenable to ionisation by EI and CI to be studied by MS. Further, the ease of use meant that ESI became the preferred ionisation technique amongst the biological community. Although ESI has been extensively applied to the analysis of biological macromolecules, it is equally suited to ionising small polar compounds. It is frequently used in areas of science where small molecules are of primary interest, including environmental science,[30] forensic science,[31] metabolomics[32] and toxicology,[33] as well as pharmaceutical science.[21]

Another useful property of ESI is that the ionisation event imparts very little energy to the analyte, leading to it being referred to as a "soft" ionisation technique.[34] The result of this phenomenon is that predominately molecular species are observed in an ESI mass spectrum with rarely any evidence of fragmentation, unless induced *via* in-source CID. Depending upon the experimental conditions used, either positive or negative ions are produced by the ion source. Molecules with basic or acidic sites can be analysed by virtue of protonation or deprotonation respectively (**Equations 1.1** and **1.2**, where M = molecule). Adduct ions can also be formed, especially for those compounds not possessing strongly basic or acidic sites. Examples of adducts observed using positive ion ESI are cationised molecules, particularly with alkali metals such as sodium ions (**Equation 1.3**). Adducts with deprotonated acid molecules, for example formate anions (**Equation 1.4**) and halide anions are common in negative ion ESI.[35] The soft nature of the ionisation event, and the consequent lack of dissociation, means that molecular mass information, and additionally elemental formulae when high-resolution mass spectrometers are employed, is easily obtainable using ESI-MS.[36, 37]

Equation 1.1 $\qquad M + H^+ \rightarrow [M + H]^+$

Equation 1.2 $\qquad M \rightarrow [M - H]^- + H^+$

Equation 1.3 $\qquad M + Na^+ \rightarrow [M + Na]^+$

Equation 1.4 $\qquad M + HCO_2^- \rightarrow [M + HCO_2]^-$

An analytically useful characteristic of ESI is that multiple-charging is observed for macromolecules *i.e.* $[M + nC]^{n+}$, where C represents a charged species such as a proton or an ammonium ion. This was first demonstrated by Wong and co-workers, who showed data for oligomers of poly(ethylene)glycol bearing up to twenty-three sodium cations.[38] Multiple-charging thus leads to a range of species of a given analyte existing in solution, differentiated only by the number of positive or negative charges on the ion for positive and negative ion ESI respectively. When the solution is electrosprayed into the mass spectrometer, these species will be recorded at different *m/z* values due to the relationship shown in **Equation 1.5**;

Equation 1.5 $$\frac{[M+nC]^{n+}}{z}$$

where: M = Molecule

C = Charged species

n = Number of charged species

z = Number of charges on ion

The resultant distribution of peaks is referred to as the "charge envelope". An example is shown in **Figure 1.2** for the proteins cytochrome C and myoglobin.[39] The reduction of the *m/z* value of a macromolecule through multiple-charging means that it can be analysed on mass spectrometers that have a low value upper mass range limit *e.g.* quadrupole mass spectrometers.[40] This increases the scope of biological MS by allowing a greater number of researchers to perform analyses in this area.[14] Another advantage of multiple-charging is that the molecular mass determination can be averaged over all of the observed charged states, leading to mass accuracies with errors of ± 0.01% *i.e.* 1 Dalton (Da) error at 10,000 Da molecular weight.[41]
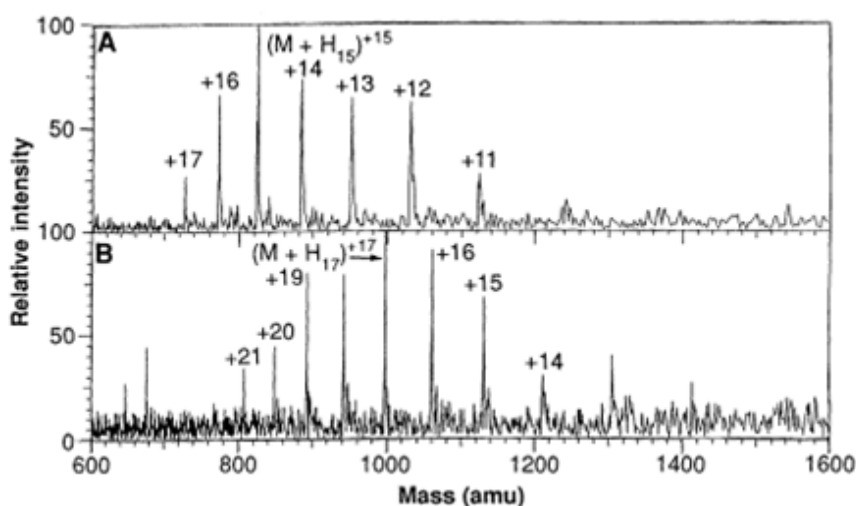
Figure 1.2 **ESI mass spectra of A) cytochrome C and B) myoglobin. The annotations show the number of protons associated with each peak. Deconvolution of the spectrum allows the determination of the molecular weight of the protein analysed**
Reproduced from reference 39 with kind permission from the American Association for the Advancement of Science

Multiple-charging is generally restricted to analytes in excess of approximately 1000 Da. Below this value, most molecules are sufficiently small that coulombic repulsion prevents the addition or removal of a second charge. Thus, small molecules are typically observed as singly charged ions, although Kaufmann and co-workers reported doubly charged ions in the ESI mass spectrum of difloxacin.[42] All of the compounds investigated in this study were analysed as singly protonated molecules *i.e.* [M + H]$^{+}$.

Finally, ESI also enables the simple coupling of separation science techniques, such high performance liquid chromatography (HPLC)[43] and capillary electrophoresis,[44] to MS. A number of interfaces were evaluated for the coupling of the two techniques,[45] such as TSP and continuous-flow (CF)-FAB,[46] with varying degrees of success. However, ESI provided one of the most robust and user-friendly approaches, and thus has become widely applied.[47] The ease of coupling, along with the high sensitivity of ESI,[48] has led to LC-ESI-MS becoming the staple technology for the analysis of pharmaceutical metabolites.[49] These analytes are typically at low levels in complex matrices, thus necessitating the strengths of LC-ESI-MS for their successful analysis.

Figure 1.3 shows a schematic of the production of ions at the tip of the capillary in an ESI ion source, which is operated at atmospheric pressure. To ionise a sample, it is first dissolved in a polar solvent; typically acetonitrile, methanol or water, or combinations thereof.[50] In the design shown, the resultant solution is passed through a metal capillary to which a high voltage of several kilovolts (kV) is applied. If positive ion ESI is being performed, this voltage is of positive polarity. The polarity is reversed for negative ion ESI. A counter electrode is held at 0 volts (V), causing a strong electric field to be created. A different approach to creating the strong electric field is to hold the capillary at 0 V, typically using a glass capillary, whilst applying a high voltage to the counter electrode; a negative voltage is used for positive ion ESI, whilst a positive voltage is applied when performing negative ion ESI. Upon reaching the end of the capillary, the electric field causes the positive ions to be attracted towards the counter electrode, leading to charge separation at the surface of the solution. The result is that the liquid forms a "Taylor cone", which protrudes from the end of the capillary with charge of the same polarity localised on the surface (**Figure 1.3**).[15] Subsequent evaporation of solvent causes the charge density on the surface of the Taylor cone to increase until the "Rayleigh limit" is reached *i.e.* when the forces of coulombic repulsion between the like charges and surface tension of the solution are equal.[40] At this point, fission occurs, thus producing smaller droplets that carry the same amount of charge.[51]
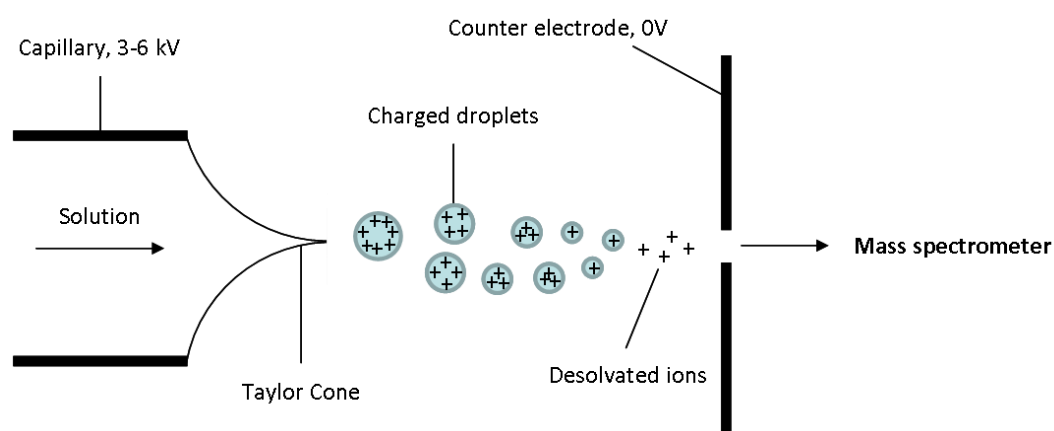
Figure 1.3   **Schematic of a Taylor cone and subsequent droplet fission in an ESI ion source operated with a positive polarity**

Repeated evaporation and fission eventually leads to the production of desolvated ions.[52] The ions present in solution are thus transferred to the gas phase. However, gas-phase reactions can cause the ions to be qualitatively different to those present in the solution phase.[53, 54]

More efficient ion production, and the capability to accept faster HPLC flow rates, is achieved by using pneumatically-assisted ESI (**Figure 1.4**). In this design, a counter-current drying gas is applied to the source; typically nitrogen. Collisions between ion-solvent complexes and the drying gas destroys the non-covalent interactions and releases desolvated ions.[55] Most ESI ion sources nowadays also use a sheath gas, which helps nebulise the solution, aids desolvation and collimates the spray; a modification originally proposed by Bruins and co-workers.[56] Application of heat can also assist desolvation, and prevent resolvation, of the ions.[57-59]
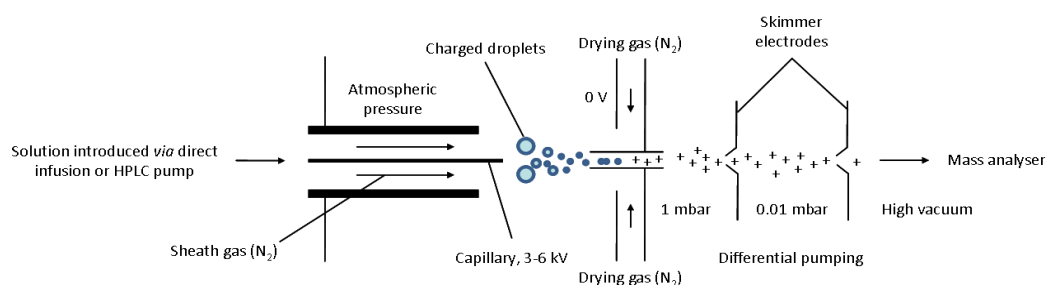
Figure 1.4   Schematic of a pneumatically-assisted ESI ion source

Two desolvation mechanisms have been proposed for the formation of isolated gas-phase ions produced by ESI. Dole and co-workers suggested the charged residue model (CRM) (**Figure 1.5**), whereby the repeated solvent evaporation and droplet fission eventually leads to a complex of an analyte with a few molecules of solvent.[11, 60] Evaporation of these solvent molecules, with concurrent retention of the droplet's charge by the analyte, forms an isolated gas-phase ion that can be sampled into the mass spectrometer.[61] Iribarne and Thomson proposed an alternative mechanism; the ion evaporation model (IEM) (**Figure 1.5**).[62, 63] This model begins as being qualitatively the same as the CRM, with repeated solvent evaporation and droplet fission steps. However, it differs when the droplets reach approximately 10 nm in radius. The model proposes

that at this point, the electrostatic force on the surface of the charged droplet is sufficiently high to overcome the solvation forces. As a result, direct field desorption of an analyte ion into the gas phase is able to take place.[53]

There is much conjecture as to which model applies, with conflicting experimental evidence and opinion.[61] However, a general consensus is that multiply-charged macromolecules are formed *via* the CRM,[64] whilst small ions are proposed to form by either the IEM[53, 65-67] or the CRM.[68, 69] These generalisations are based on a number of rationalisations, including the fact that a high activation energy barrier would exist to the desorption of macromolecules directly from the charged droplet, thus precluding the IEM.[70] However, various authors acknowledge that there are assumptions in the proposals as to which model applies for different types of analyte. There is an acceptance that a combination of the models could be involved at any one time in the formation of gas-phase ions.[71]
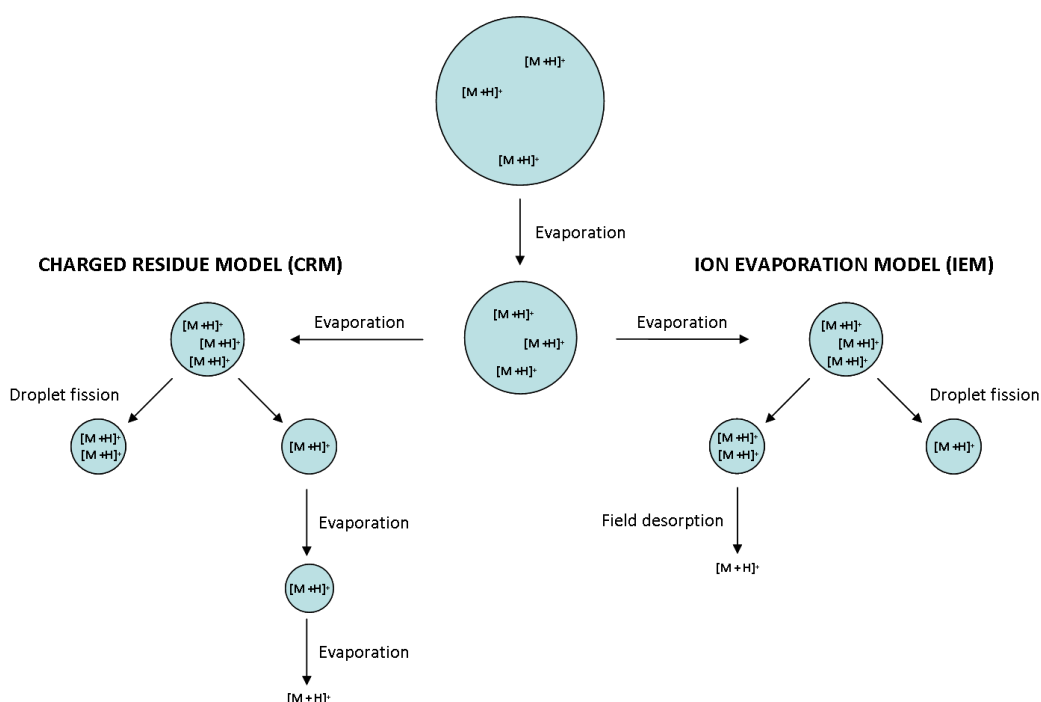
Figure 1.5   **Schematic of the desolvation of gas-phase ions as described by the charged residue model (CRM) and the ion evaporation model (IEM)**

The mixture of ions and solvent molecules generated from the tip of the capillary supersonically expands as it passes through the ESI ion source.[72] The desolvated ions, along with any surviving ion-solvent clusters, pass through the orifice in the counter electrode into the mass analyser because they experience limited diffusion over the distance traversed. The lighter solvents molecules diffuse much faster from the centre of the spray and thus are less likely to be sampled into the mass analyser. Various source configurations have been developed to maximise ion transmission whilst minimising sampling of solvent molecules, neutrals and salts.[73] For example, Voyksner and Lee demonstrated an off-axis nebuliser, positioned 90-95° from the sampling orifice, which increased the signal for the protonated molecule of lincomycin by a factor of six.[74] Upon passing through the orifice, the ions experience a pressure gradient as they travel to the mass analyser. A gradient is required to gradually lower the pressure from atmospheric pressure at the source to the high vacuum required in the mass analyser, in order to make them compatible. This gradient is created using a differentially pumped interface made up of a series of compartments separated by skimmers, which act as baffles, between the source and the mass analyser (**Figure 1.3**).[75] Initially, rotary vane vacuum pumps are used to decrease the pressure to approximately 0.01 mbar.[41] Once pressures of this order are reached, high vacuum pumps can be utilised.[76] Typically, a turbomolecular vacuum pump is attached to the mass analyser to quickly attain the high vacuum at which it operates.[41] The ion motion must be controlled during the passage along the pressure gradient to ensure high transmission efficiency. This is achieved using ion optics.[77] The use of radio frequency (RF)-only multipoles,[78] charged lenses[76] and ion funnels[79] collimates the beam of ions, thus allowing efficient transfer. The exertion of electrostatic forces also accelerates the ions and prevents their removal by the vacuum pumps. Collisions caused by accelerating the ions desolvates any remaining ion-solvent complexes, with the solvent removed by the vacuum system.[75]

1.4   Mass analysers

Once an isolated gas-phase ion has been formed, a mass analyser is used to determine its *m/z* value. The three mass analysers used in this study were a quadrupole ion trap (QIT) mass spectrometer, a quadrupole time-of-flight (QqTOF) mass spectrometer and a Fourier transform-ion cyclotron resonance (FT-ICR) mass spectrometer. All three instruments are capable of performing the tandem mass spectrometry (MS/MS) experiment.

The use of soft ionisation techniques has had a significant positive impact on the field of MS. However, the limitation of these ionisation techniques is that little or no dissociation occurs due to the low amounts of energy imparted to the molecule. Thus, little or no structural information can be derived from a single stage of mass analysis. This limitation is overcome through the use of the MS/MS experiment, which involves two stages of mass analysis.[80] Bridging these two analytical scans is a period where an "ion activation" method is used to impart energy to the ions.[81] This leads to their dissociation, thus allowing the elucidation of structural information.

1.4.1 Tandem mass spectrometry (MS/MS)

The MS/MS experiment can be performed either "in-time" or "in-space".[82] Of the mass spectrometers used in this study, the QIT and FT-ICR mass spectrometers are "in-time" MS/MS platforms, whilst the QqTOF mass spectrometer performs MS/MS "in-space". "In-time" MS/MS platforms perform the two stages of mass analysis and the ion activation in the same mass analyser but at different points in time. "In-space" MS/MS instruments have two mass analysers separated by a collision cell where the ions are dissociated, all of which are arranged in series.[83] The type of MS/MS platform *i.e.* the mass analyser(s) used and whether MS/MS is performed "in-time" or "in-space", has a bearing on the MS/MS scans that can be performed. **Figure 1.6** shows the four MS/MS scan modes that can be conducted.

	Mass analysis stage 1	Ion activation	Mass analysis stage 2
a)	Specific *m/z* value		Mass range scanned
b)	Mass range scanned		Specific *m/z* value
c)	Scanned *m/z = x*		Scanned *m/z = x - y*
d)	Specific *m/z* value		Specific *m/z* value
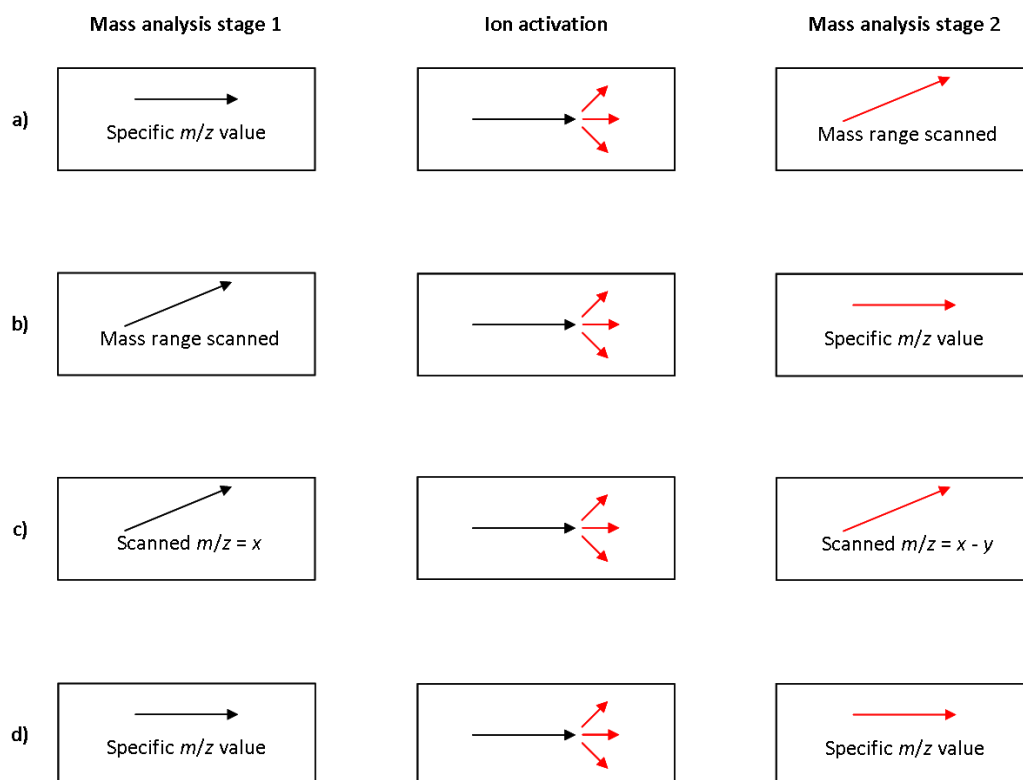
Figure 1.6   The MS/MS scan modes; a) product ion scan; b) precursor ion scan; c) constant neutral loss scan; d) selected reaction monitoring[1]

The different scan types can enable different information to be obtained about an ion of interest. All of the MS/MS experiments performed in this study were product ion scans. This experiment involves selecting a specific *m/z* value, for example that related to the protonated molecule of an analyte of interest, which is then isolated. The ions (precursor ions) then undergo activation, and all of the fragment ions (product ions) within a defined mass range are recorded by scanning the mass analyser during the second stage of mass analysis. This allows the analyst to determine structural components of the precursor ion. The precursor ion scan involves detecting a specific product ion during the second stage of mass analysis whilst scanning over a mass range during the first stage. This scan is useful for screening experiments where a group of compounds all dissociate to produce a common product ion. A frequent application of this experiment is the detection of the product ion at *m/z* 85 produced *via* the dissociation of butylester derivatives of acylcarnitines, which are biomarkers for inborn errors of fat metabolism.[84, 85] The constant neutral

loss scan is also useful for screening for a specific class of compounds. In this experiment, both mass analysers are scanned at the same rate during mass analysis. However, the second mass analyser is scanned with an offset in *m/z* value equal to the mass of a diagnostic neutral loss from the precursor ion. Thus, a signal is only generated when the specific neutral loss takes place during ion activation, allowing the recording of the product ion during the second stage of mass analysis. A recent application of this approach was reported by Bessette and co-workers, who used the constant neutral loss of 116 *m/z* units from protonated DNA adducts to identify different classes of carcinogens.[86] Finally, selected reaction monitoring experiments are used in quantitative MS to improve the limit of detection. A precursor-product ion pair is detected by scanning only for the *m/z* value of the precursor ion during the first stage of mass analysis and only for the *m/z* value of the product ion during the second. As well as lowering the limit of detection, this MS/MS scan mode also improves the selectivity of the experiment.[87]

1.4.2 Collision-induced dissociation (CID)

The MS/MS experiment requires an ion activation technique to induce dissociation of the precursor ions, with a variety of approaches reported.[81] The technique used throughout this study was CID (**Figure 1.7**). In this process, the precursor ion is accelerated and collides with an inert gas of high ionisation potential; typically helium, nitrogen or argon.[88] The collisions cause conversion of the translational energy of the precursor ions to internal energy.[89] In low-energy CID, such as that used in this study, the precursor ions undergo multiple collisions that gradually increase the internal energy.[90] High-energy CID can also be performed, using sector and time-of-flight (TOF) mass spectrometers, which can produce qualitatively different mass spectra.[91-93] The increased internal energy provides the activation energy for the dissociation reactions to occur. The stepwise heating due to multiple collisions produces a spread of energies in the precursor ions that tend towards a Boltzmann distribution.[83] Thus, precursor ions with different internal energies are produced, allowing a range of

dissociations to take place.
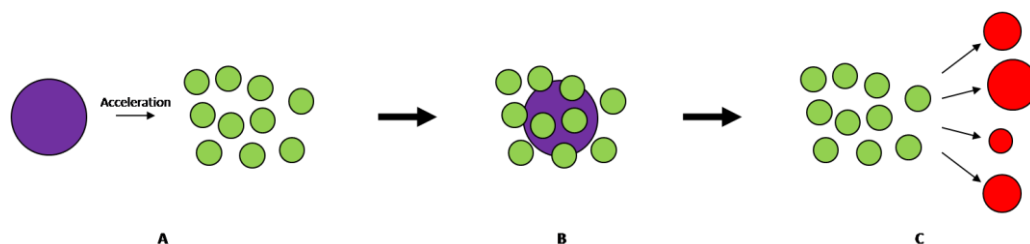
Figure 1.7 **Schematic of the collision-induced dissociation (CID) process where (A) a precursor ion (purple circle) is accelerated and (B) collides with a neutral gas (green circles) (C) leading to the formation of product ions (red circles)**

The centre-of-mass (E_{com}) reference describes the inelastic ion-neutral collision and is used to represent the maximum amount of translational energy that can be converted into internal energy.[81] **Equation 1.6** shows that increasing the translational energy of the precursor ion and/or the mass of the inert gas will allow greater internal energies to be attained.[41] Greater collision gas pressures, as well as increasing the cross-sectional area of the atom or molecule used, also increase the likelihood of a collision.[76, 81] Given that multiple collisions take place under low-energy CID conditions, these approaches provide alternative methods of increasing the internal energies of the precursor ions.

Equation 1.6
$$E_{com} = E_{lab}(\frac{m_c}{m_i + m_c})$$

where: E_{lab} = translational energy of the precursor ion provided by the electric fields in the mass spectrometer

m_i = mass of the precursor ion

m_c = mass of the inert gas

1.4.3 Quadrupole ion trap-mass spectrometry (QIT-MS)

The low-energy CID-MS/MS platform upon which much of this study was conducted was the QIT mass spectrometer. This instrument has a single mass analyser in which MS/MS is performed *i.e.* it is an "in-time" MS/MS platform.

The QIT mass spectrometer became commercially available as a result of the development of the mass-selective instability mode of operation.[94] Until this point, the QIT had mainly garnered interest amongst the physics community as a method of trapping and studying ions, either *via* mass-selective detection or mass-selective storage.[95] However, limited analytical performance in terms of mass range, mass resolution and sensitivity meant that its use as a mass spectrometer was not widespread until the work of Stafford and co-workers.[96] The QIT mass spectrometer used in this study was an LCQ Classic, which operated in the mass-selective instability mode. The key features of this process on this particular instrument are described below.

A schematic of the QIT is shown in **Figure 1.8**. The mass analyser is constructed from three electrodes; a ring electrode and two end-cap electrodes. An oscillating electric field is generated through the application of an RF voltage to the ring electrode, whilst the end-cap electrodes are held at ground potential.[97] The electric field that is created allows ions of a range of *m/z* values to be trapped.[98]
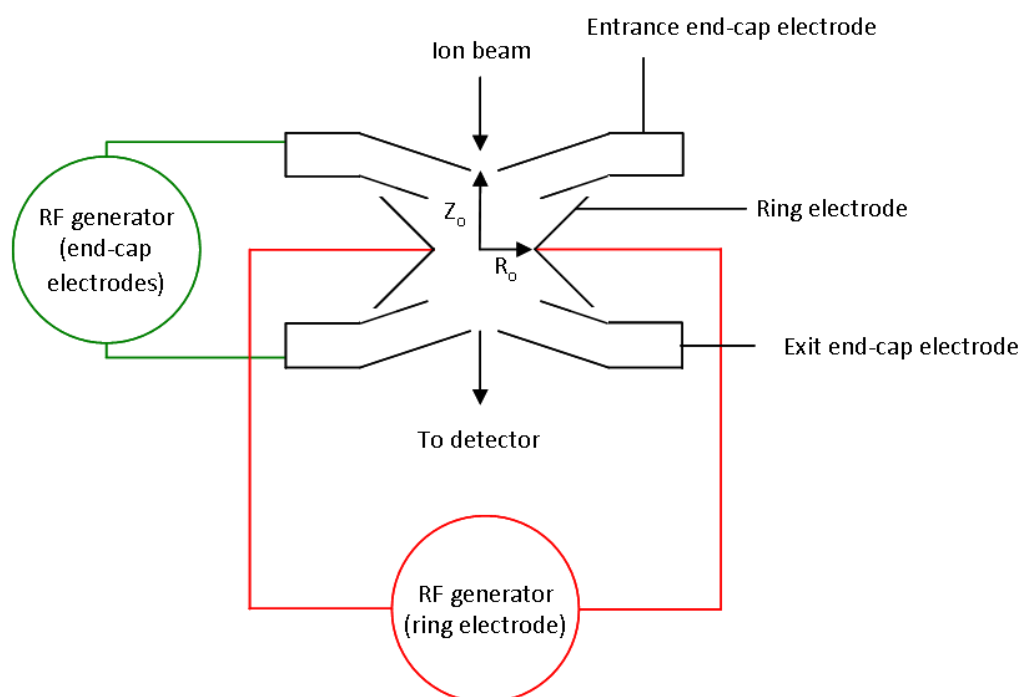
Figure 1.8   **Schematic of the two-dimensional cross section of a quadrupole ion trap (QIT) mass analyser**

The ions with a stable trajectory undertake a motion that has been likened to a "figure-of-eight".[99]   The stability of ion motion within the QIT can be determined from solutions of the Mathieu equation. These solutions allow the construction of a stability diagram in a_z, q_z space (**Figure 1.9**) where the following relationships apply (**Equations 1.7** and **1.8**);[94]

Equation 1.7 $a_z = \dfrac{-8U}{(m/z)r_o^2 \Omega^2}$ **Equation 1.8** $q_z = \dfrac{4V}{(m/z)r_o^2 \Omega^2}$

where: U = Maximum direct current (DC) potential between end-cap and ring electrodes

V = Maximum RF potential between end-cap and ring electrodes

m = Mass of ion in Da

z = Number of charges on ion

r_o = Internal radius of ring electrode

Ω = Angular frequency of RF potential
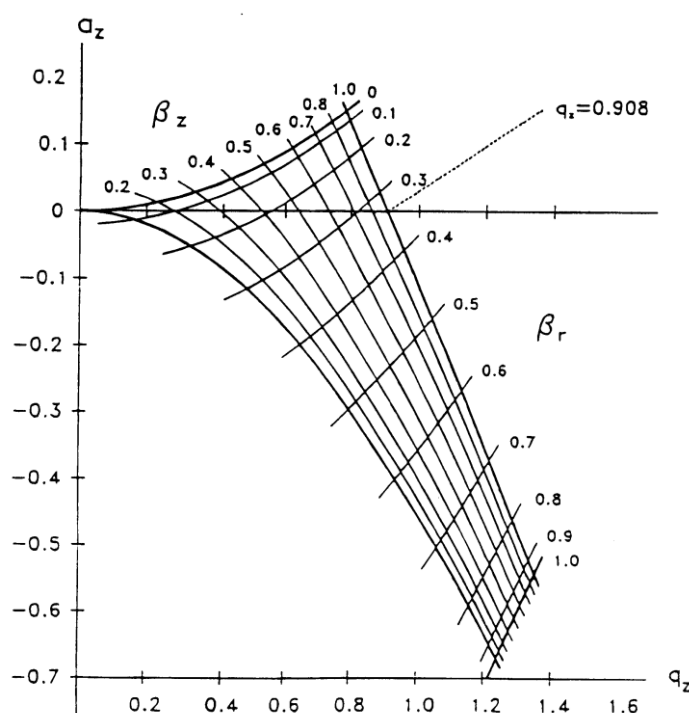
Figure 1.9   **Stability diagram in (a_z, q_z) space for a QIT mass analyser**
Reproduced from reference 105 with kind permission from John Wiley & Sons Ltd.

Ions which map onto the stability diagram within the defined boundaries have stable orbits within the electric field, and thus the QIT.[100] As no DC potential is applied using the mass-selective instability mode of operation, all of the ions have a value of zero for a_z, hence maximising the range of m/z values that can be trapped.[95] Ions are thus positioned along the q_z axis, with values inversely proportional to their m/z value. Mass analysis is achieved by linearly increasing the amplitude of the RF voltage applied to the ring electrode whilst maintaining a fixed frequency.[101] This increases the q_z value associated with each m/z value. When a particular m/z value reaches the q_z value at the boundary of the stability region, the orbits of those ions become unstable in the axial direction.[96] This leads to ejection of the ions, in order of increasing m/z value, through one of the end-cap electrodes where they impinge on an external detector. The solutions of the Mathieu equation produce a boundary of the stability diagram at $q_z = 0.98$ when $a_z = 0$. However, this value is decreased to 0.83 in the LCQ Classic QIT mass spectrometer used in this study due to the application of a supplementary RF voltage to the end-cap electrodes during mass analysis. This voltage is called the resonance ejection amplitude and is applied so that all ions of a given m/z value are ejected simultaneously. This ensures correct m/z value assignment and improves the mass resolving power of the instrument. When the ions begin to become unstable inside the QIT, their orbits increase in size and decrease in regularity. At the point in time when $q_z = 0.98$, some of the ions will be closer to the end-cap electrodes than others. This leads to the population of ions of a given m/z value leaving the trap and impinging upon the detector at different points in time. Whilst these ions are exiting the end-cap electrodes, the amplitude of the RF voltage on the ring electrode will have increased. As the QIT is calibrated such that there is a linear relationship between m/z value and RF amplitude, the ions reaching the detector at a later point in time will be detected at a higher m/z value than their true value. By applying the resonance ejection amplitude at the secular frequency of the m/z value of interest *i.e.* the characteristic frequencies with which ions oscillate within the QIT, which are dependent upon their q_z values,[95] all ions of that m/z value are caused to oscillate as a group. Thus, they are ejected from the trap

simultaneously when q_z = 0.83 and before the amplitude of the RF voltage on the ring electrode has increased. The resonance ejection amplitude is increased proportionally to the amplitude of the RF voltage on the ring electrode during mass analysis to ensure that ions of increasing *m/z* value are grouped.

Electrostatic repulsion between like charges inside the QIT decreases the mass resolving power of the instrument. The interferences between ions and the modifications of the electric fields inside the QIT caused by coulombic interactions are called space charge effects.[102] One method of overcoming space charge effects is by limiting the population of ions within the QIT using automatic gain control (AGC). AGC determines a maximum allowable ion abundance that can be tolerated inside the QIT before space charge effects occur. When this ion abundance is reached, the AGC prevents further ions entering the trap to allow optimal performance to be maintained. Another method of improving the performance of the QIT, discovered by Stafford and co-workers, is to introduce a buffer gas of helium at a pressure of approximately 1 µbar.[94] The buffer gas causes collisional cooling of the ions entering the trap. The removal of excess kinetic energy prevents collisions with the electrodes of the QIT, which would cause neutralisation and thus loss of the ions.[103] The collisional cooling also causes the ions to collapse towards the centre of the QIT where the electric field is homogeneous.[100] This enables a more uniform and efficient ejection process during mass analysis, which leads to an improvement in mass resolution, sensitivity and the limit of detection.[94]

The QIT allows structural information about an analyte of interest to be obtained using the MS/MS and mass spectrometry to the nth degree (MS^n) experiments. MS/MS and MS^n are performed in the QIT by isolating and dissociating a precursor ion of interest to yield product ions. The ability of the QIT to perform MS^n means that the genealogy of a precursor ion can be followed.[90] This allows extensive structural information to be obtained, with MS^{12} having been demonstrated.[104] MS^n is achieved by performing multiple stages of dissociation *i.e.* repeated isolation and fragmentation steps.[105] The

isolation of ions is often achieved in two stages. Firstly, the q_z value of the ion of interest is increased to 0.83. Thus, all ions of lower *m/z* values will be ejected from the trap. This process also increases the differences in the q_z values between the remaining ions in the QIT to allow more efficient isolation during the second stage, which is termed resonance ejection. This involves applying a range of RF frequencies to the end-cap electrodes in a similar manner to that used to eject the ions simultaneously during mass analysis.[101] However, the frequencies are chosen to resonate with the secular frequencies of the ions that are not required. A large voltage (approximately 100 V) is used to ensure that the ions obtain sufficient energy to cause them to undergo unstable orbits. Thus, they are ejected from the QIT. No frequency that resonates with the secular frequency of the ion of interest is applied so that it remains in the QIT. Resonance ejection can also be utilised to eject all of the unwanted *m/z* values from the QIT without the prior increase of the q_z value of the ion of interest to 0.83.[106]

Dissociation of the isolated ion of interest is achieved using low-energy CID, which is effected in the QIT by initially decreasing the amplitude of the RF voltage applied to the ring electrode. This reduces the q_z value of the isolated ions. The product ions, which for singly charged precursor ions will be of a lower *m/z* value, would instantly become unstable and be ejected from the QIT as they are formed if the q_z value of the precursor ion was not decreased from q_z = 0.83. A q_z value of 0.25 has been found to lead to optimal dissociation of the precursor ion. Application of an RF voltage to the end-cap electrodes of secular frequency of the ion of interest leads to dissociation. The amplitude used is smaller than that used to effect resonance ejection. The voltage causes the ions to become excited; hence the process is known as resonance excitation. The excitation of the ions increases their kinetic energy to facilitate higher energy collisions with the helium buffer gas.[101] The gradual increase in the internal energy inside the QIT is a "slow heating" process, taking place over time spans of the order of tens of milliseconds (ms).[107] Once formed, the product ions do not fragment further. This is because they are not in resonance

with the applied RF voltage as their q_z values are greater than 0.25 due to them being lower in *m/z* value, assuming that the precursor ion is singly charged. The amplitude of the RF potential applied to the ring electrode is then increased linearly to eject the product ions in order of increasing *m/z* value. A limitation of performing MS/MS in the QIT is that some low *m/z* value product ions formed through dissociation of the precursor ion will have q_z values greater than 0.83. Thus, they instantly have unstable orbits, causing their ejection from the QIT and preventing them from being recorded during the mass analysis stage. This is referred to as the low mass cut-off (LMCO) and results in product ions with *m/z* values of approximately one-third of the precursor ion not being observed in the product ion spectrum.[108]

Two parameters allow improved acquisition of product ion spectra using the LCQ Classic QIT mass spectrometer. These are WideBand activation and normalised collision energies. WideBand activation allows dissociation of the product ion resulting from the non-specific water loss observed for many compounds in the QIT. The transfer of energy to the precursor ion during low-energy CID in the QIT is lower than in other mass spectrometers that perform low-energy CID, such as a triple quadrupole (QqQ) instrument with a collision cell.[109] This frequently leads to the dominant, and often only, product ion being $[M + H - H_2O]^+$, as observed in the low-energy CID product ion spectrum of methyl red acquired without WideBand activation (**Figure 1.10a**). The non-specificity of this dissociation provides little useful structural information about an analyte of interest. MS^3 can be employed to fragment the $[M + H - H_2O]^+$ product ion. However, this is non-ideal when using chromatography because the extra scan event leads to fewer scans across an eluted peak. This leads to a decrease in accuracy in quantitative experiments. Further, the extra scan event decreases the number of co-eluting compounds for which structural information can be obtained. WideBand activation overcomes this problem by applying a range of excitation frequencies during low-energy CID such that product ions within a 20 *m/z* unit range below the precursor ion are dissociated.[110] Thus, WideBand activation allows the dissociation of a

protonated molecule and the $[M + H - H_2O]^+$ product ion in a single scan *i.e.* a pseudo-MS^3 scan takes place (**Figure 1.11**). This can lead to product ion spectra with greater structural information (**Figure 1.10b**).[110]
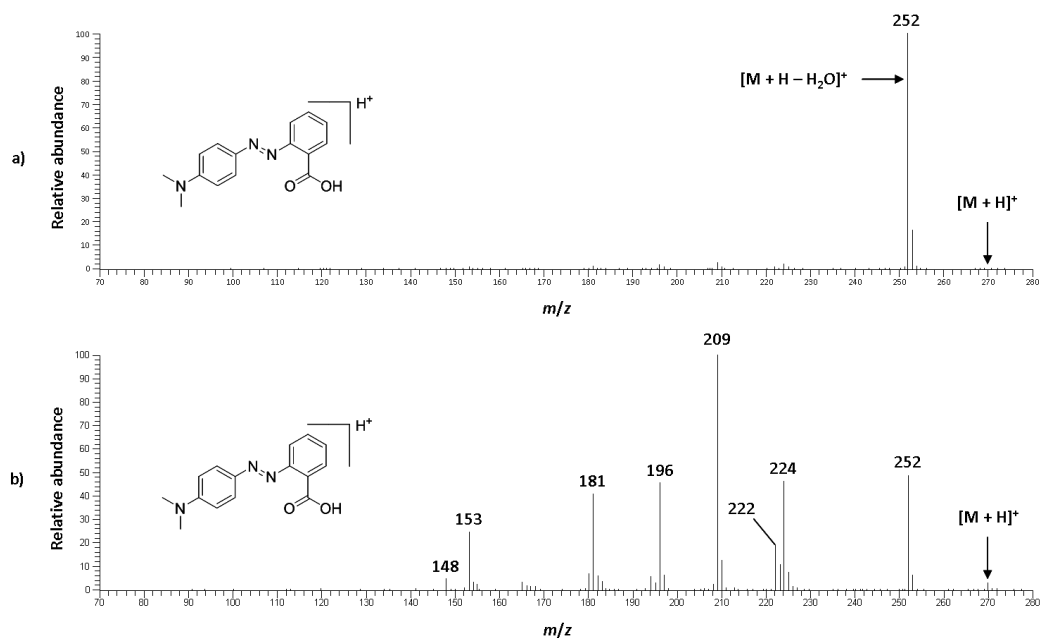
Figure 1.10   First-generation low-energy CID product ion spectra of protonated methyl red (*m/z* 270) acquired using a LCQ Classic QIT mass spectrometer with a) WideBand activation off and b) WideBand activation on
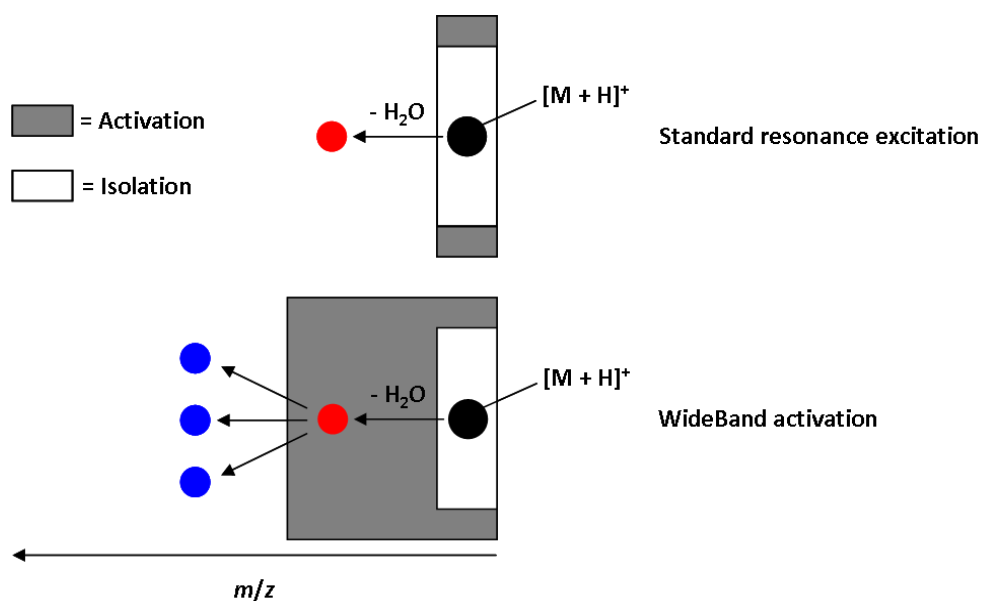
Figure 1.11   Schematic of the operation of WideBand activation
Reproduced from reference 110 with kind permission from John Wiley & Sons Ltd.

Normalised collision energies allow optimum dissociation of analytes covering a wide mass range. A high mass ion requires a greater RF voltage *i.e.* a greater collision energy, than a low mass ion for effective dissociation by low-energy CID to be achieved.[110] An approximately linear relationship exists between the *m/z* value of the precursor ion and the optimal collision energy (**Figure 1.12**). Collision energies could be applied as a percentage of the fixed maximum value of which the LCQ Classic QIT mass spectrometer is capable. In this circumstance, approximately the same amount of energy would be applied for a given percentage regardless of the *m/z* value of interest. Hence, the RF voltage used would only be optimal for a single *m/z* value. This would result in the structural information for ions of other *m/z* values being less informative. The normalised collision energy parameter scales the applied RF voltage by accounting for the linear relationship shown in **Figure 1.12**. The scaling of the RF voltage creates equivalent dissociation, and hence potentially structural information, for any precursor ion independent of its *m/z* value (**Figure 1.13**)
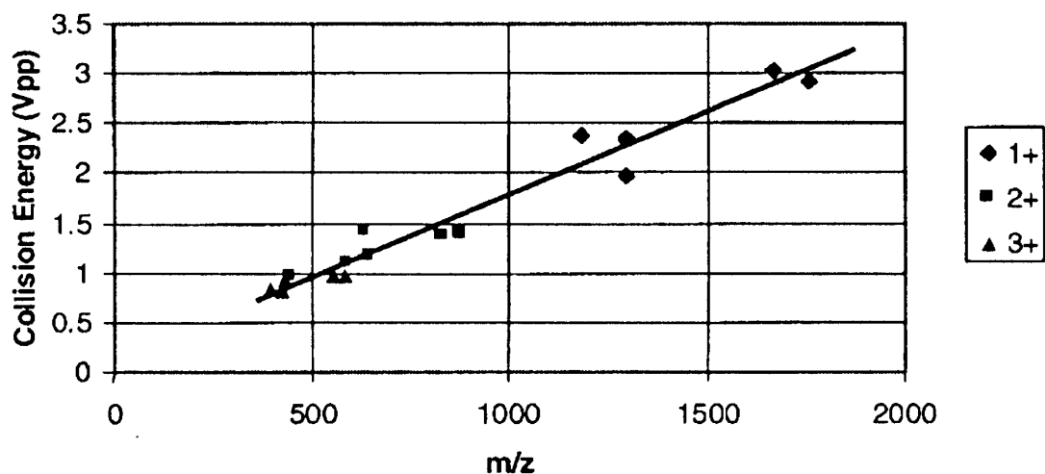
Figure 1.12 **Graph of optimal collision energy against precursor ion *m/z* value**
Reproduced from reference 110 with kind permission from John Wiley & Sons Ltd.

Normalized Collision Energy Scheme
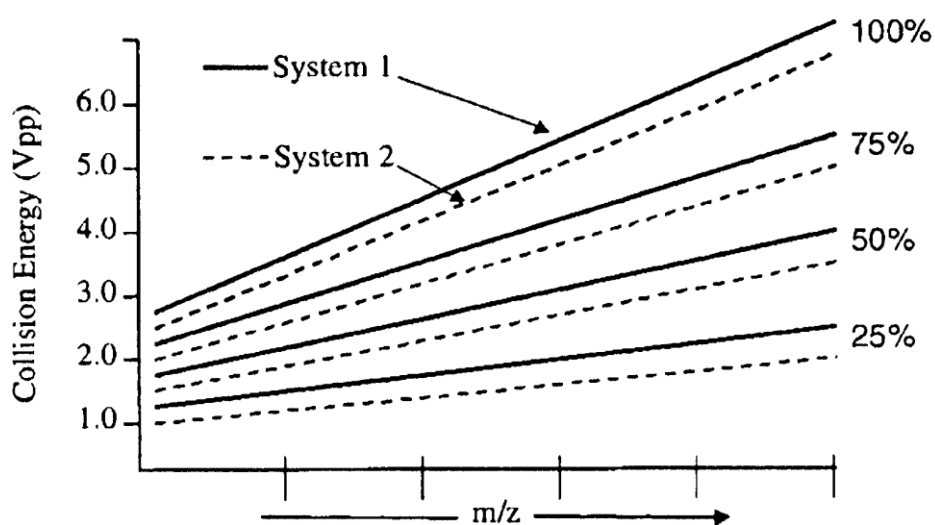
Figure 1.13   **Scaling of applied RF voltage with increasing *m/z* values for different values of normalised collision energy**
Reproduced from reference 110 with kind permission from John Wiley & Sons Ltd.

1.4.4 Quadrupole time-of-flight-mass spectrometry (QqTOF-MS)

The second low-energy CID-MS/MS platform used in this study was the QqTOF mass spectrometer. This is a hybrid instrument made up of two different mass analysers; a quadrupole mass analyser and a TOF mass analyser, coupled *via* a collision cell where low-energy CID takes place. The components are arranged in series. Thus, the QqTOF mass spectrometer is an "in-space" MS/MS platform. The instrument benefits from the ability of the quadrupole to isolate precursor ions with unit mass resolution and the TOF's low limit of detection and capacity to record mass spectra with high speed and mass resolution, thus making accurate mass measurements (AMMs) of complex mixtures possible.[41, 111]

The first QqTOF mass spectrometer was reported by Glish and Goeringer.[112] This instrument was constructed such that the quadrupole and the TOF were aligned on the same axis. This configuration was compatible with the ionisation technique selected; thermal ionisation following desorption from a probe. The compatibility arises from the requirement of the acceleration plates of the TOF to be operated in a pulsing fashion, thus facilitating transfer of ions along the flight tube (**Figure 1.14**).[1] Thus, TOFs can only accept packets of ions that are

created by pulsed ionisation techniques. Therefore, the Glish and Goeringer designed instrument would not have been compatible with ionisation techniques that create ions continuously, such as ESI, because the TOF could not tolerate the ion beam.
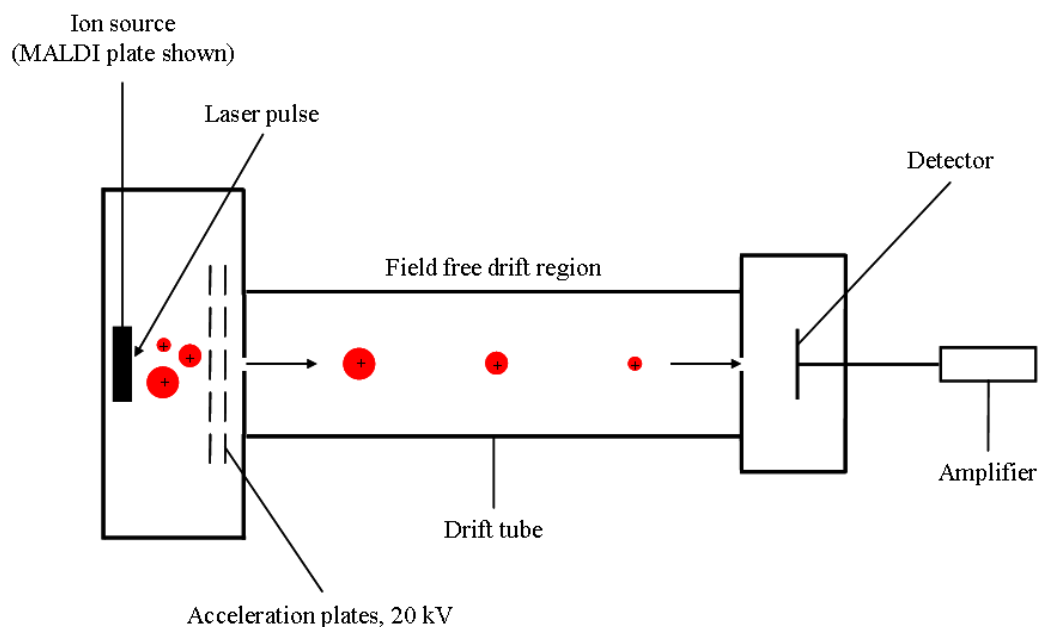
Figure 1.14   Schematic of a time-of-flight (TOF) mass analyser

The interfacing of continuous ionisation techniques with TOFs was solved by Dawson and Guilhaus, who reported an orthogonal acceleration (oa)-TOF mass spectrometer.[113] This configuration involves arranging the TOF perpendicular to the beam of ions produced by the ion source (**Figure 1.15**). The ion beam is collimated by a charged lens and then directed into the orthogonal accelerator. A voltage of like potential to the ions of interest is applied to the orthogonal accelerator for short time periods, typically 10-100 nanoseconds (ns), to repel the ions and direct them into the flight tube.[114] These short voltage pulses thus make the TOF compatible with the continuous ion source generating the ion beam. The orthogonal accelerator also imparts a number of other advantages.[115] The filling time of the orthogonal accelerator is approximately equal to the time taken for ions to travel along the drift tube and reach the detector. This means that mass analysis can take place whilst the orthogonal accelerator is filling with the next packet of ions, thus leading to a high duty
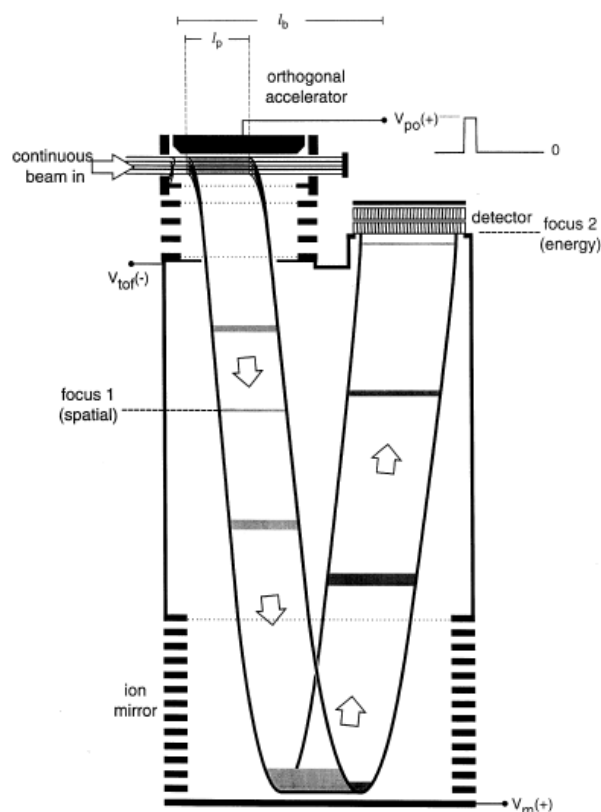
Figure 1.15   Schematic of an orthogonal acceleration-time-of-flight (oa-TOF) mass spectrometer
Reproduced from reference 115 with kind permission from Elsevier Ltd.

cycle.   Further, collimation of the ion beam and collisional cooling in the orthogonal accelerator leads to a population of ions that have very similar velocities in the axis of the TOF.[76] This leads to the ions passing through the acceleration plates at the same time, which results in an enhancement in mass resolving power. Additional increases in mass resolving power are derived from the ion beam being dispersed along the axis of the orthogonal accelerator, which means that the subset sampled into the TOF are spread sufficiently to obviate space charge effects. Finally, any neutral species produced by the ion source will not be affected by the electric pulse generated by the orthogonal accelerator. Hence, no neutrals will enter the TOF, which can lead to improved sensitivity and prevention of contamination of the mass analyser and detector.

The ability of an orthogonal accelerator to interface continuous ionisation techniques, specifically ESI, with TOFs led to interest from the biological

community and paved the way for the development of the QqTOF mass spectrometer as a commercially available instrument.[116] The oa-TOF was used as the basis for the design of the QqTOF mass spectrometer, which has an additional quadrupole mass analyser and a hexapole collision cell preceding the orthogonal accelerator (**Figure 1.16**). The construction and operation of the two mass analysers in this hybrid instrument will be discussed below.
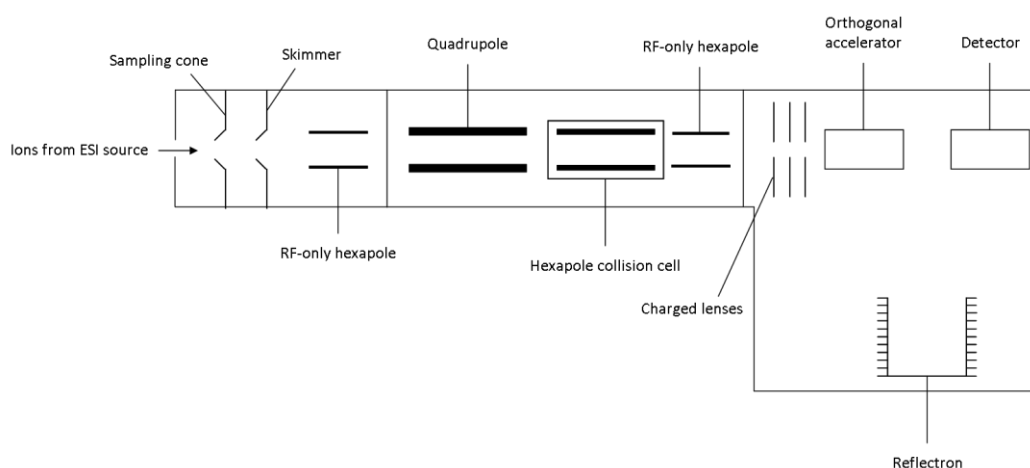
Figure 1.16   **Schematic of a quadrupole time-of-flight (QqTOF) mass spectrometer with an orthogonal accelerator**[116]

Quadrupoles are made up of four cylindrical metal rods arranged equidistant from one another. Opposite pairs of rods are electrically connected as denoted by "A" and "B" in **Figure 1.17**.
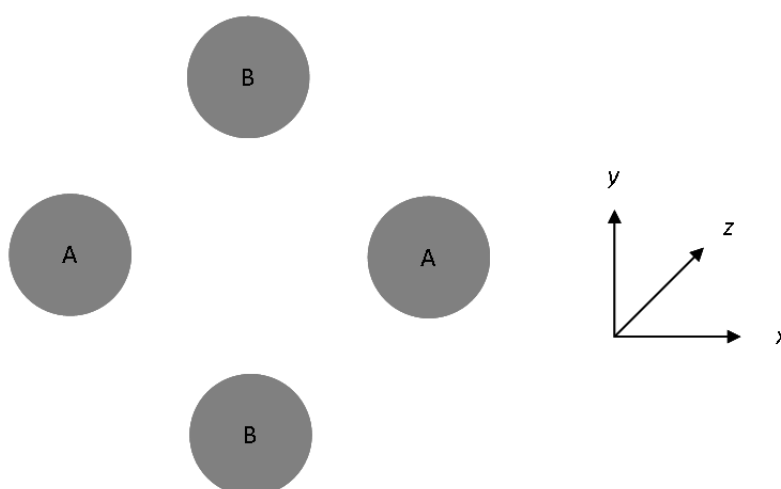
Figure 1.17   **Schematic of a two-dimensional cross section of a quadrupole mass analyser**

During the operation of a quadrupole, a positive potential with both a DC and an RF component is initially applied in the *x* direction *i.e.* to the "A" rods. At the same time, an equal negative potential, also with DC and RF components, is applied in the *y* direction *i.e.* to the "B" rods.[117] Throughout the operation of the quadrupole, the polarities of the two pairs of rods are alternated rapidly *i.e.* from their initial states, the "A" rods change to a negative polarity and the "B" rods to a positive polarity, and then back to their initial conditions. The connection of the pairs of rods with opposite polarities creates an electric field in the x-y plane (**Figure 1.17**). Ions enter the quadrupole along the z-axis and begin to oscillate in the x-y plane.[99] Assuming that the ions are positively charged and the polarities of the rods are in the initial state described above, the ions will be attracted towards the "B" rods. However, the rapid switching of polarities means that the ions will then be repelled by the "B" rods and attracted towards the "A" rods, a situation that will again be reversed when the polarities are changed once more. These cycles of attraction and repulsion lead to the ions undergoing a spiralling motion as they travel along the quadrupole. As for the QIT, the stability of the ions within the electric field is determined by whether their *a* and *q* values from the simplified Mathieu equation, as given by **Equations 1.9** and **1.10**, produce a coordinate in the stable region of the stability diagram.[118]

Equation 1.9 $\quad a_x = -a_y = \dfrac{4zU}{m\omega^2 r_o^2}$ $\qquad$ **Equation 1.10** $q_x = -q_y = \dfrac{2zV}{m\omega^2 r_o^2}$

where: $\qquad$ z = Number of charges on the ion

$\qquad\qquad$ U = Amplitude of the applied DC voltage

$\qquad\qquad$ V = Amplitude of the applied RF voltage

$\qquad\qquad$ m = Mass of ion in Da

$\qquad\qquad$ ω = Angular frequency of the applied RF voltage

$\qquad\qquad$ r_o = Distance from centre to an electrode

Because there is a DC component contributing to the *a* value, both components of the coordinate will have a positive value on the stability diagram (**Figure 1.18**). Ions with a_z, q_z coordinates that map onto the stability diagram will have a stable trajectory through the quadrupole. Those ions with a_z, q_z coordinates outside of it will have unstable trajectories, thus leading to them striking the quadrupoles and becoming neutralised.
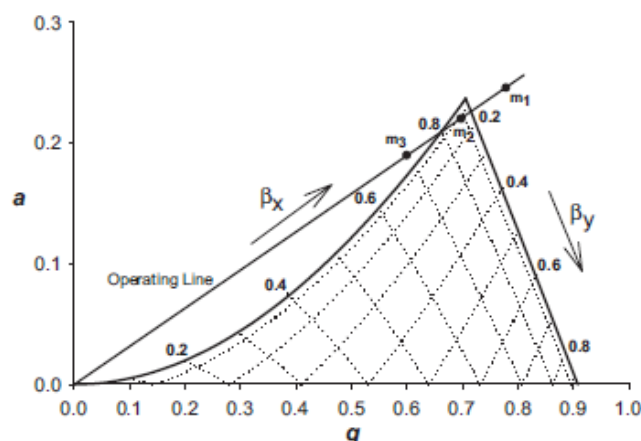
Figure 1.18   Stability diagram in (*a, q*) space for a quadrupole mass analyser
Reproduced from reference 117 with kind permission from John Wiley & Sons Ltd.

The only variables in **Equations 1.9** and **1.10** are the amplitudes of the DC and RF voltages.[1] Thus, these values are varied during mass analysis and determine whether an ion of given *m/z* value has a stable trajectory or not. The ratio of the amplitudes is fixed at a constant value, which defines the operating line (**Figure 1.18**).[76] Judicious selection of the ratio will ensure that only ions that map onto the stability diagram at the apex are stable. The stable region defines the mass resolving power of the instrument because it determines how many *m/z* values have stable trajectories through the quadrupole for a given DC:RF amplitude ratio. Thus, fixing the ratio such that only a small range of *m/z* values have stable trajectories at any one time maximises the mass resolving power.[118] In the example shown in **Figure 1.18**, m_2 has a stable trajectory at the specific DC and RF amplitudes selected, whilst m_1 and m_3 have unstable trajectories. Thus, only m_2 would travel the length of the quadrupole and reach the next mass analyser or detector, depending upon the configuration of the specific

instrument. To acquire a mass spectrum, the amplitudes of the DC and RF voltages are increased over a range whilst maintaining a fixed ratio. This sequentially changes, in an increasing fashion, the *m/z* values that have a_z, q_z coordinates at the apex of the stability diagram, and thus stable trajectories through the quadrupole.[117]

The TOF mass spectrometer is structurally simple, consisting of a flight tube held in a vacuum, a set of acceleration plates to direct ions along the tube, and a detector (**Figure 1.14**).[119] The depicted configuration is referred to as a "Wiley-McLaren" or linear TOF mass spectrometer.[120] The flight tube is referred to as a field-free region because neither electric nor magnetic fields are used in the operation of a TOF mass spectrometer. Mass analysis in a TOF mass spectrometer is performed by measuring the time that it takes for an ion to travel along the flight tube and strike the detector. The variation in flight times for ions of different *m/z* value arises from the relationship between the potential energy of the ion when present in the electric field created by the acceleration plates, and its subsequent kinetic energy derived through conversion of its potential energy. An ion in the electric field created by the acceleration plates will have a potential energy given by **Equation 1.11.** When the ion is pushed along the flight tube by the voltage of the acceleration plates, it obtains a kinetic energy as described by **Equation 1.12**. Assuming quantitative conversion of this energy, **Equation 1.13** can be formed.[1]

Equation 1.11 $\qquad E_p = zV \qquad$ where: E_p = Potential energy

$\qquad\qquad\qquad\qquad\qquad\qquad\qquad$ z = Number of charges on ion

$\qquad\qquad\qquad\qquad\qquad\qquad\qquad$ V = Accelerating voltage

Equation 1.12 $\qquad E_k = \dfrac{1}{2}mv^2 \qquad$ where: E_k = Kinetic energy

$\qquad\qquad\qquad\qquad\qquad\qquad\qquad$ m = Mass of ion in *m/z* units

$\qquad\qquad\qquad\qquad\qquad\qquad\qquad$ v = Velocity

Equation 1.13 $\qquad zV = \dfrac{1}{2}mv^2$

The velocity term can be expressed in terms of the time, t, required to travel the length of flight tube, d (**Equation 1.14**);

Equation 1.14 $\qquad v = \dfrac{d}{t}$ $\qquad$ where: v = Velocity

$\qquad\qquad\qquad\qquad\qquad\qquad\qquad$ d = Distance

$\qquad\qquad\qquad\qquad\qquad\qquad\qquad$ t = Time

Substitution of **Equation 1.14** into **Equation 1.13** produces **Equation 1.15**;

Equation 1.15 $\qquad zV = \dfrac{1}{2}m(\dfrac{d}{t})^2$

Rearrangement of **Equation 1.15** to express t in terms of the other parameters shows that the time taken to travel the length of the flight tube is proportional to the square root of the *m/z* value of the ion (**Derivation 1.1**).[121] This can be simplified to **Equation 1.16** because V and d are constant and hence can be expressed as k. Thus, ions with lower *m/z* values will have shorter flight times than those of greater *m/z* values.

Derivation 1.1 $\qquad zV = \dfrac{1}{2}m(\dfrac{d}{t})^2$

$\qquad\qquad \equiv \qquad \dfrac{2zV}{m} = (\dfrac{d}{t})^2$

$\qquad\qquad \equiv \qquad \dfrac{2zV}{m} = \dfrac{d^2}{t^2}$

$\qquad\qquad \equiv \qquad t^2 = \dfrac{m}{z}\dfrac{d^2}{2V}$

$\qquad\qquad \equiv \qquad t = \sqrt{\dfrac{m}{z}}\dfrac{d}{\sqrt{2V}}$

Equation 1.16 $t = k\sqrt{\dfrac{m}{z}}$

Thus far, a linear TOF mass spectrometer has been discussed *i.e.* the ions travel in a straight line between the acceleration plates and the detector. However, this arrangement leads to very poor mass resolution; approximately 300-500 full width at half maximum (FWHM).[122] This is because ions of the same *m/z* value generated by the ion source have both a spatial distribution *i.e.* they do not occupy an infinitesimally small space, and an energy distribution. The spatial distribution means that ions of a given *m/z* value will reach the acceleration plates at different times. Therefore, once accelerated, they will also reach the detector at different times, leading to peak broadening. The energy distribution causes ions of the same *m/z* value to have different kinetic energies. **Derivation 1.1** shows that the flight time is inversely proportional to the square root of the accelerating voltage. Therefore, if ions of the same *m/z* value have different amounts of kinetic energy, their flight times will be different and peak broadening will result. Furthermore, there are variations in the effect that the electric field has on the ions, which results from their spatial distribution. This leads to ions of the same *m/z* value receiving different amounts of energy when they are accelerated, thus leading to a spread of kinetic energies. Again, this leads to broader peaks than would be obtained if all ions of the same *m/z* value had equal kinetic energies. The combined effects of the spatial and energy distribution of the ions leads to a significant deterioration in the mass resolving power of the linear TOF mass spectrometer.[123]

Two approaches are used to improve the mass resolving power of TOF mass spectrometers. The first is the use of time-lag focussing (TLF),[120] which is sometimes referred to as pulsed-ion extraction (PIE)[124] or delayed extraction (DE).[125] This feature decouples the extraction of ions from the ion source and their acceleration down the flight tube *i.e.* ions are not continuously accelerated as soon as they are formed by the ion source.[123] By allowing a short period of

time (between hundreds of ns to several microseconds [μs])[1] to elapse before applying the acceleration voltage, the ions are allowed to cool in the ion source. This helps to minimise the distribution of kinetic energies of ions of the same *m/z* value such that the spread of their flight times is tighter once accelerated.[50] Further, the ions separate according to their kinetic energies during the period between their formation and their acceleration because no force is acting upon them. This results in ions of the same *m/z* value with greater kinetic energies drifting towards the detector due to the enhanced effect of the potential gradient. When they are extracted from the ion source and accelerated along the flight tube, the applied voltage has a greater effect on those ions that have spent longer in the source and are further from the detector *i.e.* those with lower kinetic energies.[1] The net result of the ions receiving different amounts of kinetic energy from the application of the accelerating voltage is that the ions that initially possessed less kinetic energy catch up with those that were more energetic at the outset. Thus, the kinetic energy and spatial distributions of the ions are reduced, resulting in improved mass resolving power.[41]

The second approach to improve the mass resolving power of a TOF mass spectrometer is the addition of a reflectron to the instrument (**Figure 1.16**). This is a stack of ring electrodes that typically have equal differences in voltage between them, creating a linear electric field.[41] The lowest voltage is applied to the electrode nearest the orthogonal accelerator and the detector, with the far most electrode having the highest voltage. The applied voltage creates an electric field that acts in the direction opposite to that produced by the orthogonal accelerator.[76] This has the effect of reversing the flight direction of the ions. The purpose of the reflectron is to correct for the differing velocities of ions of the same *m/z* value, which results from them possessing different amounts of kinetic energy. This is achieved by causing ions with greater amounts of kinetic energy to undergo longer flight paths than ions of slower velocities.[41] The ion beam penetrates into the reflectron after its passage from the orthogonal accelerator, whereby the ions are eventually repelled back towards the detector. However, the distance of penetration by a given ion is

dependent upon its kinetic energy. Increasing kinetic energies allow increased penetration, and thus longer residence times in the reflectron, before the ion's direction is reversed.[126] Therefore, for ions of the same *m/z* value but different kinetic energies, the faster travelling ions will traverse the flight tube quicker and enter the reflectron before the slower ones arrive. However, the ions with greater kinetic energies will spend longer in the reflectron than the ions with less kinetic energy. Hence, the difference in residence time, and thus flight path length, means that the ions of the same *m/z* value but different kinetic energies strike the detector at the same time, thus improving mass resolving power.[127] The use of a reflectron further increases the mass resolving power of a TOF mass spectrometer because the flight length is increased without having to make the instrument bigger, which would necessitate greater vacuum pumping capacity.[121] Mass resolving power is increased because flight times scales linearly with the distance to be travelled (**Derivation 1.1**). Thus, two ions of different *m/z* values with a constant difference in velocity will become increasingly separated in arrival time at the detector as the flight length increases. This leads to a lower chance of overlap between peaks of different *m/z* values, thus improving the mass resolving power.

Low-energy CID is performed on a QqTOF mass spectrometer using a collision cell, which is positioned between the two mass analysers. This is an RF-only quadrupole, hexapole or octopole that contains the gas with which the ions of interest collide, leading to an increase in their internal energy.[76] The pressure inside the cell is typically maintained at approximately 10 μbar, although this can be varied to affect the number of collisions that the ions undergo and thus the extent to which their internal energy is raised (**Equation 1.6**).[128] The collision energies can be tuned through varying the accelerating voltages applied to the poles of the cell. Only RF voltages are used so that all of the precursor and product ions have stable trajectories inside the collision cell. This is because the absence of a DC component means that all of the ions will be positioned on the *q*-axis of the stability diagram (**Figure 1.18**). This region is within the boundaries that define whether an ion has a stable trajectory or not

as it passes through the poles. Hence, as all of the ions have stable trajectories, no mass filtering will take place. Thus, all of the ions will traverse the collision cell and enter the orthogonal accelerator, and subsequently the TOF mass analyser. Unlike the QIT, dissociation of product ions can take place inside a collision cell. This is because the acceleration of ions of as they pass through the collision cell does not discriminate between precursor and product ions *c.f.* QIT where resonance excitation only causes the precursor ion to undergo high-energy collisions with the buffer gas. Thus, the formed product ions can undergo energetic collisions with the gas atoms or molecules before exiting the cell, which causes an increase in their internal energies. This can facilitate further fragmentation, which is referred to as second-generation dissociation.

1.4.5 Fourier transform-ion cyclotron resonance-mass spectrometry (FT-ICR-MS)

The final low-energy CID-MS/MS platform used in this study was the FT-ICR mass spectrometer. This instrument was used to acquire AMMs. The ultra-high mass resolving power of this instrument makes AMMs possible, with accuracies of sub-parts-per-million (ppm) having been reported by McKenna and co-workers in the identification of vanadyl porphorins.[129]

FT-ICR-MS instruments have a trap mass analyser, which uses a combination of electric and magnetic fields to trap the ions *c.f.* a QIT which uses only electric fields.[130] The magnetic field is typically generated using a superconducting magnet rather than a permanent magnet or an electromagnet. This is because the latter two varieties are only capable of producing weak magnetic fields, and as will be seen below, advantages are gained from using increasingly strong magnets.[131, 132]

Figure 1.19 shows a schematic of an FT-ICR-MS cell. The cell is made up of three pairs of electrically connected plates; trapping plates, excitation plates and detection plates. Ions enter the cell along the axis of the magnetic field but initially feel no force from it in this direction.

Figure 1.19   **Schematic of a cubic FT-ICR-MS cell detailing the electrical connection of the pairs of plates and the direction of the magnetic field, B**
Reproduced from reference 134 with kind permission from John Wiley & Sons Ltd.

To retain the ions in the cell, an electric current is applied to the trapping plates to create a potential well.[133] The plates are positioned perpendicular to the magnetic field and a low potential of approximately 1 V is used to trap the ions.[130] The magnetic field does impart a force on the ions in the plane perpendicular to their motion as they enter the cell. The force, known as the Lorentz force, is given by **Equation 1.17**.

Equation 1.17 $F_L = z$VB   where: z = Number of charges on ion

V = Velocity of ion

B = Magnetic field strength

The Lorentz force causes the ions to be bent into a circular motion that is perpendicular to the plane of the magnetic field (**Figure 1.20**). This is referred to as the cyclotron motion.[134]
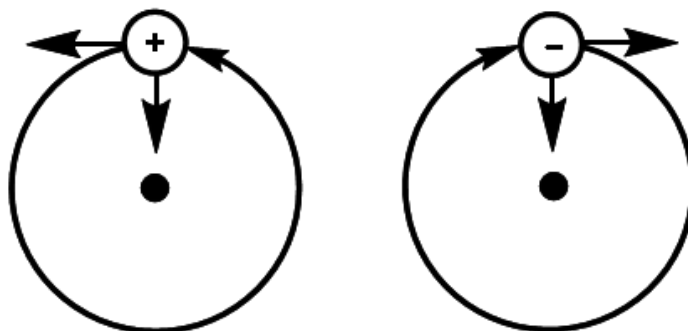
Figure 1.20   **The cyclotron motion of ions in a uniform magnetic field. The magnetic field is in the direction of the plane of the paper. Positive and negative ions orbit in opposite directions**

The ions also describe two other motions inside the cell. The ions undergo simple harmonic oscillation in the direction of the electric field created by the trapping plates; the so-called trapping motion. Finally, the combination of the electric and magnetic fields induces a third motion called the magnetron motion. This causes the ions to move in larger circular orbits in terms of radius than those described by the cyclotron motion, as shown in **Figure 1.21**.[133]
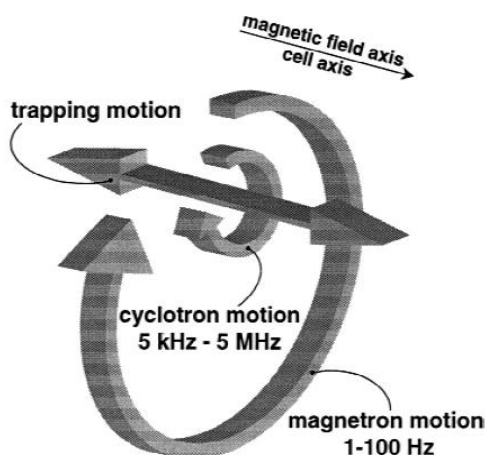
Figure 1.21   **Three fundamental motions described by ions trapped in an FT-ICR-MS cell**
Reproduced from reference 131 with kind permission from John Wiley & Sons Ltd.

Only the cyclotron motion is analytically useful. From the frequency of these orbits, the *m/z* value of an ion can be determined. The equation for cyclotron frequency (**Equation 1.18**) shows that the only variable is the *m/z* value of the ion.

Equation 1.18 $$f_c = \frac{zB}{m2\pi}$$ where: z = Number of charges on ion

B = Magnetic field strength

m = Mass of ion in Da

The high mass resolving power of FT-ICR-MS stems from the fact that the *m/z* value of the ions is the sole variable that dictates the cyclotron frequency. Thus, the cyclotron frequency is independent of an ion's velocity, which correlates with its kinetic energy, and its location in the cell. Hence, no energy or spatial focussing is required to allow accurate *m/z* values to be determined, which results in the ability to acquire high-resolution mass spectra *c.f.* TOF mass analysers whereby an increased spatial and energy distribution of the ions leads to a deterioration in the mass resolving power.[135]

To measure the cyclotron frequency of an ion, it is first excited to increase the radius of the cyclotron motion. The initial radius is much smaller than the dimensions of the cell and is insufficient to generate a recordable signal in the detection plates.[133] The radius of the orbits of ions of a given *m/z* value is increased by applying an RF voltage to the excitation plates with a frequency that is in resonance with the *m/z* value's characteristic cyclotron frequency.[136] This causes the ions to experience an outward force, which increases their kinetic energies and results in them moving coherently to an orbit of larger radius in a spiralling motion (**Figure 1.22**).[133] A number of *m/z* values can be excited to larger radii cyclotron orbits by applying a range of frequencies. This is achieved by performing a fast frequency sweep, referred to as an RF chirp.[133]

Detection of ions is achieved by measuring the alternating current induced in the detection plates by the orbiting packet of ions, referred to as the image current.[137] As the ions move past each detection plate, they attract electrons through the external circuit towards the plate (**Figure 1.22**). The movement of electrons from one plate to the other as the ions orbit creates the alternating current, the frequency of which is equal to the reduced cyclotron frequency *i.e.*
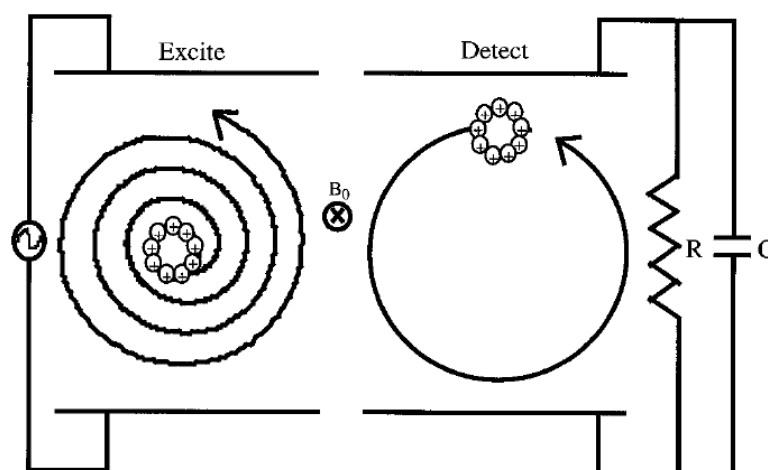
Figure 1.22   **Excitation of ions to a larger radius cyclotron motion by the application of a resonant frequency RF voltage to the excitation plates and detection of ions using the image current generated in an external circuit**
Reproduced from reference 134 with kind permission from John Wiley & Sons Ltd.

the difference between the cyclotron frequency and the magnetron frequency. The magnetron frequency is proportional to the trapping voltage used (**Equation 1.19**).[133] Therefore, the cyclotron frequency of a given *m/z* value will be reduced by increasing amounts with increasing trapping voltage. This prevents the frequency of the image current being used to determine the *m/z* value of the ion creating it from **Equation 1.18**. However, this does not prevent AMMs being acquired using FT-ICR-MS, because calibration of the instrument can account for the reduction in the cyclotron frequency that results from the applied electric field used to trap the ions.[133] The use of standard compounds of known elemental composition allows reduced cyclotron frequencies to be assigned to particular *m/z* values. This allows for the production of a calibration line, applicable at the specific trapping voltage, from which the *m/z* value of an unknown can be interpolated from its recorded reduced cyclotron frequency.[133]

Equation 1.19 $f_m = \dfrac{\alpha V}{\pi a^2 B}$

where: α = Geometry factor dependent upon the shape of the cell

V = Amplitude of the applied trapping voltage

a = Distance between the trapping plates

B = Magnetic field strength

If multiple ion packets of different *m/z* values are detected, the signal that is produced is an overlay of sinusoidal waves of different frequencies and amplitudes (**Figure 1.23**).[130] This complex signal is referred to as a transient, and is in the time domain. The complexity of the signal prevents simple mathematical treatment to derive the *m/z* value of the ions from the calibration line because it is a composite of a number of signals. However, frequency components from the time domain transient can be derived by applying a fast Fourier transform. This deconvolutes the signal and generates a frequency spectrum, which can be converted to a mass spectrum using the previously determined calibration line.[133]
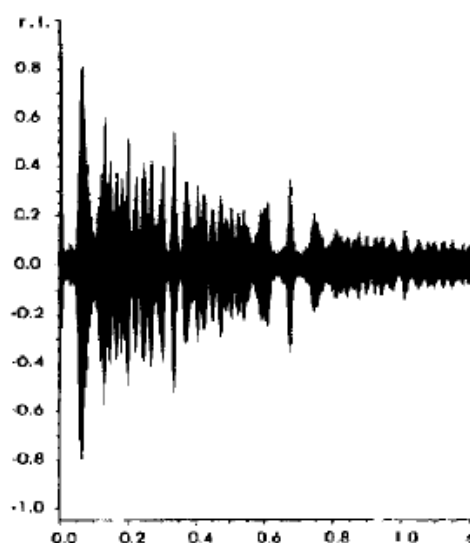
Figure 1.23   A time domain transient
Reproduced from reference 133 with kind permission from John Wiley & Sons Ltd.

Improved signal-to-noise ratio and mass resolving power is obtained with transients of increasing lengths of time, as detailed by the relationships in **Equations 1.20** and **1.21**. Acquisition of long transients is possible because the detection process is non-destructive. Thus, the ions can be remeasured on a number of occasions. To prevent ion loss, and thus enable remeasurement, an

ultra-high vacuum is used to maintain pressures of 1 x 10^{-8} – 1x10^{-9} mbar inside the cell. This minimises the numbers of neutrals present that can collide with the ions, thus causing their neutralisation. Transient lengths are not infinite however, with residual neutral molecules eventually causing loss of coherence of the ion packets. The longest transients are of the order of a minute in length.[133]

Equation 1.20 $\quad$ $S:N=\sqrt{n}$ $\quad$ where: n = number of scans

Equation 1.21 $\quad$ $R=\dfrac{f_c T}{2}$ $\quad$ where: f_c = cyclotron motion frequency

$\qquad\qquad\qquad\qquad\qquad\qquad\qquad\qquad$ T = duration of transient

Although both "in-time" MS/MS trapping instruments, low-energy CID is performed in a slightly different manner in the FT-ICR mass spectrometer compared to the QIT mass spectrometer. Firstly, the collision gas is pumped into the FT-ICR cell in a pulsing fashion. This briefly increases the pressure inside the cell to facilitate low-energy CID, but can not be maintained there due to its hindering effect on detection and is thus rapidly pumped away *c.f.* QIT where the helium gas is present in the mass analyser throughout the experiment. This process can take several seconds (s), meaning that low-energy CID-MS/MS experiments using FT-ICR mass spectrometers have a low duty cycle.[138] The second key difference is that there is no LMCO, meaning that all product ions can be trapped and mass analysed.[139] Like the QIT, the trapping capability of the FT-ICR mass spectrometer facilitates MS^n experiments.[138]

Isolation of the precursor ion of interest is most commonly performed using the stored-waveform inverse Fourier transform (SWIFT) technique.[140] This waveform excites all ions present in the cell to orbits of larger radii. The energy imparted to the undesired ions is sufficient to increase the radii such that they collide with the walls of the cell, thus leading to their neutralisation and subsequent removal by the vacuum system.[136] Concurrently, the ion of interest

is also excited to a larger cyclotron motion radius, leading to an increase in its kinetic energy. However, only half the energy imparted to the undesired ions is applied to the ion of interest so that its cyclotron motion radius is not increased to such an extent that it strikes the walls of the cell.[133] The excited ions of interest then undergo collisions with the gas that is pumped into the cell, which increases their internal energy and facilitates dissociation.

The excitation frequency used to excite the precursor ions of interest to a larger cyclotron motion radius is "off-resonance" *i.e.* not equal to the frequency of the ion's cyclotron motion. Hence, the activation technique is referred to as sustained off-resonance excitation (SORI)-CID.[141] This approach is used to enable more efficient detection of the product ions than is possible with an "on-resonance" excitation frequency like the one used in the QIT.[133] Using an on-resonance excitation frequency, the product ions are a significant distance from the centre of the cell when they are produced, which means that they cannot be formed into as coherent a packet for detection. This has an adverse effect on the mass resolution of the resulting mass spectrum.[133] Low-energy SORI-CID overcomes this by applying an excitation frequency that is slightly off-resonance of the cyclotron frequency of the precursor ions of interest. This results in the precursor ions being alternately in-phase and out-of-phase with the applied frequency.[133] Hence, the precursor ions experience periodic increases and decreases in their cyclotron motion radii, and therefore their kinetic energy.[136] The amplitude of the applied frequency is maintained at a low value so that the precursor ions do not travel far from the centre of the cell.[133] This, in combination with their intermittent decrease in radii towards the centre of the cell, means that the product ions formed from dissociation of the precursor ion are also located at the centre of the cell. This then allows them to be excited as a coherent packet for detection. Thus, low-energy SORI-CID improves the efficiency and mass resolution with which the product ions can be detected.[133]

Chapter 2

The use of mass spectrometry in pharmaceutical drug metabolite identification and characterisation

2.1   Introduction to pharmaceutical drug metabolism

The term metabolism describes a reaction, or series of reactions, in a biological system that converts a given molecule into a different compound or compounds.[142]   The intermediates and products of these reactions are called metabolites.[143]   Metabolites are produced from compounds that have essential biological functions *e.g.* carbohydrates, lipids, vitamins *etc.*, and also xenobiotics.   A xenobiotic is defined as any compound that is not ordinarily present in a biological organism or is present at a concentration much higher than usual due to uptake from an external source.[144]   A pharmaceutical compound is therefore classed as a xenobiotic.

Pharmaceutical compounds are metabolised because the biological organism (either human or animal) recognises it as a xenobiotic.   As a defence mechanism to prevent accumulation of xenobiotics, the organism reacts by attempting to eliminate the compound through a combination of physical and chemical means.   Physical elimination takes place by means of excretion, primarily *via* urine or faeces.[144]   To expedite the drug's excretion, chemical changes are made to the compound, which constitutes its metabolism.   The urinary excretion of the lipophilic parent drug compound is an inefficient process due its limited solubility in water.   Therefore, the organism metabolises the compound, typically converting the lipid-soluble parent drug compound into a more hydrophilic metabolite.[145]   The increased hydrophilicity of the metabolite compared to the parent compound makes it more water-soluble, and hence easier to excrete *via* the kidneys.   Thus, metabolism increases the rate of a drug's excretion from the body.[146]

Metabolism of pharmaceutical drugs consists of two stages of reactions; phase I metabolism and phase II metabolism. Phase I metabolism involves functionalisation reactions that either produce or uncover a functional group through oxidation, reduction or hydrolysis. Phase II metabolism involves the conjugation of an endogenous polar molecule, such as glucuronic acid, to a functional group either produced by phase I metabolism[147] or already present in the parent compound.[144] The phase II reactions are those that generally cause a significant increase in the hydrophilicity of the drug. This facilitates its excretion from the body, and also decreases its volume of distribution.[148] Thus, phase II metabolism is deemed to be the detoxifying process. The phase I reactions do not deactivate the drug, and in some cases can create a metabolite that itself has pharmacological activity. This behaviour can be used to positive effect in the case of prodrugs, which become pharmacologically active upon metabolism.[147]

The focus of the presented study was to identify structurally dependent dissociation pathways that could be used to characterise oxidised metabolites formed during phase I metabolism. The major enzymes involved in the oxidation of xenobiotics, including pharmaceutical drugs, are cytochrome P450s (CYP450s), which account for more than 90% of all oxidative reactions of this type.[149] CYP450s are a superfamily of haem-containing enzymes with many different forms, which are present in all eukaryotic organisms and some prokaryotes.[150] The different forms are divided into families based upon the similarity in their DNA sequences, with a 40% overlap indicating that two CYP450s are in the same family. Further subdivision within a family can be obtained if the sequence similarity reaches 55%. Each family has a number, and subfamilies are denoted by a letter in alphabetical order *e.g.* CYP3A, CYP3B. Individual family members, which must differ in DNA sequence by greater than 3% compared to the other family members, are denoted by a number after the subfamily letter *e.g.* CYP3A4.[151] A total of fifty-seven CYP450 genes belonging to different families have been identified in humans.[152] Although structurally different, all CYP450s are mono-oxygenases that metabolise xenobiotics *via* a

redox reaction.[153] The generalised reaction is shown below;[154]

$$\text{Drug} + \text{NADPH} + \text{O}_2 + \text{H}^+ \quad \rightarrow \quad \text{Drug-O} + \text{NADP}^+ + \text{H}_2\text{O}$$
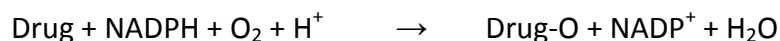
Briefly, the mechanism of the redox reaction initially involves binding of the drug molecule to the active site of the CYP450 (**Figure 2.1**, **step 1**). An electron is then transferred from reduced nicotinamide adenine dinucleotide phosphate (NADPH) to the haem portion of the CYP450, which is in the ferric (Fe^{3+}) state. This causes its reduction to a ferrous (Fe^{2+}) enzyme (**Figure 2.1**, **step 2**).[155] The reaction is mediated by a second enzyme; NADPH-CYP450 reductase.[156] The reduced haem then binds a molecule of oxygen (**Figure 2.1**, **step 3**). Addition of a second electron to the complex, donated by NADPH, in conjunction with a proton creates an iron-hydroperoxo intermediate *i.e.* Fe(II)-OOH (**Figure 2.1**, **steps 4 and 5**).[155] Cleavage of the oxygen-oxygen bond, with concomitant addition of a second proton, releases a molecule of water (**Figure 2.1**, **step 6**).[154] This leaves an electron-deficient FeO^{3+} complex, which abstracts either a hydrogen atom or an electron from the drug compound depending upon whether a carbon atom or heteroatom is being oxidised (**Figure 2.1**, **step 7**).[157] The radical drug molecule then reacts with the hydroxyl group or the radical oxygen atom in the complex. This results in the insertion of the oxygen atom into the molecular structure of the drug to form the metabolite (**Figure 2.1**, **step 8**).[154] The change in the drug's molecular structure and physicochemical properties are such that the complex separates to release the metabolite. This final step converts the CYP450 back to its original form and allows it to catalyse the biotransformation of another substrate molecule.[157]

The variation in structure between CYP450s leads to different active site shapes, which lends a degree of substrate specificity to different isozymes.[158] As a result, five forms of CYP450 are responsible for the oxidation of a vast majority of drug molecules; CYP1A2, CYP2C9, CYP2C19, CYP2D6 and CYP3A4.[159] In particular, CYP3A4 is very prominent in the metabolism of pharmaceutical compounds, catalysing the oxidation of greater than 50% of commonly used
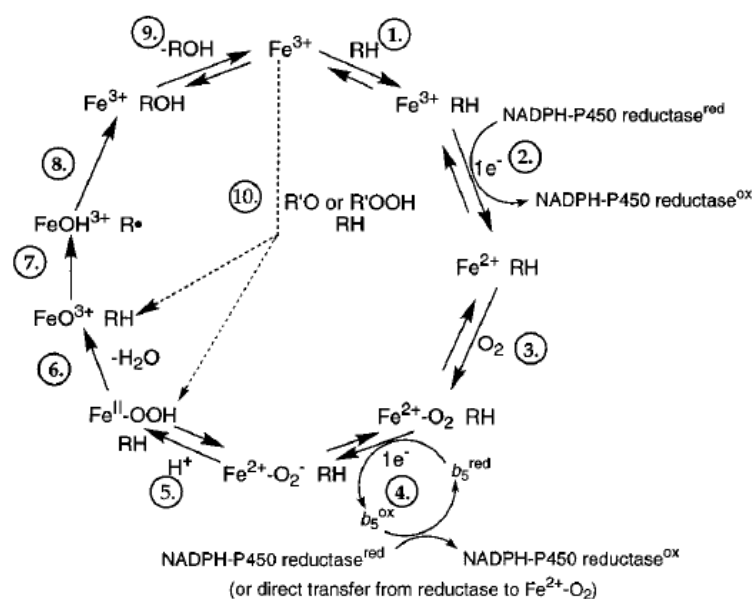
Figure 2.1 **Generalised catalytic cycle of the oxidation of xenobiotics by CYP450s**
Reproduced from reference 154 with kind permission from the American Chemical Society

clinical drugs.[160] These forms are predominately found in the liver, which is thus the primary site of pharmaceutical drug metabolism,[161] although CYP450s can be found throughout the human body.[151, 162] In the liver, CYP450s are situated on the membranes of mitochondria or endoplasmic reticula.[150]

Understanding the metabolism of a NCE is of key importance to the pharmaceutical industry. Metabolite identification studies are performed throughout the drug discovery and development process to detect, structurally characterise and quantify metabolites of pharmaceutical compounds.[163] In early drug discovery, these studies provide many pieces of information that indicate whether a given NCE is suitable to proceed further along the discovery stage and into development. The structural characterisation of the metabolites of a NCE can indicate those parts of the molecule that are prone to alteration by the metabolising enzymes. This information, in conjunction with quantitative data gained from clearance studies, can allow medicinal chemists to synthesise more or less stable analogues of the NCE. This can allow tailoring of the pharmacokinetics of the compound by altering its metabolic stability.[164] Another aim of metabolite identification studies is to identify those metabolites

that are not inactivated as a result of their structural change. This can lead to the formation of active metabolites *i.e.* those that have pharmacological activity. This activity can either be synergistic or inhibitory to the parent compound, which would affect the organism's response to a specific dosage. In contrast, the active metabolite may elicit a different pharmacological response than that intended by the drug as a result of acting on a different target.[147] Therefore, the identification of active metabolites can enable pharmacodynamic results to be rationalised.[165] Finally, metabolite identification studies need to determine whether any reactive metabolites are formed, which can result in drug-induced toxicity.[166] Identification of NCEs that form reactive metabolites in the early drug discovery stage allows a judicious selection of candidates to proceed to the more costly development stage.[167] The identification of active and reactive metabolites is of particular interest in the pharmaceutical industry at this current time due to the recent publication of the "Metabolites in Safety Testing" (MIST) guidelines by the Food and Drug Administration (FDA).[168] The MIST guidelines propose that additional safety assessments should be performed for compounds that produce metabolites that are only detectable in human plasma, or are present at much greater levels in man compared to the other species used to test the safety of the NCE.[169] Additional safety tests are required in this circumstance because the effect of the metabolite in man can not be extrapolated from the results in animals at these greater levels of production. Further, any metabolite that has a systemic exposure of greater than 10% of the parent compound at steady state should raise a safety concern.[169] If this metabolite is active and present at greater than 10% of the parent compound, then the body may be unable to tolerate the extra burden in pharmacological terms if both compounds have a similar effect. Therefore, additional safety assessments should be conducted before the drug is used in further clinical studies.

To obtain an understanding of how a compound is metabolised, a combination of *in vitro* and *in vivo* studies are utilised in drug discovery and development.[170] Oxidised metabolites, which are the focus of the presented study, are

investigated in the early drug discovery process using *in vitro* assays that allow phase I metabolites to be formed. The most commonly used *in vitro* test systems are liver microsomes and hepatocytes, with liver slices also being used on occasion.[171] Liver microsomes, either from human or animals, offer a simple system to assess phase I metabolism. Microsomes are artifactual vesicles formed through disruption of endoplasmic reticula, which retain the activity of the key enzymes involved in phase I metabolism, including CYP450s.[170, 172] A group of enzymes involved in phase II metabolism, the uridine diphosphate (UDP) glucuronyl transferases, are also microsomal. However, the cofactor required for glucuronidation, UDP-glucuronic acid (GA), is cystolic and thus is not present. Addition of the cofactor to the test system facilitates phase II metabolism *in vitro*. Other enzymes involved in phase II metabolism, for instance sulfotransferases, are not present in microsomes.[173] Thus, microsomes do not provide a complete representation of the metabolism of a NCE. Further, cofactors required for metabolism, such as NADPH are not present and their addition to the system is required to activate it.[173] These limitations are offset by the accessibility of microsomes, which are commercially available, and their retention of activity even after long-term freezing.[171, 174] This makes microsomes a suitable *in vitro* test system for the high-throughput analyses required by the pharmaceutical industry. Hepatocytes are whole-cell systems which offer the advantage of containing all of the metabolising enzymes and associated cofactors at physiologically relevant concentrations.[175] This means that both phase I and phase II metabolism can be investigated in a single test system. However, hepatocytes quickly lose their activity, meaning that fresh cultures are favoured to provide accurate and robust results. Thus, the availability of fresh hepatocytes are a restriction to their usage in metabolite identification studies.[176] Further, isolated hepatocytes can show different enzymatic activity to those in a biological environment, limiting the *in vitro-in vivo* correlation that can be deduced.[175] Liver slices represent the most complete *in vitro* model.[171] These systems closely replicate metabolism *in vivo* because all of the relevant enzymes and cofactors are present at physiological relevant concentrations and retain their activity.[170] However, liver slices are

more expensive and difficult to prepare than microsomes and hepatocytes, and are thus seldom used.

2.2 Analytical approaches for the identification of pharmaceutical drug metabolites

A range of analytical approaches are used in metabolite identification studies to detect, characterise and quantify the metabolites of a NCE during drug discovery and development. These include nuclear magnetic resonance (NMR) spectroscopy,[148] ultra-violet (UV) spectroscopy[176] and HPLC with radioactivity detectors.[177] The primary analytical approach utilised in early drug discovery metabolite identification studies is MS (see **Chapter 1**).[178] This is because only small amounts of NCEs are typically available for metabolite identification studies. Thus, the analytical techniques used must be capable of a low limit of detection to facilitate the analysis of all of the metabolites formed. MS is capable of very low limits of detection, and this characteristic, in addition to its high selectivity when the MS/MS experiment is utilised, means that it has become the technique of choice for early drug discovery metabolite identification studies. The ability of MS to rapidly provide structural information about the metabolites using MS/MS experiments also means that its use is favoured.[148] Finally, MS is easily interfaced to HPLC. A separation science is required because the matrices in which metabolites are present are complex mixtures containing biological molecules, such as proteins and lipids, salts and other endogenous compounds.[145] Reversed phase (RP)-HPLC is favoured in pharmaceutical analyses because most drugs and metabolites are amenable to ionisation by ESI, which necessitates delivery of the sample in the solution phase using a polar solvent.[178] RP-HPLC can separate the mixture of compounds such that they enter the mass spectrometer at different times. The separation of the metabolites from the matrix components is critical to the success of metabolite identification studies for two reasons. Firstly, metabolism of a NCE can result in the formation of isomeric metabolites *e.g.* two metabolites that have both been oxidised but at different locations.[145] If these

two species are ionised and enter the mass spectrometer at the same time *e.g.* introduction by direct infusion, the peak due to the protonated parent compound plus 16 *m/z* units would be a composite of the two species. Thus, the tandem mass spectrum would also be a composite, which could make the structural characterisation of the metabolites a more time-consuming and difficult task than if the species were separated in time. Secondly, and arguably more importantly, separation helps to alleviate the problems related to matrix effects. The term matrix effects refers to either enhancement or suppression of the mass spectrometric signal of an analyte of interest by a co-eluting compound that is present in the sample matrix.[179] Ion suppression is the most problematic matrix effect in the context of metabolite identification studies. This is because a metabolite present in the sample may not be ionised, hence meaning that it is not detected nor identified *i.e.* a false negative result would be obtained. King and co-workers conducted an in-depth comparative study to investigate whether solution or gas phase processes have a greater effect on the suppression of an analyte's ionisation.[180] This was achieved by comparing the suppression of the ionisation of caffeine, phenacetin and urapidil, as well as two proprietary compounds, using both ESI and APCI. They concluded that, although gas phase processes contribute to ion suppression, solution phase processes predominate. Their findings suggested that ESI is more sensitive to matrix effects than APCI, and thus greater ion suppression will be encountered using the former. This conclusion has been supported by the research of other groups.[181-184] However, reports of ion suppression in bioanalytical assays using APCI exist in the literature.[184-186] This indicates that approaches towards eliminating, or at least minimising, matrix effects must be taken regardless of the ionisation technique utilised when performing metabolite identification studies by API-MS/MS. Separation of the matrix components from the analytes of interest in time using RP-HPLC, along with the removal of interferences using sample preparation techniques, are the most commonly used methods of eliminating or reducing matrix effects.[187, 188]

The causes and mechanisms of ion suppression differ depending upon whether

ESI or APCI is being considered.[189] In ESI, interferences that increase the surface tension of the charged droplets prevent solvent evaporation.[190] This leads to fewer desolvated ions reaching the mass analyser, thus leading to a suppression of the signal compared to that obtained for a single component sample solely containing the analyte. Matrix components that typically suppress ions by this mechanism are endogenous phospholipids, which are thought to coat the surface of the charged droplet, preventing evaporation of the solvent and hence droplet fission. Phosphotidylcholines, which are zwitterions, are a major cause of ion suppression because of their ability to ionise using both positive ion and negative ion ESI.[191] Non-polar analytes, such as phospholipids, are more difficult to separate from analytes of interest using RP-HPLC, and thus are more likely to co-elute and cause ion suppression.[192] The presence of non-volatile compounds, such as salts, is proposed to have numerous ion suppressing effects.[180] Firstly, the non-volatile compound may increase the boiling point and surface tension of the charged droplet. This would slow the rate of solvent evaporation, potentially to the extent that the ions do not reach a radius of around 10 nm, which prevents field desorption as described by the IEM.[189] Further, the non-volatile compound will precipitate as the solvent evaporates from the charged droplet. The analyte may co-precipitate with the non-volatile compound, leading to a reduction in the number of molecules which form gas-phase ions.[180] A further posited mechanism of ion suppression in ESI is the competition between analytes for space at the surface of the charged droplet, as described by Enke's equilibrium partitioning model for singly charged ions.[193] Saturation of the surface with analyte is thought to occur at high concentrations of the order of greater than 10^{-5} molar (M), which is when the ESI response typically becomes non-linear.[194] The competition between analytes leads to preferential ionisation of those at the surface, which have greater likelihood of entering the gas phase.[15] The analytes that are more solvated and positioned in the bulk of the charged droplet are prevented from being desorbed. Thus, they fail to form gas-phase ions.[189] This form of ion suppression is proposed to affect polar analytes, which are more likely to be positioned in the bulk of the charged droplet.[195] A study by Cech and Enke demonstrated this by using a series of

peptides, as well as surface active analytes.[196] Their work showed that ESI response was related to the non-polar character of the peptide. Further, it demonstrated that the ESI response of surface active analytes is not affected by a high concentration of solvated species. Conversely, a suppression of the ESI response of solvated compounds was observed as the concentration of surface active analytes increased. The final mechanism postulated for ion suppression using ESI is neutralisation of the analytes caused by reactions with interfering compounds after desolvation *e.g.* deprotonation of positively charged ions.[190] This is a gas-phase mechanism as opposed to the solution-phase processes detailed above. This mechanism is proposed to occur when the interferences have high gas-phase basicities or acidities, to effect deprotonation or protonation respectively, and concentrations are sufficiently high to facilitate ion-molecule reactions.[189]

The mechanisms of ion suppression using APCI are different to those when ESI is employed because there is no competition between analytes and interferences to enter the gas phase, and much less competition to become charged. Entrance into the gas phase is not competitive because all of the thermally stable neutral species are transferred from the solution phase by the heated gas stream in the source.[189] The competition to become charged occurs at higher concentrations than in ESI because an excess of reagent ions is typically formed. Thus, more interfering compounds can be tolerated before ion suppression occurs.[197] Gas-phase reactions are a major source of ion suppression in APCI, as the ionisation technique is ideally suited to facilitating ion-molecule reactions. Therefore, as with ESI, suppression can occur *via* gas-phase reactions with interferences possessing high gas-phase basicities or acidities.[189] A related mechanism is the change in the efficiency of charge transfer from the corona discharge needle as a result of the matrix components.[185] Finally, because APCI is a gas-phase ionisation technique, the precipitation of non-volatile interfering compounds as the solution evaporates may cause co-precipitation of analyte molecules, leading to their loss and thus suppression of the ion signal.[180]

Once a metabolite has successfully formed a gas-phase ion and been sampled into the mass analyser, the typical protocol to identify and characterise it by MS is to first acquire a full scan spectrum *i.e.* no ion activation technique is utilised to induce dissociation. From the protonated molecule observed, the structural change can be deduced. For example, a mass shift of +16 *m/z* units for a metabolite compared to the parent compound would suggest that oxidation has taken place, whilst a mass shift of -14 *m/z* units would indicate that demethylation has occurred. The metabolite is then dissociated, routinely by low-energy CID, so as to facilitate its structural characterisation. The interpretation approach most commonly used to localise the site of metabolism is the "Shift technique".[198] This involves comparing the low-energy CID product ion spectra of the parent compound and the metabolite and looking for major product ions that are mass shifted. Based upon the assumption that the dissociation of the two ions are very similar as only a small modification has been made, the product ions of the metabolite that are mass shifted compared to the parent compound are those that have been structurally altered during metabolism (**Figure 2.2**). The schematic shows a parent drug compound that dissociates to form three product ions; A, B and C (**Figure 2.2a**). Upon oxidation of the portion of the molecule that forms product ion C, the metabolite dissociates to form product ions A and B at the same *m/z* values as for the parent compound (**Figure 2.2b**). However, as the result of the addition of an oxygen atom, the product ion due to the C part of the molecule is mass shifted by +16 *m/z* units compared to that observed for the parent compound (**Figure 2.2b**). The peak denoted in red represents that originally observed in the low-energy CID product ion spectrum for the parent compound, which is mass shifted to the *m/z* value equal to "C + O" in the low-energy CID product ion spectrum of the oxidised metabolite.

The limitation of the Shift technique is that unambiguous assignments are frequently not possible. This is particularly true for oxidised metabolites. For example, a product ion mass shifted by +16 *m/z* units in the low-energy CID product ion spectrum of the metabolite compared to the parent compound
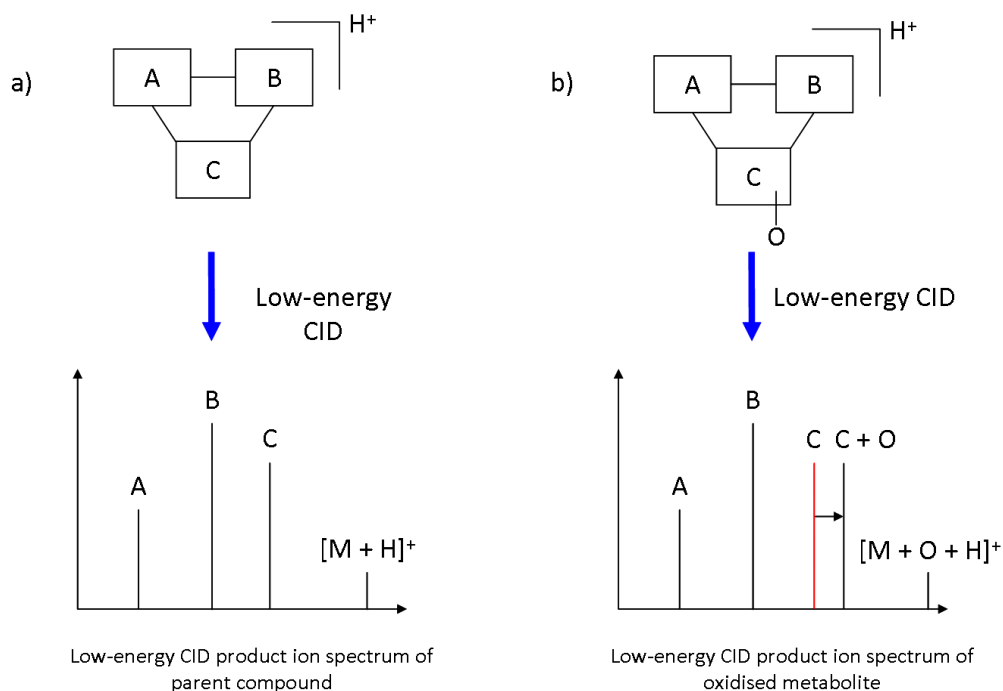
Figure 2.2 **Schematic of the Shift technique approach to the identification of the site of metabolism of a NCE using low-energy CID-MS/MS**

would lead to the deduction that oxidation has taken place on the portion of the molecule represented by that ion. However, oxidation can take place at carbon, nitrogen and sulfur atoms; all common constituents of small molecule NCEs. Thus, the product ion may contain more than one atom that can be oxidised, precluding the definitive identification of the site of oxidation. A recent example of this ambiguity was observed in the investigation of the *in vitro* metabolism of dasatinib in rat, monkey and human (**Figure 2.3**).[199] In this study, the authors were only able to localise oxidations to the *N*-(2-chloro-6-methylphenyl)formamide and the 2-(piperazin-1-yl)ethanol substructures. Many other such examples of ambiguity in the characterisation of oxidised metabolites formed both *in vitro* and *in vivo* exist in the literature.[175, 200-203]
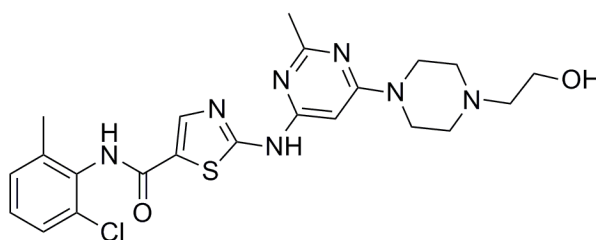
Figure 2.3 **Molecular structure of dasatinib**

Being able to specify the portion of a NCE that is metabolised is useful information to medicinal chemists in their endeavours to improve its metabolic stability. However, faster and more efficient production of metabolically stable analogues could be achieved if the specific atom that has been oxidised could be identified.

A number of approaches have been reported in the literature to discriminate between *C*-, *N*- and *S*-oxides, many of which can be achieved rapidly. Further, some of the methods also facilitate the definitive localisation of the site of oxidation. The approaches for the identification and characterisation of *C*-. *N*- and *S*-oxides will be considered in turn.

A number of wet chemistry approaches have been reported for identifying *C*-oxidised metabolites, one of the most commonly applied being the use of solution-phase hydrogen/deuterium (H/D) exchange experiments. These can be conducted either off-line[204] or on-line using HPLC.[205, 206] Further, gas-phase H/D exchange has also been demonstrated.[207, 208] Oxidation of a carbon atom creates a hydroxyl group, whilst oxidation at nitrogen and sulfur atoms forms N^+-O^- and S^+-O^- bonds respectively. Thus, only *C*-oxidation creates a functional group with an exchangeable hydrogen atom.[171] This can be exchanged for a deuterium atom in solution when the metabolite is dissolved in a solvent containing acidic deuterons *e.g.* deuterium oxide (D_2O). Therefore, if the oxidised metabolite has been hydroxylated, its recorded *m/z* value will mass shift according to the number of deuterium atoms incorporated into its structure *e.g.* 1 *m/z* units for a mono-oxidised metabolite, 2 *m/z* units for a di-oxidised metabolite *etc.*, plus an equal number of *m/z* units to the number of exchangeable hydrogen atoms in the parent compound's ion structure. The absence of any additional exchangeable hydrogen atoms in a *N*- or *S*-oxide compared to the parent compound means that both the parent compound and the metabolite will be mass shifted by the same number of *m/z* units. Thus, a *C*-oxide can be discriminated from an *N*- or *S*-oxide. The drawback of this method is that it can not always determine which carbon atom has been oxidised.

Instead, it can only provide information on the portion of the molecule that has been biotransformed. Further, the cost of deuterated solvents is high, meaning that routine application may be precluded. Derivatisation reagents can also be used to selectively react with hydroxyl groups to identify their presence. The use of derivatisation in metabolite identification studies has been reviewed by Liu and Hop.[209] Many derivatisation reagents will not only show selectivity for hydroxyl functionalities, thus discriminating between and *C*-oxides and *N*- and *S*-oxides, but will also demonstrate selectivity towards either aliphatic or aromatic hydroxyl groups. This can aid in determining the site of oxidation. For example, discrimination between aliphatic and aromatic hydroxyl groups can be achieved using acetic anhydride in water. This reagent will selectively acetylate aromatic hydroxyl groups whilst being unreactive towards aliphatic hydroxyl functionalities. The drawback of this approach is that partial or complete acetylation of amine groups can also occur.[171] This is particularly true under aqueous conditions, whereby the more nucleophilic amine groups are readily acetylated whilst the hydroxyl groups are prohibited from reacting due to the presence of water.[209] Therefore, more stringent control of reaction conditions is required for this method to be successful. Diazomethane and diazoethane can also be used to selectively react with aromatic hydroxyl groups. However, these reagents can also react with other functionalities, in this case carboxylic acids, which may complicate data interpretation.[209] The use of Jones reagent (chromium trioxide in concentrated sulfuric acid) can allow discrimination between primary and secondary alcohols, because the former produces a carboxylic acid upon oxidation whilst the latter forms a ketone.[210] A reported example is the discrimination of two hydroxylated metabolites of pioglitazone (**Figure 2.4**).[211]
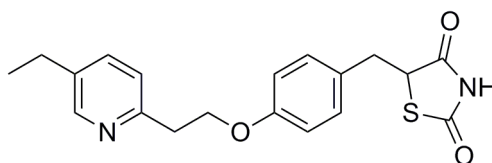
Figure 2.4   Molecular structure of pioglitazone

In this study, a previously unreported oxidised metabolite was identified. The MS/MS dissociation pattern was used to identify the oxidation product as a hydroxylated compound, due to the loss of water, and localise the site of oxidation to the 2-(5-ethyl-2-pyridyl)ethyl substructure. However, it was not possible to determine whether the hydroxylation site was a primary, secondary or aromatic carbon atom. A known oxidised metabolite of pioglitazone (**Figure 2.5**), which has a hydroxyl group on the α-carbon of the ethyl group, also has the same MS/MS dissociation pattern but a different retention time in the HPLC chromatogram.
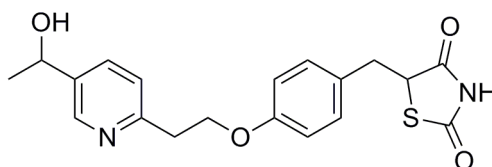
Figure 2.5   **Molecular structure of known hydroxylated pioglitazone metabolite**

Treatment of the crude sample with Jones reagent produced two different products. The known metabolite formed a keto-product as expected, and thus formed a compound that gave a signal 2 *m/z* units lower than the precursor. The unknown metabolite formed a product that was 16 *m/z* units greater in mass than the precursor. This indicated that a carboxylic acid-containing species had been formed. From this conclusion, it was deduced that the precursor must contain a primary alcohol and hence the metabolite was definitively structurally characterised as shown in **Figure 2.6**.
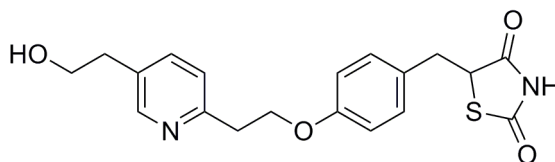
Figure 2.6   **Molecular structure of unknown hydroxylated pioglitazone metabolite deduced using derivatisation with Jones reagent and HPLC-MS/MS**

The limitations of all of these derivatisation methods are that extra analysis

time is required,[212] which also increases costs, and that losses of trace metabolites can occur during the reaction. In many cases, definitive localisation of the site of oxidation is also not possible. A faster approach to derivatisation that minimises the possibility of sample degradation is the use of ion-molecule reactions in the gas phase between a protonated analyte and neutral reagent gas; a process which can be automated. The use of dimethylethoxyborane (DEMB) facilitates a reaction with primary, secondary and tertiary hydroxyl groups, resulting in the formation of an adduct minus a molecule of methanol.[213] However, DEMB is not selective and will also react with aldehydes, esters, ethers and ketones in the same manner. This was overcome in the reported study by using gas-phase H/D exchange experiments after the derivatisation reaction. The hydroxyl derivatives contain a single exchangeable hydrogen atom; a structural feature that is not found in any of the other derivatives. Hence, hydroxyl-containing precursors could be distinguished.[213] The number of hydroxyl groups in a polyol can also be determined using ion-molecule reactions with either DEMB[214] or trimethylborate (TMB).[215] This can discriminate a *C*-oxide from *N*- and *S*-oxides because the former will have one greater number of hydroxyl groups than the parent compound, whilst the other two types of metabolite will have the same number. The study using DEMB was demonstrated to be compatible with HPLC, which is crucial in metabolite identification studies. However, the limitation of ion-molecule reactions, as with condensed-phase derivatisation, is that definitive identification of the carbon atom that has been oxidised is frequently not possible. Further, the cited studies were all performed on FT-ICR mass spectrometers, which are expensive and thus not readily available. Hence, implementation as a routine application is unlikely. An analytical approach that can allow the discrimination of aliphatic and aromatic hydroxylation is through the use of diagnostic dissociation behaviour. The loss of water under low-energy CID conditions has been suggested as being an indicator of aliphatic hydroxylation.[216] In a study of loratadine metabolism, the loss of water was favoured from the aliphatic hydroxylated metabolite compared to the aromatic hydroxylated desloratadine metabolite. This allowed discrimination between the two metabolites in this

study. However, a comprehensive study assessing whether aliphatic hydroxylation always leads to a more favourable loss of water than aromatic hydroxylation has yet to be conducted. Further, the robustness of this approach to discriminate between *C*-oxides and *N*- and *S*-oxides is questionable. This is because in the same study, the piperidine-*N*-oxide and pyridine-*N*-oxide metabolites of loratadine, neither of which contained hydroxyl groups, also showed losses of 18 *m/z* units, which corresponds to a molecule of water, in their low-energy CID product ion spectra.[216]

Both analytical and wet chemistry approaches have also been demonstrated to identify *N*-oxides. Ramanathan and co-workers showed that *N*-oxides undergo thermally-induced deoxygenation when using APCI; a trait not reported for *C*- and *S*-oxides.[216] Subsequent work observed similar behaviour using an ESI ion source with a heated transport capillary and proved that the loss of oxygen was not due to in-source CID.[217] The abundance of the loss of oxygen was also shown to be independent of the length of the heated capillary/ion transfer tube, indicating that the kinetics of the reaction are fast.[218] The same loss has also been observed using APPI.[219] Another analytical approach utilises the chromatographic behaviour of *N*-oxides using RP-HPLC. Under these conditions, *N*-oxidised metabolites have been observed to elute after the parent compound, despite being of greater polarity.[165, 199, 220-222] However, this is not generic behaviour, and examples of *N*-oxidised metabolites that elute prior to the parent compound are also reported in the literature.[216, 223] Wet chemistry approaches are also evident in the literature for the identification of *N*-oxides. Selective reduction of *N*-oxides back to their amine parent compounds has been achieved by adding titanium chloride (TiCl$_3$) directly to plasma and urine matrices.[224] The identification of an *N*-oxide was demonstrated for a proprietary compound where the low-energy CID product ion spectrum was ambiguous and suggested the formation of either a *C*- or *N*-oxide. Further, TiCl$_3$ was able to quantitatively reduce the *N*-oxide group in a di-oxidised metabolite containing both an oxidised piperidine nitrogen and an oxidised thioether sulfur, thus demonstrating the selectivity of the reagent. The drawback of the

method is the long reaction time (60-90 minutes), thus limiting its usage in a high-throughput environment. The Kenttämaa group has published a number of papers detailing functional group selective ion-molecule reactions between protonated analytes and neutral reagent gases. Reagents have been identified that can characterise monofunctional primary amine-*N*-oxides,[225] aromatic tertiary amine-*N*-oxides[226, 227] and aliphatic tertiary amine-*N*-oxide.[227] The adduct-forming reactions with dimethyl disulfide,[225] 2-methoxypropene,[226] tri(dimethylamino)borane[227] have potential application in metabolite identification studies because the reagents selectively react with *N*-oxides but not amine functionalities. However, as with the ion-molecule reactions used to identify hydroxyl-containing compounds, all of the studies were performed on instruments with limited availability; either FT-ICR or modified QqQ mass spectrometers. Thus, the experiments may not be possible in all laboratories. Further, the reactions occur on an extended time-scale; generally in the region of seconds. Therefore, the duty cycle of the experiment *i.e.* the time taken for the gas-phase ion-molecule reaction to take place and the products to be detected by the mass spectrometer, may not be compatible with the time-scale of the chromatographic separations used in metabolite identification studies. Indeed, none of the cited studies used HPLC as a method to introduce the samples into the mass spectrometer. Reaction times of the order of 500 ms have been suggested as being suitable for HPLC-MS applications.[228] A limitation common to all of the discussed approaches for *N*-oxide identification is that they give no indication of the site of oxidation, except for the ion-molecule reaction between protonated primary *N*-oxides and dimethyl disulfide.[225] Two examples of definitive localisation of the site of oxidation for *N*-oxides involve structurally dependent dissociation pathways. Ma and co-workers elucidated a thermally induced structurally dependent dissociation pathway that definitively identified the oxidised nitrogen atom in a series of model *N*-oxide metabolites.[219] They showed that a Meisenheimer rearrangement preceded the loss of an aldehyde or a ketone, which took place at a tertiary amine-*N*-oxide containing an alkyl or benzyl group. This structural specificity allowed the nitrogen atoms in the analysed compounds (both pharmaceuticals and other

small molecules) to be discriminated. The rearrangement and thermally induced dissociation was shown to be specific for the tertiary amines analysed because the analogous loss was not observed for the aromatic *N*-oxide metabolite of 2-(methylsulfonylmethyl)-pyridine-*N*-oxide. Lay and co-workers utilised high-energy FAB-MS and FAB-CID-MS/MS to show that the losses of dimethylamine and *N,N*-dimethylhydroxylamine were observed for a series of ethylenediamine, ethanolamine and propylamine antihistamine drugs and their tertiary amine-*N*-oxides respectively.[229] These diagnostic losses provided an approach to localise the site of oxidation to the tertiary amine substructure. However, equivalent data under low-energy CID conditions has never been reported.

Of the three types of oxidised metabolite, *S*-oxides have the fewest reported rapid and definitive identification approaches in the literature. No examples of derivatisation reagents that are selective towards *S*-oxide functionalities are evident in the literature.[148, 209] Further, no details of ion-molecule reactions that facilitate their identification could be sourced. Thus, the only reported method for rapid and definitive identification of sulfoxides is based on their diagnostic dissociation behaviour.[230] This study showed that the group bonded to the sulfoxide functionality is lost as a radical using low-energy CID-MS/MS. The corresponding radical loss was not observed for the parent compound. Thus, a radical loss in the low-energy CID product ion spectrum of an oxidised metabolite could be indicative of an *S*-oxide. Further, the site of oxidation could be inferred by characterising the radical loss, as the leaving group was originally bonded to the sulfoxide functionality.

In summary, the existing approaches for identifying and discriminating between oxidised metabolites often do not provide definitive localisation of the site of oxidation. Further, those that can are often not applicable to routine application. The inability to localise the specific site of oxidation on a pharmaceutical compound is problematic if there are two or more potential oxidation sites for which a given approach is diagnostic *e.g.* two nitrogen atoms

that could be oxidised and then identified following reduction using TiCl$_3$. In this circumstance, the analyst must rigorously interrogate the low-energy CID product ion spectrum of the metabolite to assign the site of oxidation. However, this approach may still result in an ambiguous assignment, as demonstrated in the case of dasantinib.[199] The work of Wright and co-workers, in conjunction with that performed by the groups of Ma and Lay, suggest that the elucidation of structurally dependent dissociation pathways could provide a means to definitively localise the site of oxidation in oxidised metabolites. This is supported by the work of the Desaire and Langley groups, who have shown diagnostic losses for the identification and localisation of other functional groups in small molecules using low-energy CID-MS/MS. The Desaire group have demonstrated that the loss of carbon dioxide (44 *m/z* units) in a negative ion low-energy CID-MS/MS product ion spectrum is indicative of a carboxylic acid.[231] The observation of the loss also provides structural information about the chemical environment in which the carboxylic acid functionality is positioned, with certain substructures precluding the loss of carbon dioxide *e.g.* dicarboxylic acids where the acid groups are separated by three carbon atoms do not lose carbon dioxide under low-energy CID conditions. A further paper showed that carboxylic acid-containing metabolites formed through hydrolysis of lactones can be differentiated from their parent compounds through diagnostic neutral losses from both the parent molecule and the metabolite.[232] Finally, the localisation of the site of sulfation in phase II metabolism was achieved, with diagnostic product ions and losses used to classify the sulfation site as one of four possibilities.[233] This enabled prediction of the metabolite's biological effect, which is important as conjugation of the sulfate group to benzylic alcohol, allylic alcohol or aromatic hydroxylamine functionalities gives rise to carcinogenic species. The Langley group have also conducted work into the elucidation of structural motifs that drive dissociation pathways.[234, 235] Their studies showed that class-specific product ions and losses could be identified for a number of groups of small molecules. Further, they demonstrated that the different classes of compounds would cluster using principal component analysis (PCA) based upon the ions observed in their low-energy CID product ion

spectra. This therefore indicated that the structure of the molecule drives its dissociation under low-energy CID conditions. The information in the literature therefore suggested that there was scope to elucidate structurally dependent dissociation pathways using low-energy CID-MS/MS that would allow discrimination and characterisation of oxidised pharmaceutical drug metabolites. It was envisaged that such information could have immediate benefit to the metabolite identification community by enabling faster interpretation of data; a recognised bottleneck in metabolite identification studies.[178] This is because an analyst would, as a first approach, be able to just look for key diagnostic information in a low-energy CID product ion spectrum of an unknown metabolite, rather than rigorously interrogating the data. Thus, faster throughput would be possible using such a protocol, and hence the presented study was conducted.

Chapter 3

Experimental

3.1   Introduction

The experimental conditions detailed below are the generic protocols used for a majority of the work in the presented study.   Deviations from the generic protocol, or specific experiments not conducted throughout the study, are detailed in the relevant chapters.

3.2   Chemicals

Solutions were prepared in LC-MS grade methanol and analytical grade methanoic acid [99.9:0.1, volume by volume (v/v)] (Fisher Scientific UK Ltd., Loughborough, UK) for QIT-MS and FT-ICR-MS experiments. The concentrations were 10 micrograms per millilitre (μg mL^{-1}) for the QIT-MS experiments and 1 μg mL^{-1} for the FT-ICR-MS experiments.   QqTOF-MS experiments were performed using solutions prepared at 1 μg mL^{-1} in LC-MS Chromasolv® acetonitrile [1:1, v/v] (Sigma-Aldrich Company Ltd., Gillingham, UK) and HPLC grade water (Millipore, Bedford, MA, USA).   Solution-phase H/D exchange experiments were performed by preparing the compound in >99.5% deuterated methanol with either 99.5% methanoic acid [99.9:0.1, v/v] or 99.5% ethanoic acid [99:1, v/v] (Apollo Scientific Ltd., Stockport, UK). The concentration of the solutions for the solution-phase H/D exchange experiments were 10 μg mL^{-1}. Reserpine (Sigma-Aldrich Company Ltd., Gillingham, UK) was prepared at 100 nanogram per millilitre (ng mL^{-1}) in LC-MS grade methanol and analytical grade methanoic acid [99.9:0.1, v/v] for calibration of the FT-ICR mass spectrometer. All chemicals were used without further purification.

3.3   Instrumental

"In-time" low-energy CID product ion spectra were acquired using a LCQ Classic QIT mass spectrometer (Thermo Fisher Scientific, San Jose, CA, USA). Positive ion ESI-MS/MS was performed by infusing the solutions directly into the ion source at a constant flow rate of 3 microlitres per minute (μL min^{-1}). Nitrogen was used as the sheath and auxiliary gas. The ion source conditions varied between experiments and will be detailed in the individual chapters. Low-energy CID product ion spectra were acquired using an isolation width of 6 *m/z* units (1 *m/z* unit for solution-phase H/D exchange experiments), an activation Q of 0.250 and an activation time of 30 ms. Acquisitions were performed for twenty scans. Helium was used as the buffer gas. The value of the normalised collision energy and the WideBand activation setting were varied between experiments and will be detailed in the individual chapters. Data acquisition was performed using XCalibur version 1.2 (Thermo Fisher Scientific, San Jose, CA, USA).

"In-space" low-energy CID product ion spectra were acquired using a Premier QqTOF mass spectrometer (Waters Ltd., Elstree, UK) coupled to an Acquity ultra performance liquid chromatography (UPLC) instrument (Waters Ltd., Elstree, UK). Separation was achieved using a Sunfire C_{18} column, 50 millimetre (mm) x 2.1 mm internal diameter (i.d.), 3.5 μm particle size (Waters Ltd., Elstree, UK). The column oven temperature was set to 40°C. The mobile phases were; (A) HPLC grade water and LC-MS Chromasolv® acetonitrile [95:5, v/v] containing 0.1% analytical grade methanoic acid and (B) LC-MS Chromasolv® acetonitrile containing 0.1% analytical grade methanoic acid. The gradient conditions are shown in **Table 3.1**. The eluent flow rate was 200 μL min^{-1} and the injection volume was 5 μL.

Table 3.1   Gradient conditions for the UPLC-QqTOF-MS/MS analyses

Time / min	% A	% B
0	95	5
1	95	5
8	2	98
9	2	98
9.1	95	5
13	95	5

Positive ion ESI-MS/MS was performed using the following ion source conditions; cone gas flow, 40 litres per hour (L hr^{-1}); desolvation gas flow, 650 L hr^{-1}; capillary voltage, 3.2 kV; sampling cone, 25 V; extraction cone, 4 V; ion guide, 2.5 V; source temperature, 120 degrees Celsius (^{o}C); desolvation temperature, 350°C. Nitrogen was used as the cone and desolvation gas. Low-energy CID product ion spectra were acquired at collision energies of 15, 20 and 25 electron volts (eV) using argon as the collision gas. The mass spectrometer was operated in the "V" mode. The scan time was 0.2 s and the interscan time was 0.05 s. Data acquisition was performed using MassLynx version 4.1 (Waters Ltd., Elstree, Herts., UK).

AMM "in-time" low-energy SORI-CID product ion spectra were acquired using an Apex III FT-ICR mass spectrometer (Bruker, Billerica, MA, USA) equipped with a 4.7 Tesla actively shielded superconducting magnet, an Infinity cylindrical analyser cell and an Apollo ESI ion source. Positive ion ESI-MS/MS was performed by infusing the solutions directly into the ion source at a constant flow rate of 3 μL min^{-1}. Nitrogen was used as the drying gas. The ion source conditions and excitation amplitude varied between experiments and will be detailed in the individual chapters. Positive ions were accumulated in the hexapole ion guide for 0.2 s prior to transfer into the ICR cell. The conditions for the acquisition of "in-time" low-energy SORI-CID product ion spectra varied between experiments and will be detailed in the individual chapters. However, argon was always used as the collision gas. The instrument was calibrated using the first-generation low-energy SORI-CID product ion spectrum of reserpine.

Data acquisition was performed using XMass version 7.0.8 (Bruker, Billerica, MA, USA).

Chapter 4

Evidence for an *ortho*-effect on the fragmentation of 4-benzenesulfinyl-3-methylphenylamine

4.1   Introduction

Herein, an *ortho*-effect on the fragmentation of a model *S*-oxide leading to a 50 *m/z* unit loss is described.   *Ortho*-effects are common observations in EI-MS and have been extensively investigated.[236-239]   They are less frequent under low-energy CID conditions, although reports do exist for protonated,[240, 241] deprotonated[242-244] and adduct molecules.[241, 245]   Further, Mendes and co-workers demonstrated an *ortho*-effect in both the EI and low-energy CID mass spectra of *ortho*-*N*-chlorophenyl- and *ortho*-*N*-bromophenyl-2-aminobenzamidine.[246]   The 50 *m/z* unit loss discussed below is of interest as a potential tool for metabolite identification because oxidation at a sulfur atom is a common phase I biotransformation, both *in vitro* and *in vivo*.[247]   The dissociation behaviour discussed could possibly be of use during drug discovery for definitively identifying the sulfur atom in a pharmaceutical compound that has undergone *S*-oxidation.

4.2   Experimental

4.2.1 Chemicals

4-Benzenesulfinyl-3-methylphenylamine (**Compound 4.1**), 4-benzenesulfinylphenylamine (**Compound 4.2**), 3-methyl-4-phenylsulfanylphenylamine (**Compound 4.4**), (4-methanesulfinyl-3-methylphenoxy)acetic acid (**Compound 4.5**) and 3-dimethylaminomethyl-4-(4-methanesulfinyl-3-methylphenoxy)benzenesulfonamide (**Compound 4.6**) were provided by Pfizer Global Research and Development (Sandwich, UK).   2-Aminofluorene (**Compound 4.3**) was purchased from Alfa Aesar (Heysham, UK).

Solutions of **Compounds 4.1-4.6** were prepared for QIT-MS experiments as detailed in **Chapter 3**. Further solutions of **Compound 4.1** were prepared for FT-ICR-MS, QqTOF-MS and solution-phase H/D exchange experiments as detailed in **Chapter 3** and at 20 µg mL^{-1} in LC-MS grade methanol and analytical grade methanoic acid [99.9:0.1, v/v] for the MS^4 experiment using QIT-MS.

4.2.2 Instrumental

QIT-MS experiments were performed as detailed in **Chapter 3** to acquire "in-time" low-energy CID product ion spectra. The ion source conditions were; sheath gas, 30 arbitrary units; auxiliary gas, 5 arbitrary units (45 arbitrary units for the solution-phase H/D exchange experiment); spray voltage, 4 kV; capillary voltage, 17 V; capillary temperature, 140°C; tube lens offset, 10 V. The experiments performed, the setting of the WideBand activation parameter and the normalised collision energy value are shown in **Table 4.1**.

Table 4.1   **Experiment performed, WideBand activation parameter setting and normalised collision energy value for the QIT-MS analyses of Compounds 4.1-4.6**

Compound	Experiment	WideBand activation on/off	Normalised collision energy / %
4.1	MS/MS	On	50
4.1	MS/MS	Off	30
4.1	MS^3	Off	35, 35
4.1	MS^4	Off	40, 40, 30
4.2	MS/MS	On	55
4.3	MS/MS	Off	35
4.4	MS/MS	On	60
4.5	MS/MS	On	50
4.6	MS/MS	On	50

QqTOF-MS experiments were performed as detailed in **Chapter 3** to acquire "in-space" low-energy CID product ion spectra of **Compound 4.1**.

FT-ICR-MS experiments were performed as detailed in **Chapter 3** to acquire an AMM "in-time" low-energy SORI-CID product ion spectrum of **Compound 4.1**.

The ion source conditions were; capillary voltage, -4.5 kV; end plate voltage, -3.8 kV; capillary exit voltage, 100 V; skimmer 1, 11 V; skimmer 2, 6 V; offset, 1.25; RF amplitude, 600 Hertz (Hz); dry gas temperature, 250°C; dry gas flow rate, 30 arbitrary units; nebulising gas pressure, 50 pounds-per-square-inch (psi). The excitation amplitude was 3.7 decibels (dB). A low-energy SORI-CID product ion spectrum was acquired for eight scans using 512K data points. The MS/MS parameters were; corr sweep pulse length, 1000 µs; corr sweep attenuation, 28.5 dB; ejection safety belt, 3000 Hz; user pulse length, 1000 µs; ion activation pulse length, 250000 µs; ion activation attenuation, 38.9 dB; frequency offset from activation mass, - 500 Hz; user delay length, 3 s.

4.2.3 Molecular modelling

The gas-phase proton affinity of **Compound 4.1** was calculated using Spartan '02 (Wavefunction, Inc, CA, USA). The gas-phase proton affinity is defined as the negative of the enthalpy change at 298 Kelvin (K) for the protonation reaction (**Equation 4.1**):[1]

Equation 4.1

Four different conformers of the molecule were modelled. For each of these models, one conformer protonated at the amine nitrogen and four conformers protonated at the sulfoxide oxygen were modelled through the addition of a proton at the relevant site. Four different conformers of the protonated sulfoxide oxygen were modelled from each neutral species to account for different spatial orientations that the proton can assume in the gas phase when protonation occurs at this functional group.

The structures were minimised and the energies calculated at the density functional theory (DFT) level (B3LYP) using the 6-31G** basis set. The equilibrium geometry was calculated at the ground state starting from AM1 geometry. The total charge was set to cation for the protonated species and

neutral for the molecule. The calculated energies were converted from atomic units to kilocalories per mole (kcal mol^{-1}) using the conversion factor of 627.5.[248] The enthalpy change was calculated by subtracting the energy of the molecule from the energy of each protonated species. The obtained values corresponded to the ΔH value and were converted to proton affinities by multiplying by -1 (see **Equation 4.1**).

4.3   Results and discussion

The fragmentation of protonated 4-benzenesulfinyl-3-methylphenylamine (**Compound 4.1**) (**Figure 4.1a**) was investigated. A 50 *m/z* unit loss was observed in the first-generation low-energy CID product ion spectrum acquired with WideBand activation on (**Figure 4.2**).[110] It was proposed that this loss is the result of an *ortho*-effect due to the presence of the methyl group on the phenylamine ring. This hypothesis was suggested because the des-methyl homologue, protonated 4-benzenesulfinylphenylamine (**Compound 4.2**) (**Figure 4.1b**), did not display a 50 *m/z* unit loss in the first-generation low-energy CID product ion spectrum acquired with WideBand activation on. Instead, a 48 *m/z* unit loss was observed, which corresponded to the loss of sulfur monoxide (**Figure 4.3**). Thus, the 50 *m/z* unit loss from protonated **Compound 4.1** was proposed to be a loss with the elemental formula H_2SO. Further experiments were conducted to confirm this loss and investigate the fragmentation.
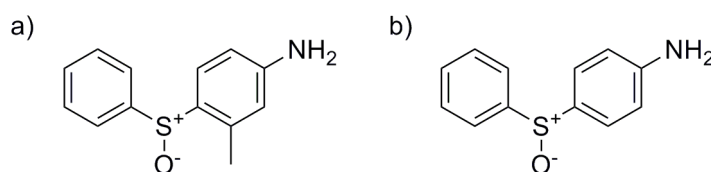
Figure 4.1   Molecular structures of a) 4-benzenesulfinyl-3-methylphenylamine (Compound 4.1) and b) 4-benzenesulfinylphenylamine (Compound 4.2)

It was noted that the 50 *m/z* unit loss from protonated **Compound 4.1** was only observed when the low-energy CID product ion spectrum was acquired with WideBand activation on. With the parameter switched off, no signal was
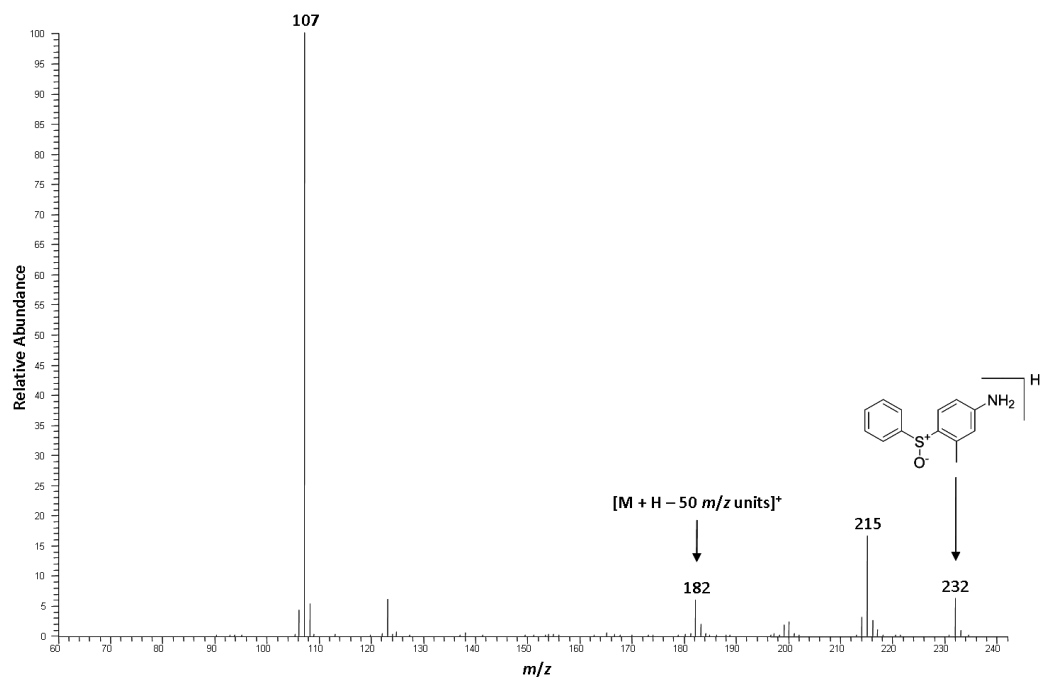
Figure 4.2   **First-generation low-energy CID product ion spectrum of protonated Compound 4.1 (*m/z* 232) acquired using a LCQ Classic QIT mass spectrometer with WideBand activation on**

observed at *m/z* 182 (**Figure 4.4**). This is consistent with the suggestion that the product ion is not formed directly from protonated **Compound 4.1**. It appeared that the 20 *m/z* unit activation window created with WideBand activation on was required to form the product ion. Thus, it was hypothesised that the product ion at *m/z* 182 is formed through a two-step fragmentation process *via* the other major ion in the activation window, namely *m/z* 215. To test this hypothesis, an MS^3 experiment was performed with WideBand activation off using the ion at *m/z* 215 as the precursor ion for the second stage of mass analysis.   The second-generation low-energy CID product ion spectrum of protonated **Compound 4.1** displays an ion at *m/z* 182 (**Figure 4.5**). This proves that the product ion at *m/z* 182 is formed by fragmentation of the ion at *m/z* 215 and not directly through dissociation of the protonated molecule. Thus, the loss of 50 *m/z* units from protonated **Compound 4.1** occurs in a two-step process through sequential losses of 17 and 33 *m/z* units. As a loss with the elemental formula H_2SO had been proposed previously, the identities of the sequential losses were thought to be a hydroxyl radical and a thiol radical. However, this could not be determined by means of the preservation or
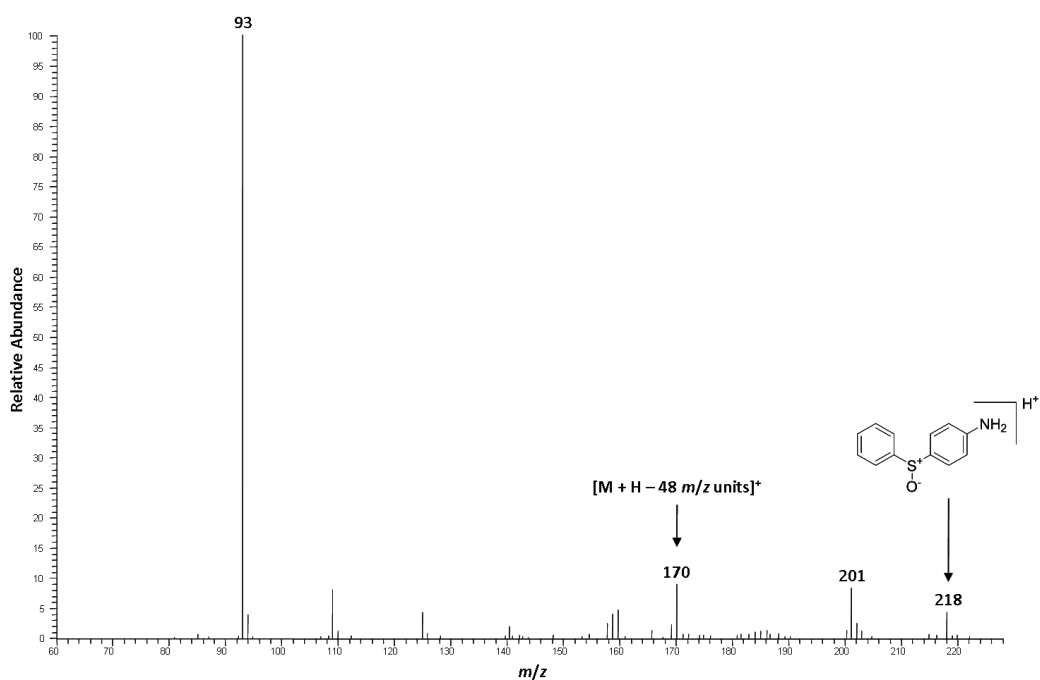
Figure 4.3 First-generation low-energy CID product ion spectrum of protonated Compound 4.2 (*m/z* 218) acquired using a LCQ Classic QIT mass spectrometer with WideBand activation on

Figure 4.4 First-generation low-energy CID product ion spectrum of protonated Compound 4.1 (*m/z* 232) acquired using a LCQ Classic QIT mass spectrometer with WideBand activation off

Figure 4.5   **Second-generation low-energy CID product ion spectrum of protonated Compound 4.1 (*m/z* 232) using the ion at *m/z* 215 as the precursor ion for the second stage of mass analysis acquired using a LCQ Classic QIT mass spectrometer with WideBand activation off**

disappearance of the ^{34}S isotope pattern for the peaks of interest due to the difficulties associated with observing the true isotope pattern using a QIT mass spectrometer. An alternative identity for the loss of 17 *m/z* units could have been ammonia, particularly if **Compound 4.1** protonated at the amine nitrogen. Further experiments were utilised to investigate the identity of the losses.

Molecular modelling calculations were utilised to support the proposed loss of a hydroxyl radical during the first stage of mass analysis. The gas-phase proton affinities for the two most likely sites of protonation on **Compound 4.1**, the sulfoxide oxygen and the amine nitrogen, were calculated. A number of conformers of **Compound 4.1** were modelled to represent some of the spatial orientations that the molecule can assume in the gas phase. Using the neutral species, the protonated molecules were modelled by adding a proton at the relevant site. Four different conformers protonated at the sulfoxide oxygen were modelled for each neutral species. This is because rotation of the S-O bond alters the spatial orientation of the proton, which could affect the overall

energy of the ion. Only a single protonated amine nitrogen species was modelled for each neutral conformer due to rotation of the C-N bond having no effect on the overall structure of the ion. A number of conformers were investigated for the molecules, and the corresponding protonated species, to verify that the same site of protonation was favoured regardless of the spatial orientation. However, it must be noted that this approach does not define the absolute site of protonation; the conformers investigated were not exhaustive of all of those that can exist in the gas phase. The energies of the protonated species were compared to the relevant neutral conformer to determine the most likely site of protonation. The lower the energy of the protonated species then the more likely it is to occur in the gas phase due to the ion being more energetically stable. The calculations showed that the protonated sulfoxide oxygen species were lower in energy by between 21.9 and 24.7 kcal mol^{-1} compared to the protonated amine nitrogen species across the investigated conformers. These values are comparable to those used to assign the sulfoxide oxygen as the site of protonation in a previous study.[230] Hence, it can be concluded that the most energetically favourable site of protonation for **Compound 4.1** is the sulfoxide oxygen. This finding suggested that the 17 *m/z* unit loss from protonated **Compound 4.1** was more likely to be a hydroxyl radical than the alternative, a molecule of ammonia. This is because protonation at the sulfoxide oxygen facilitates the loss of a hydroxyl radical. To support the molecular modelling calculations and determine the number of exchangeable hydrogen atoms in the overall 50 *m/z* unit loss, solution-phase H/D exchange experiments were performed. The 18 *m/z* unit loss indicated that a deuterohydroxyl radical was lost from the fully exchanged, deuterated molecule, [M + D]$^{+}$ (**Figure 4.6**). This definitively proved that **Compound 4.1** protonates at the sulfoxide oxygen. The experiment also showed that one exchangeable hydrogen atom was involved in the overall 50 *m/z* unit loss due to the mass difference between the precursor ion and the product ion of interest being 51 *m/z* units under deuterated conditions. Isomerisation prior to dissociation *i.e.* scrambling of the deuterium label, prior to dissociation can be excluded because the relative abundance of the ion at *m/z* 185 is insufficient to

Figure 4.6 **First-generation low-energy CID product ion spectrum of fully exchanged, deuterated Compound 4.1 (*m/z* 235) acquired using a LCQ Classic QIT mass spectrometer with Wideband activation on**

suggest that a combination of 50 and 51 *m/z* unit losses have occurred concurrently.

The single exchangeable hydrogen atom is accounted for in the first stage of fragmentation through the loss of the hydroxyl radical. Thus, the 33 *m/z* unit loss during the second stage of fragmentation is likely to be accounted for by a thiol radical involving a non-exchangeable hydrogen atom. As an *ortho*-effect had been postulated, the source of this non-exchangeable hydrogen atom was proposed to be the methyl group bonded to the phenylamine ring. To confirm the elemental formulae of the losses, AMMs were performed using a FT-ICR mass spectrometer. The elemental formulae with the lowest mass measurement error (MME) values were consistent with the loss of a hydroxyl radical and a thiol radical (**Figure 4.7**). The rings plus double bond equivalents values were 8 for the product ion at *m/z* 215.0762 and 8.5 for the product ion at *m/z* 182.0965. These values indicate that the structures were odd- and even-electron ions respectively,[249] supporting the hypothesis of sequential radical
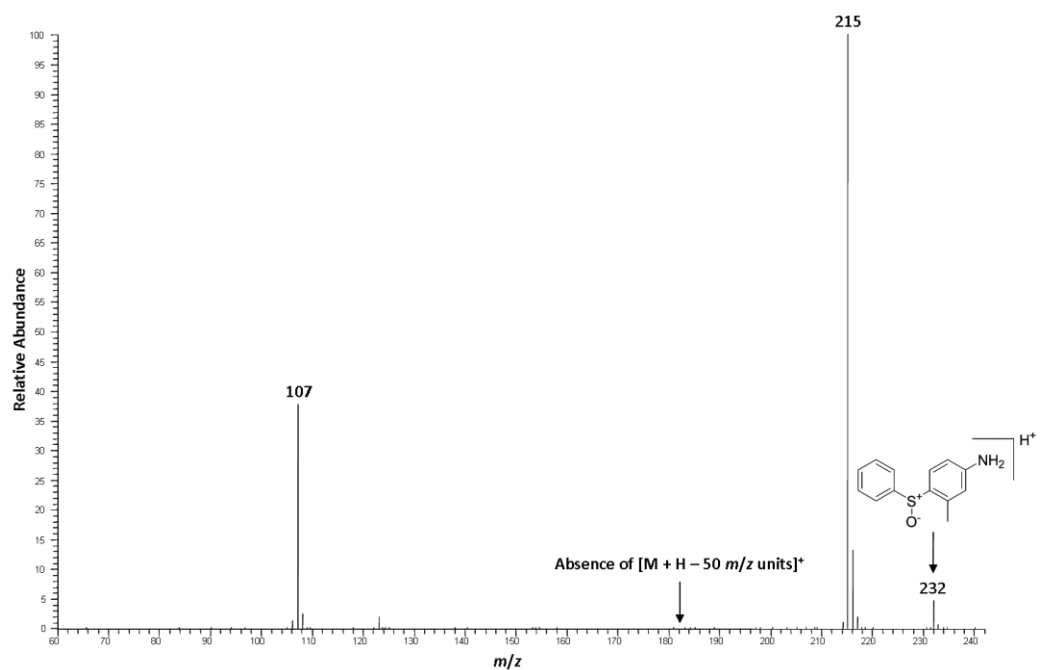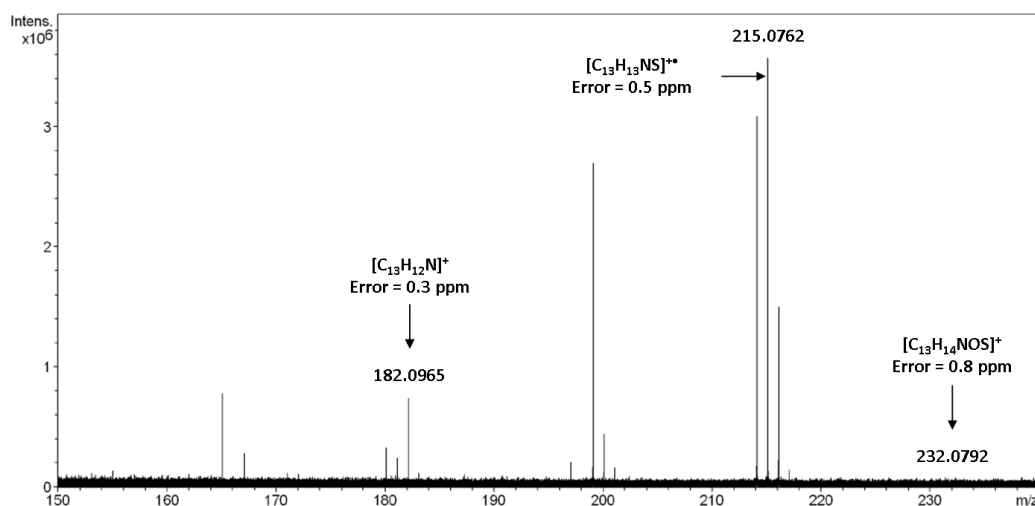
Figure 4.7 **First-generation low-energy SORI-CID product ion spectrum of protonated Compound 4.1 (*m/z* 232) acquired using an Apex III FT-ICR mass spectrometer**

losses. Because of the deficiency of the even-electron ion value by 0.5 due to the addition of a proton to the molecule,[250] it was deduced that the number of rings and double bond equivalents in the product ion was 9. This is consistent with a protonated aminofluorene, which was proposed as the structure of the product ion at *m/z* 182 (**Figure 4.8**). To verify this conclusion, a commercially available sample of 2-aminofluorene (**Compound 4.3**) was used to acquire the first-generation low-energy CID product ion spectrum of the protonated molecule, *m/z* 182 (**Figure 4.9**). The spectrum was compared to the third-generation low-energy CID product ion spectrum of protonated **Compound 4.1** *i.e.* acquired using *m/z* 182 as the precursor ion (**Figure 4.10**). Both spectra displayed a loss of 17 *m/z* units. For protonated **Compound 4.3**, this correlated to the loss of a molecule of ammonia. It is expected that, regardless of the position of the amine group on the fluorene substructure, the dissociations of the different protonated aminofluorenes will be the same *i.e.* loss of a single molecule of ammonia. It has been shown previously that the hydroxyl group is lost during the first stage of mass analysis for protonated **Compound 4.1**. Therefore, it was concluded that the further loss of 17 *m/z* units was the loss of a molecule of ammonia. Hence, the results are consistent with a protonated aminofluorene being the structure of the product ion at *m/z* 182.

Figure 4.8 Proposed structure of the product ion at *m/z* 182, a protonated aminofluorene

Figure 4.9 First-generation low-energy CID product ion spectrum of protonated Compound 4.3 (*m/z* 182) acquired using a LCQ Classic QIT mass spectrometer with WideBand activation off
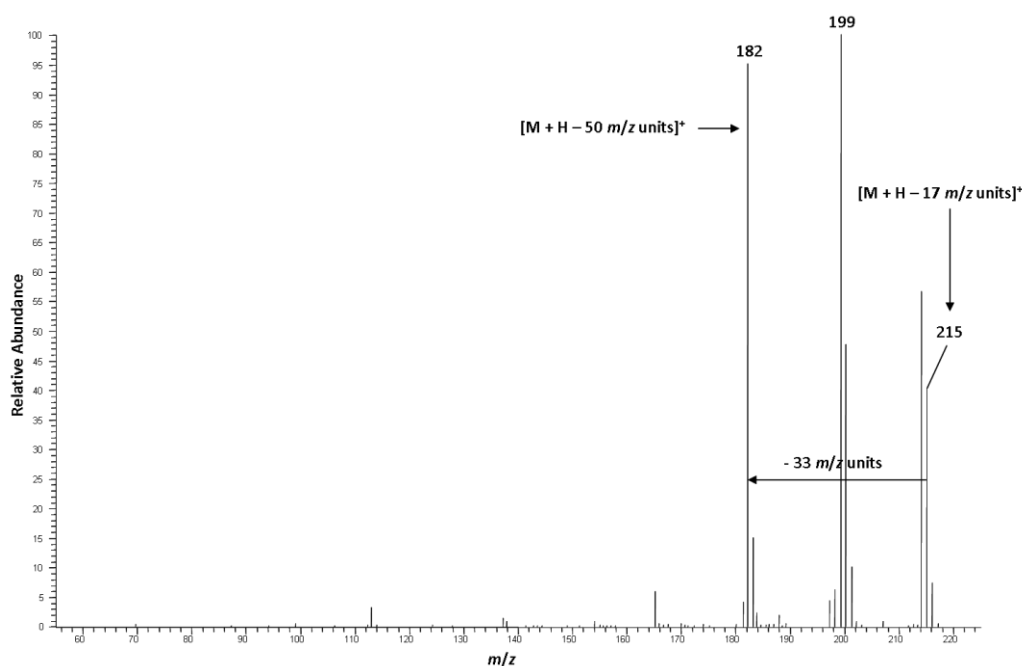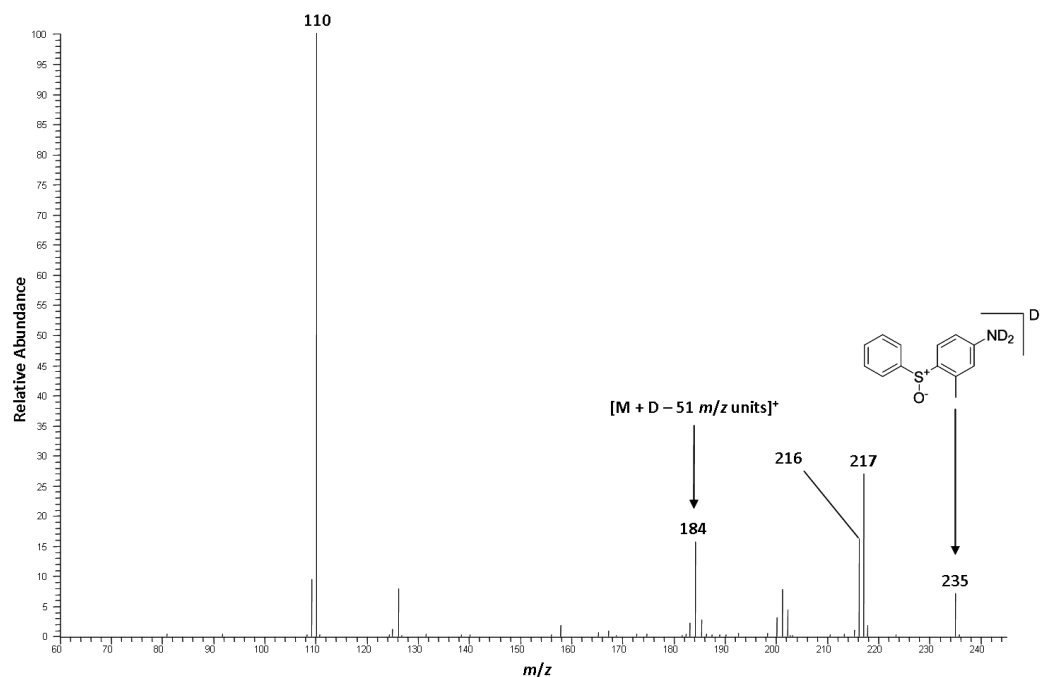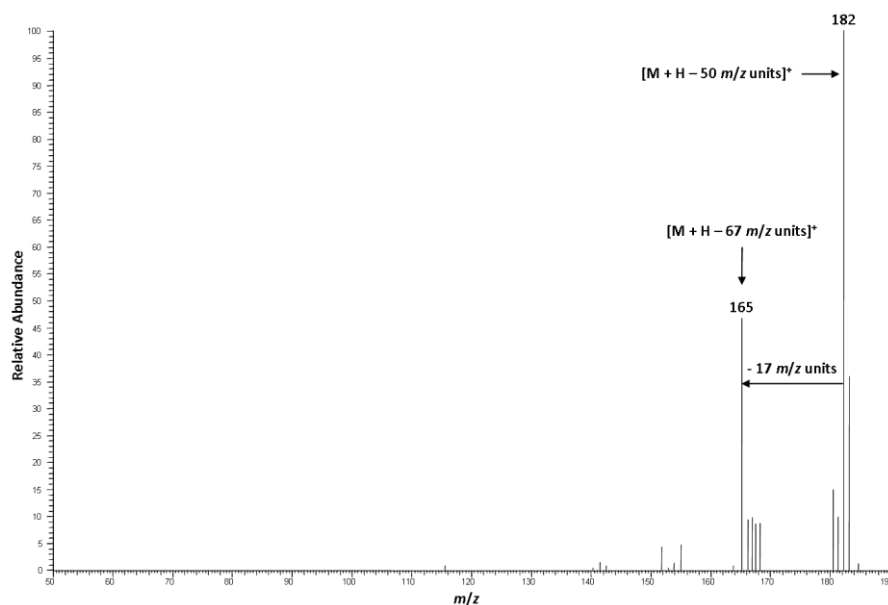

Figure 4.10 Third-generation low-energy CID product ion spectrum of protonated Compound 4.1 (*m/z* 232) using the ions at *m/z* 215 and 182 as the precursor ions for the second and third stages of mass analysis acquired using a LCQ Classic QIT mass spectrometer with WideBand activation off

A dissociation mechanism for the formation of protonated **Compound 4.3** from protonated **Compound 4.1** is proposed (**Figure 4.11**). The production of protonated 4-aminofluorene can not be precluded and a mechanism for this dissociation is also suggested (**Figure 4.12**). However, this could not be verified because 4-aminofluorene was not commercially available.
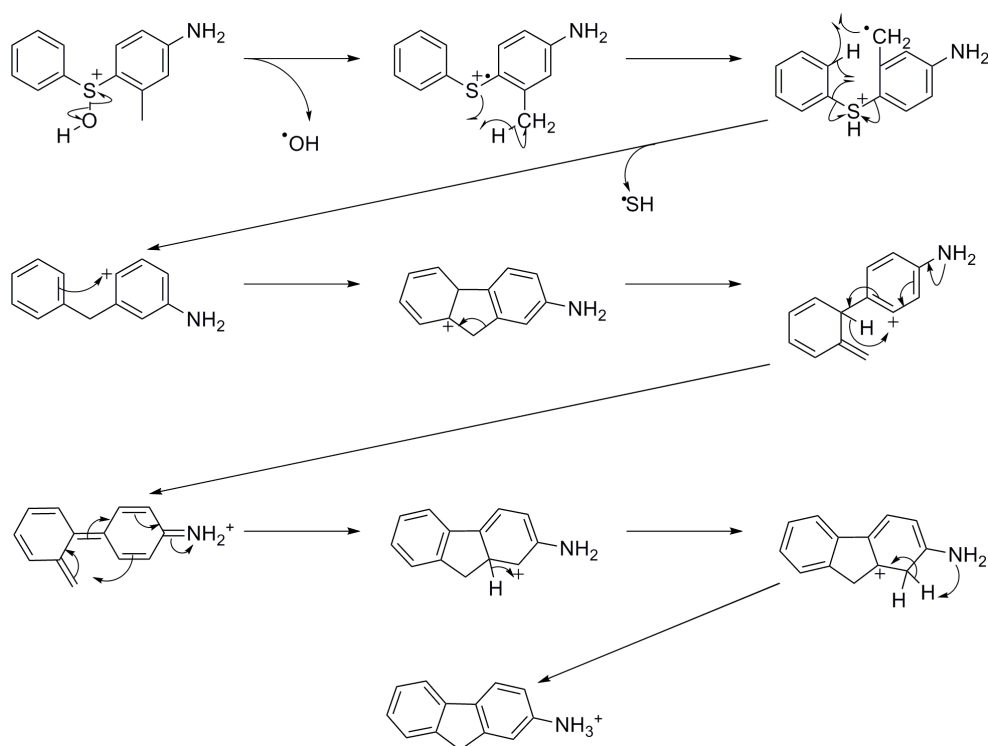
Figure 4.11   **Proposed dissociation mechanism for the formation of protonated Compound 4.3 by dissociation of protonated Compound 4.1 through sequential losses of a hydroxyl radical and a thiol radical**
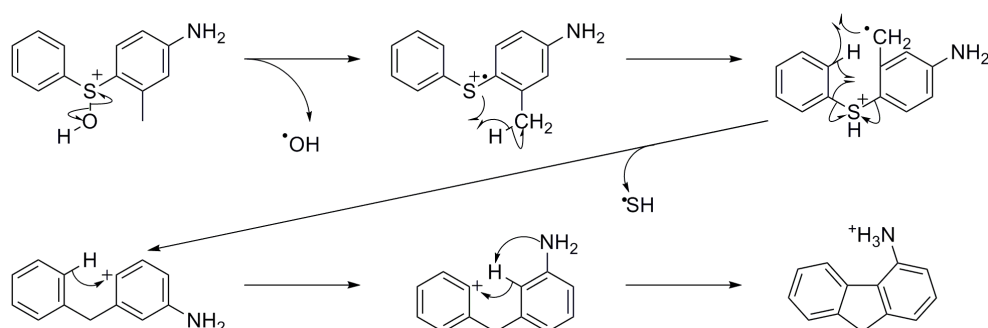
Figure 4.12   **Proposed dissociation mechanism for the formation of protonated 4-aminofluorene by dissociation of protonated Compound 4.1 through sequential losses of a hydroxyl and a thiol radical**

In both cases, the driving force for the dissociation appears to be product ion stability, with the planar structures likely to make the transitions energetically favourable (**Figure 4.13**).
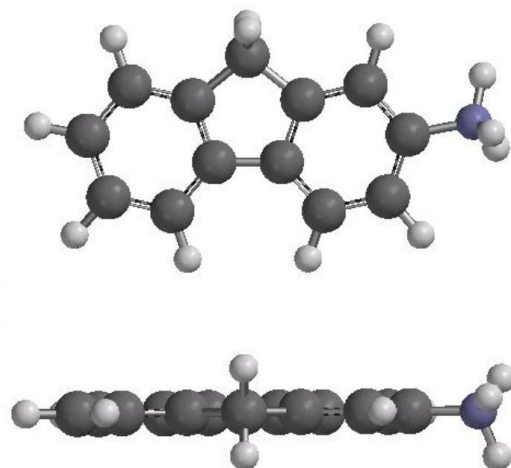
Figure 4.13   Molecular model of protonated Compound 4.3 demonstrating the planar structure of the ion

The discussed dissociation behaviour has potential as a tool for identifying the site of oxidation of a NCE during the drug discovery process. This is because the loss was not observed for protonated 3-methyl-4-phenylsulfanylphenylamine (**4**), the unoxidised analogue of the model *S*-oxide *i.e.* equivalent to the parent compound (**Figure 4.14**). The hydroxyl radical can not be lost without prior oxidation of the sulfur atom. Therefore, a 50 *m/z* unit loss in the low-energy CID product ion spectrum of a drug metabolite may suggest oxidation at a sulfur atom that is positioned *ortho* to a methyl group. This may rule out other sulfur atoms in the molecule as sites of oxidation because they lack the required chemical environment. Thus, rapid and definitive assignment of the site of *S*-oxidation could be achieved based upon a single loss in the low-energy CID product ion spectrum. The observed loss could be used as a tool to identify *S*-oxidised metabolites using both "in-time" and "in-space" MS/MS platforms. This is because the same dissociation was recorded using a QqTOF mass spectrometer operated over a range of collision energies (**Figure 4.15**). However, the investigation of the observed loss and the understanding of the mechanism were more effectively achieved using the QIT mass spectrometer.
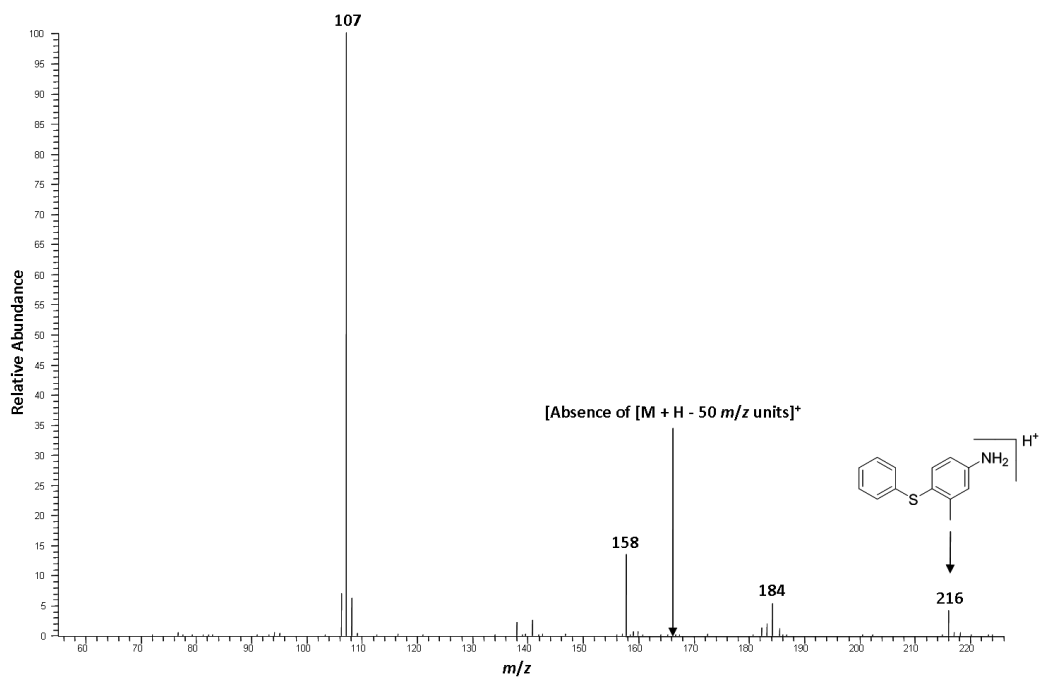
Figure 4.14 First-generation low-energy CID product ion spectrum of protonated Compound 4.4 (*m/z* 216) acquired using a LCQ Classic QIT mass spectrometer with WideBand activation on
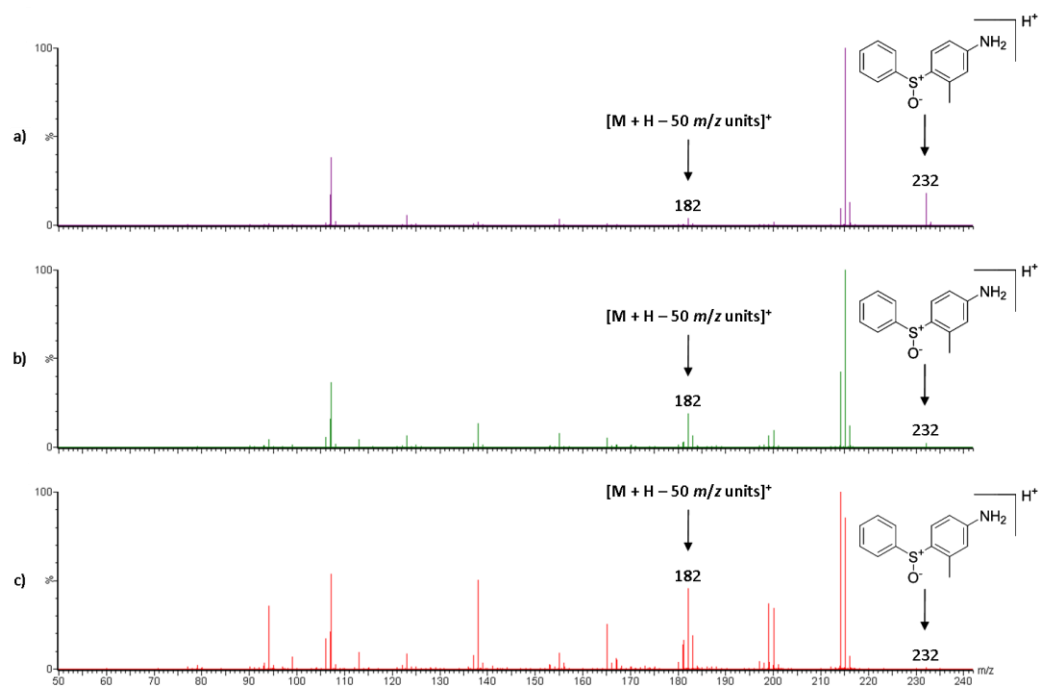
Figure 4.15 First-generation low-energy CID product ion spectra of protonated Compound 4.1 (*m/z* 232) acquired using a Premier QqTOF mass spectrometer operated at collision energies of a) 15 eV, b) 20 eV and c) 25 eV

The inability of the QqTOF mass spectrometer to perform MS^n experiments, in addition to the assumption that even-electron precursor ions dissociate to form even-electron product ions,[251] could result in an analyst proposing that the loss of 50 *m/z* units takes place in a single step. It is unlikely that sequential radical losses from even-electron precursor ions would be postulated under low-energy CID conditions, as a rationalisation based upon a neutral molecule loss would be sought in agreement with extensive experimental observations.[252] However, the ability of the QIT mass spectrometer to acquire MS^3 data allowed the elucidation of the sequential radical losses that constitute the loss of 50 *m/z* units.

It is hypothesised that two aromatic substructures bonded to the sulfoxide group, as well as the *ortho* methyl group, are required for the 50 *m/z* unit loss to be observed. This is because the loss was not observed for two compounds with sulfoxide functionalities bonded to a single aromatic ring and a methyl group; (4-methanesulfinyl-3-methylphenoxy)acetic acid (**Compound 4.5**) and 3-dimethylaminomethyl-4-(4-methanesulfinyl-3-methylphenoxy)benzenesulfonamide (**Compound 4.6**) (**Figures 4.16a and 4.16b**).
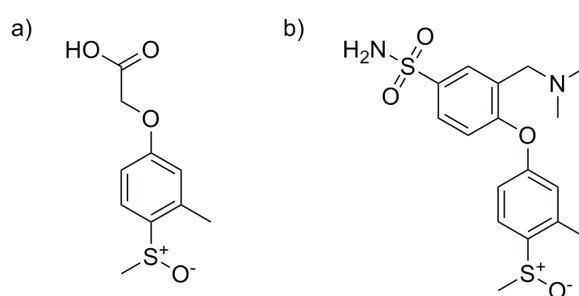
Figure 4.16   Molecular structures of a) (4-methanesulfinyl-3-methylphenoxy)acetic acid (Compound 4.5) and b) 3-dimethylaminomethyl-4-(4-methanesulfinyl-3-methylphenoxy)benzenesulfonamide (Compound 4.6)

The absence of a 50 *m/z* unit loss in their first-generation low-energy CID product ion spectra, acquired with WideBand activation on, (**Figures 4.17 and Figure 4.18**) suggests that the loss of a hydroxyl radical and a thiol radical is not
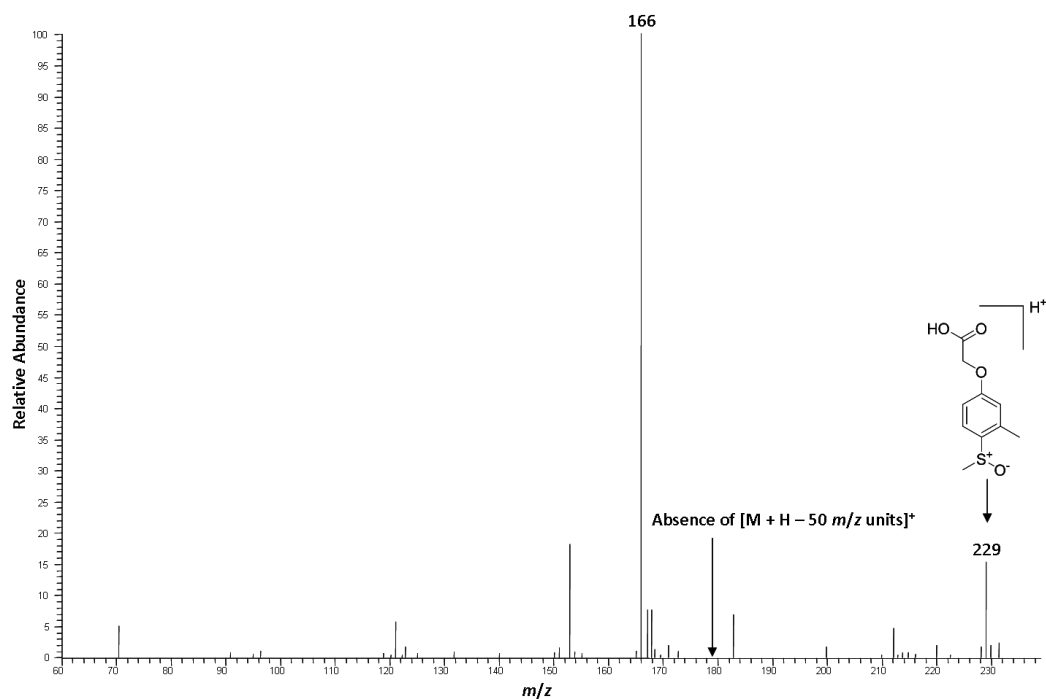
Figure 4.17 **First-generation low-energy CID product ion spectrum of protonated Compound 4.5 (*m/z* 229) acquired using a LCQ Classic QIT mass spectrometer with WideBand activation on**
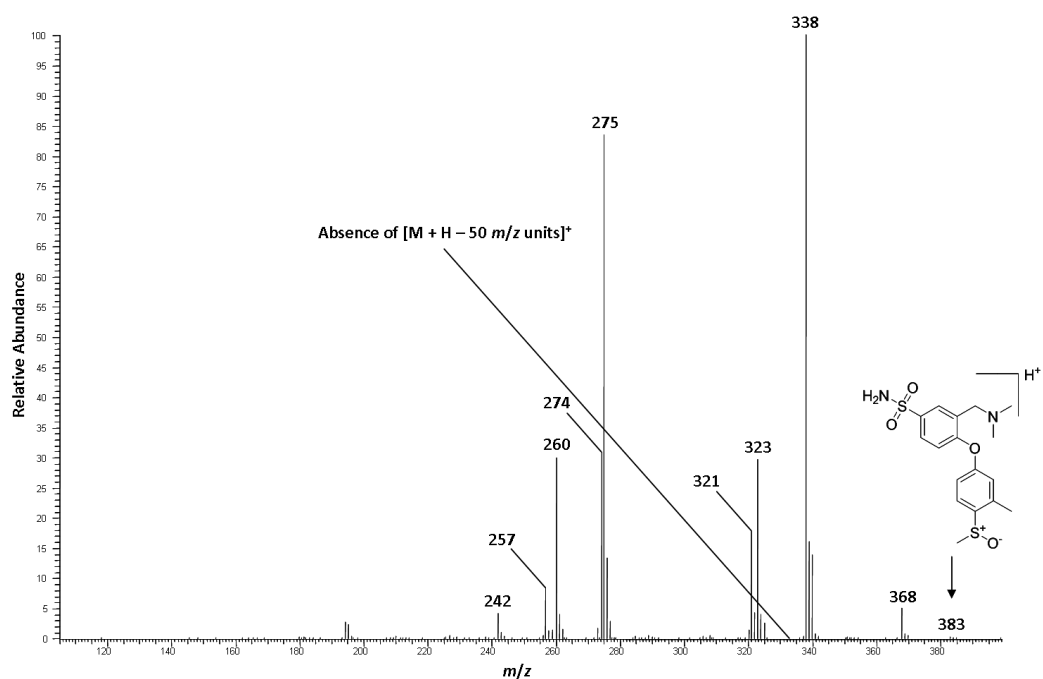
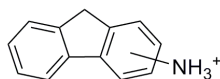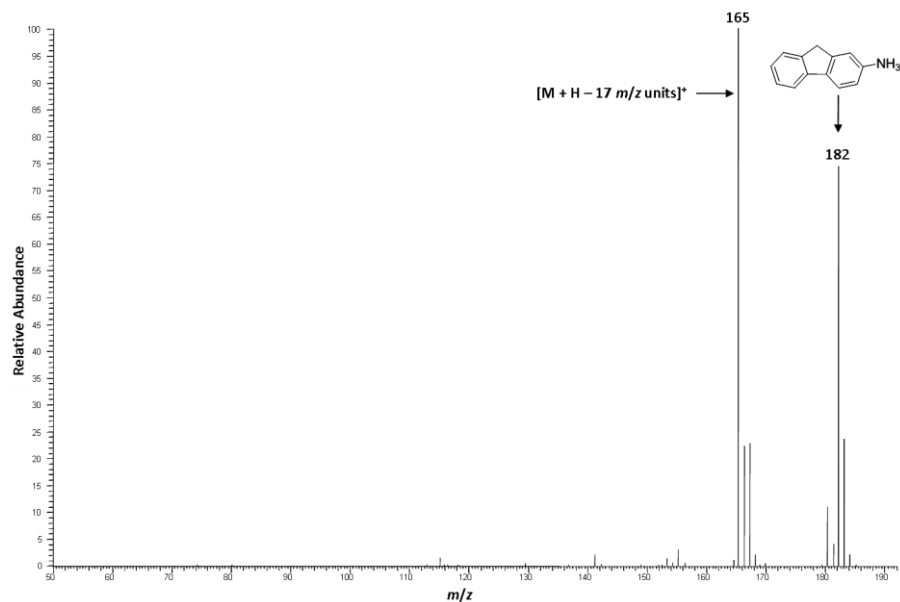**Figure 4.18** **First-generation low-energy CID product ion spectrum of protonated Compound 4.6 (*m/z* 383) acquired using a LCQ Classic QIT mass spectrometer with WideBand activation on**

energetically favourable without a second aromatic ring bonded to the sulfoxide group. Without two aromatic groups, a planar fluorene product ion-type structure can not be formed. Hence, it is hypothesised that the planar structure of the product ion is the driving force for the dissociation in this case. A further proposal concerning the dissociation is that the identity of the functional group positioned *ortho* to the sulfoxide functionality that facilitates the 50 *m/z* unit loss may not be restricted to a methyl group. However, suitable compounds to test these hypotheses were not available for this study.

4.4   Conclusions

The experimental investigation of the loss of 50 *m/z* unit loss from protonated **Compound 4.1** has been presented. Comparison of the low-energy CID product ion spectrum with that of the homologue lacking a methyl group on the phenylamine ring, **Compound 4.2**, led to the proposal of an *ortho*-effect on the dissociation. The findings indicated that the dissociation was a two-step process involving sequential losses of a hydroxyl radical followed by a thiol radical; a rare observation under low-energy CID conditions when even-electron precursor ions are fragmented. Solution-phase H/D exchange experiments showed that only one exchangeable hydrogen atom was involved in the fragmentation and that it was located on the hydroxyl group formed during protonation. Thus, definitive assignment of the site of protonation was achieved using the solution-phase H/D exchange approach. The involvement of a non-exchangeable hydrogen atom during the loss of the thiol radical supported the hypothesis of an *ortho*-effect due to the methyl group. Molecular modelling calculations complemented these findings by demonstrating that the most likely site of protonation was the sulfoxide oxygen, thus facilitating the loss of the hydroxyl radical. Accurate mass FT-ICR-MS product ion data confirmed the elemental formulae of the two radical losses. The elemental formula derived from the AMM of the resultant product ion was consistent with the calculated rings plus double bond equivalents for a protonated aminofluorene. The hypothesised product ion structure was

verified by comparison of the low-energy CID product ion spectrum of commercially available protonated **Compound 4.3** with that acquired by dissociation of the product ion derived through the loss of 50 *m/z* units from protonated **Compound 4.1**. Possible dissociation mechanisms are proposed.

The loss of H_2SO has potential application in fields where structural elucidation is of interest, particularly the pharmaceutical industry. In this area, a 50 *m/z* unit loss in the low-energy CID product ion spectrum of a drug metabolite may indicate that *S*-oxidation has taken place at a sulfur atom bonded to two aromatic rings with a methyl group positioned *ortho* to it. During drug discovery, this could facilitate rapid and definitive identification of *S*-oxidation. Further, it could discriminate between multiple sulfur atoms in a compound as the site of oxidation based upon the chemical environment required for the loss to take place.

Chapter 5

An example of how unexpected dissociation behaviour could preclude correct assignment of sites of metabolism

5.1   Introduction

The principal method of assigning the site of metabolism of a NCE using MS/MS involves comparing the low-energy CID product ion spectrum of the parent compound with that of the metabolite. The analyst interrogates the spectra for mass shifts of the major peaks to determine which part of the molecule has been altered *i.e.* the Shift technique.[198] However, unambiguous assignments by this approach are frequently not possible (see **Chapter 2**). Furthermore, the high-throughput nature of modern drug discovery means that multiple mass spectrometric-related structural elucidation experiments *e.g.* isotopic labelling, derivatisation *etc.*, which could assist in definitively identifying the site of metabolism, may not be performed.   Thus, there is a risk that incorrect assignment of sites of metabolism could arise, which is restrictive on timely completion of metabolite identification studies. This is a particular likelihood given that fragmentation under low-energy CID conditions is still not fully understood, with unexpected rearrangements being previously reported in the literature for both peptidic and small molecules.[253-256]   Herein, a further example of unanticipated dissociation behaviour, observed for the model sulfoxide metabolite 3-dimethylaminomethyl-4-(4-methanesulfinyl-3-methylphenoxy)benzenesulfonamide, demonstrates how incorrect assignment of the sites of metabolism of a NCE could occur if a rigorous analytical approach is not applied.

5.2 Experimental

5.2.1 Chemicals

3-Dimethylaminomethyl-4-(4-methanesulfinyl-3-methylphenoxy)benzenesulfonamide (**Compound 5.1**) and 3-dimethyl-^{2}H$_6$-aminomethyl-4-(4-methanesulfinyl-3-methylphenoxy)benzenesulfonamide (**Compound 5.2**) were provided by Pfizer Global Research and Development (Sandwich, UK). Solutions of both compounds were prepared for QIT-MS experiments as detailed in **Chapter 3**. Further solutions of **Compound 5.1** were prepared for FT-ICR-MS, QqTOF-MS and solution-phase H/D exchange experiments as detailed in **Chapter 3**.

5.2.2 Instrumental

QIT-MS experiments were performed as detailed in **Chapter 3** to acquire "in-time" low-energy CID product ion spectra. The ion source conditions were; sheath gas, 35 arbitrary units; auxiliary gas, 5 arbitrary units; spray voltage, 4.5 kV; capillary voltage, 11 V; capillary temperature, 220°C; tube lens offset, 35 V. For both MS/MS and MS^3 experiments, the normalised collision energy was set to 50% and WideBand activation was switched on.

QqTOF-MS experiments were performed as detailed in **Chapter 3** to acquire "in-space" low-energy CID product ion spectra of **Compound 5.1**.

FT-ICR-MS experiments were performed as detailed in **Chapter 3** to acquire an AMM "in-time" low-energy SORI-CID product ion spectrum of **Compound 5.1**. The ion source conditions were; capillary voltage, -4.5 kV; end plate voltage, -3.8 kV; capillary exit voltage, 100 V; skimmer 1, 11 V; skimmer 2, 6 V; Offset, 1.25; RF amplitude, 600 Hz; dry gas temperature, 250°C; dry gas flow rate, 30 arbitrary units; nebulising gas pressure, 50 psi. The excitation amplitude was 3.7 dB. A low-energy SORI-CID product ion spectrum was acquired for eight scans using 1024K data points. The MS/MS parameters were; corr sweep pulse length, 1000 μs; corr sweep attenuation, 37.5 dB; ejection safety belt, 3000 Hz;

user pulse length, 1000 µs; ion activation pulse length, 250000 µs; ion activation attenuation, 37.2 dB; frequency offset from activation mass, - 500 Hz; user delay length, 3 s.

5.3   Results and discussion

As part of the presented study, a series of pharmaceutical compounds and model metabolites were analysed using QIT-MS to identify product ions and losses that could facilitate rapid and definitive identification of pharmaceutical drug metabolites. During these studies, the dissociation of a model *S*-oxidised metabolite, 3-dimethylaminomethyl-4-(4-methanesulfinyl-3-methylphenoxy)benzenesulfonamide (**Compound 5.1**) (**Figure 5.1**), was investigated.
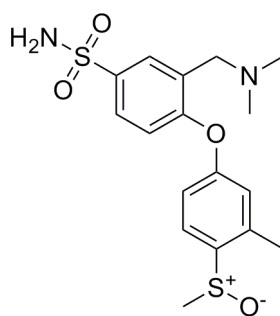
Figure 5.1   **Molecular   structure   of   3-dimethylaminomethyl-4-(4-methanesulfinyl-3-methylphenoxy)benzenesulfonamide (Compound 5.1)**

The first-generation low-energy CID product ion spectrum of the protonated molecule is shown in **Figure 5.2**. A loss of 62 *m/z* units was observed, forming the product ion at *m/z* 321. The same loss was not seen for the parent compound (data not shown). The dissociation thus appeared dependent upon the biotransformation *i.e.* oxidation. Hence, the loss was thought to be of potential use in metabolite identification. This proposal was supported by the observation of the same loss using a QqTOF mass spectrometer (**Figure 5.3**). This demonstrated that the dissociation could be recorded using both "in-space" and "in-time" MS/MS platforms *i.e.* the dissociation was instrument-
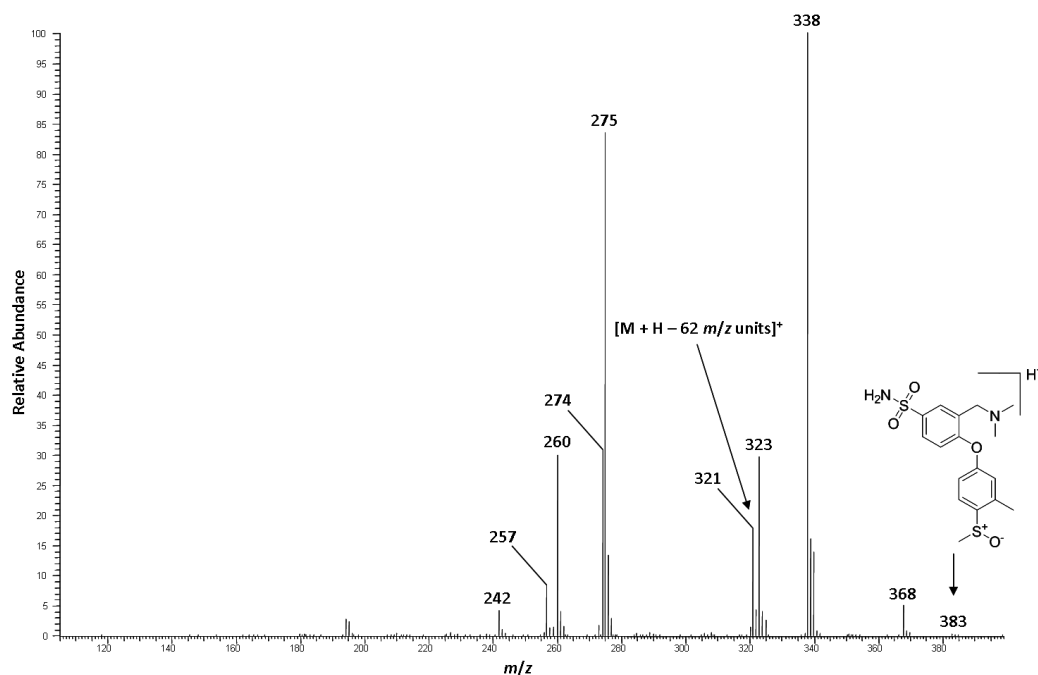
Figure 5.2 First-generation low-energy CID product ion spectrum of protonated Compound 5.1 (*m/z* 383) acquired using a LCQ Classic QIT mass spectrometer with WideBand activation on
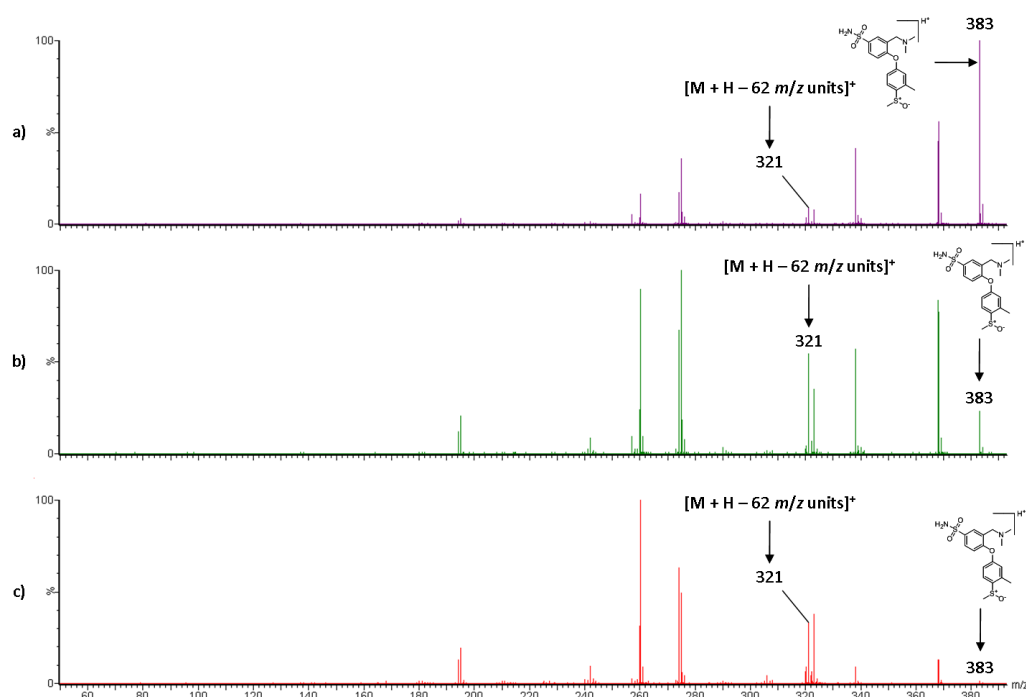
Figure 5.3 First-generation low-energy CID product ion spectra of protonated Compound 5.1 (*m/z* 383) acquired using a Premier QqTOF mass spectrometer operated at collision energies of a) 15 eV, b) 20 eV and c) 25 eV

configuration independent. This was important to establish because mass spectrometers with many different mass analysers are employed for the purpose of metabolite identification.[175, 257-261]

Involvement of the oxygen atom was inferred and the loss was assigned as methanethial, *S*-oxide (CH$_2$SO). This hypothesis was attractive because *S*-oxidation of the parent compound produces an ideal candidate for the loss of 62 *m/z* units through the well-documented processes of charge-remote fragmentation[262] and 1,3-proton shifts[263] *via* four-centred rearrangements (**Figure 5.4**). The dissociation was thought to be energetically favourable due to the conformance of the proposed product ion with the even-electron rule.[251] However, the loss could not be confirmed by a change in the ^{34}S isotope pattern for the product ion compared to the precursor ion due to the difficulties associated with observing the true isotope pattern using a QIT mass spectrometer. The overlapping of the second isotope peak of the product ion at *m/z* 321 with the monoisotopic peak of the product ion at *m/z* 323 further precluded this approach to structural elucidation.
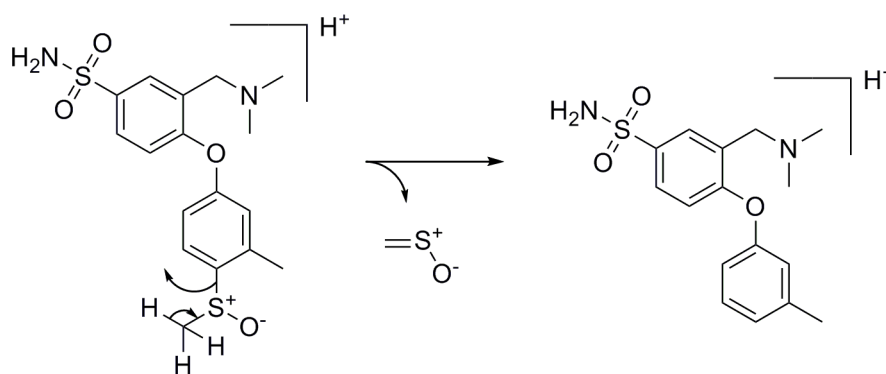
Figure 5.4   **Proposed mechanism for the loss of methanethial, *S*-oxide from protonated Compound 5.1 *via* a four-centred rearrangement**

It was noted that the proposed 62 *m/z* unit loss did not involve any of the three exchangeable hydrogen atoms on the precursor ion. Thus, if the assignment of the loss were correct, the *m/z* of the product ion for the loss of methanethial, *S*-oxide would mass shift by 3 *m/z* units to *m/z* 324 in the low-energy CID product ion spectrum of the fully exchanged, deuterated species (**Figure 5.5**). The
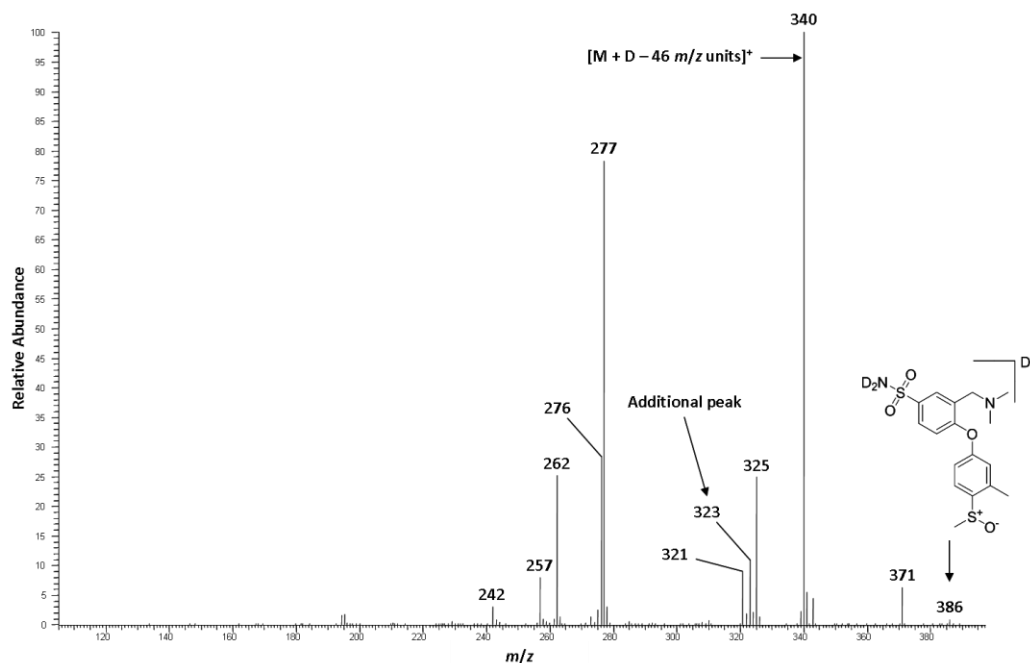
Figure 5.5   **First-generation low-energy CID product ion spectrum of fully exchanged, deuterated Compound 5.1 (*m/z* 386) acquired using a LCQ Classic QIT mass spectrometer with WideBand activation on**

absence of a peak at *m/z* 324 under deuterated conditions indicated that the initially posited loss was incorrect. Further, an additional peak was observed at *m/z* 323 in the low-energy CID product ion spectrum of the fully exchanged, deuterated species that was not seen for the protonated molecule. It should be noted that this product ion was different to that seen at *m/z* 323 in the low-energy CID product ion spectrum of the protonated molecule, which is mass shifted to *m/z* 325 under deuterated conditions.   The observation of an additional peak led to the deduction that two nominally isobaric product ions were formed through dissociation of the protonated molecule. The product ions only became mass-resolved when the fully exchanged, deuterated molecule was dissociated due to the retention of different numbers of deuterium atoms by the two product ions. Thus, the solution-phase H/D exchange experiment showed that two losses of 62 *m/z* units took place, neither of which being that initially postulated. The loss of all of the deuterium atoms to form the product ion at *m/z* 321 indicated that the primary amine group had been lost during the dissociation. This was because exchange of the

two hydrogen atoms in the primary amine group for two deuterium atoms would have occurred in solution. The peak at *m/z* 323, formed through a loss involving one deuterium atom, indicated that this product ion retained the primary amine. Further, it suggested that the ionising deuteron was lost during the dissociation, and hence the loss included a site of ionisation.

Further experimentation was undertaken to characterise the two losses of 62 *m/z* units. To this end, the first-generation low-energy CID product ion spectrum of a deuterium-labelled analogue, 3-dimethyl-^{2}H$_6$-aminomethyl-4-(4-methanesulfinyl-3-methylphenoxy)benzenesulfonamide (**Compound 5.2**) (**Figure 5.6**), was acquired (**Figure 5.7**).
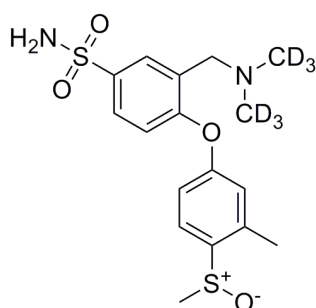
Figure 5.6   Molecular structure of 3-dimethyl-^{2}H$_6$-aminomethyl-4-(4-methanesulfinyl-3-methylphenoxy)benzenesulfonamide (Compound 5.2)

In the mass range of interest, the low-energy CID product ion spectrum resembled that of protonated **Compound 5.1**, with only two peaks being observed. This indicated that the product ions were nominally isobaric again and neither product ion retained the six deuterium labels. Thus, both losses of 62 *m/z* units in **Figure 5.2** involved the tertiary amine group. The solution-phase H/D exchange experiment had shown that one product ion also lost the primary amine group; thus, the overall loss was postulated to be $C_2H_{10}N_2$. The same experiment had also shown that one product ion retained the primary amine and lost the ionising deuteron. From this information, it was deduced that the tertiary amine group was a site of protonation. Further, it suggested that the remaining loss of 17 *m/z* units for the product ion that retained the primary
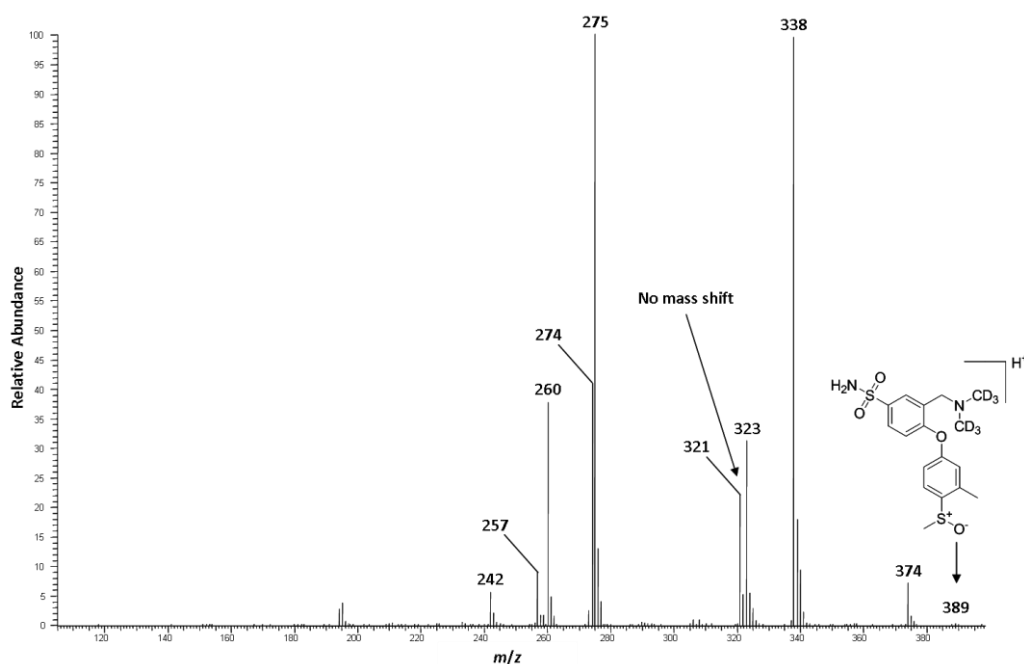
Figure 5.7 **First-generation low-energy CID product ion spectrum of protonated Compound 5.2 (*m/z* 389) acquired using a LCQ Classic QIT mass spectrometer with WideBand activation on**

amine group (62 *m/z* units minus 45 *m/z* units for the tertiary amine group plus the ionising proton) was likely to be a hydroxyl radical; an overall proposed loss of $C_2H_8NO^\bullet$.

To confirm the hypothesised losses, AMMs were acquired using FT-ICR-MS. **Figure 5.8** shows the first-generation low-energy SORI-CID product ion spectrum of protonated **Compound 5.1** in the mass range of interest. The high resolving power of the FT-ICR mass spectrometer allowed mass resolution of the two nominally isobaric product ions at *m/z* 321. The lowest MME elemental formulae, given the precursor ion formula, were consistent with those postulated and confirmed that the two losses of 62 *m/z* units were $C_2H_{10}N_2$ and $C_2H_8NO^\bullet$.

The verification of the elemental composition of the losses allowed postulation of dissociation mechanisms leading to the decomposition of the precursor ion. The product ion with an elemental formula of $C_{15}H_{13}O_4S_2^+$ (**Compound 5.3**) had a ring plus double bond equivalents value of 9.5, confirming that it is an even-
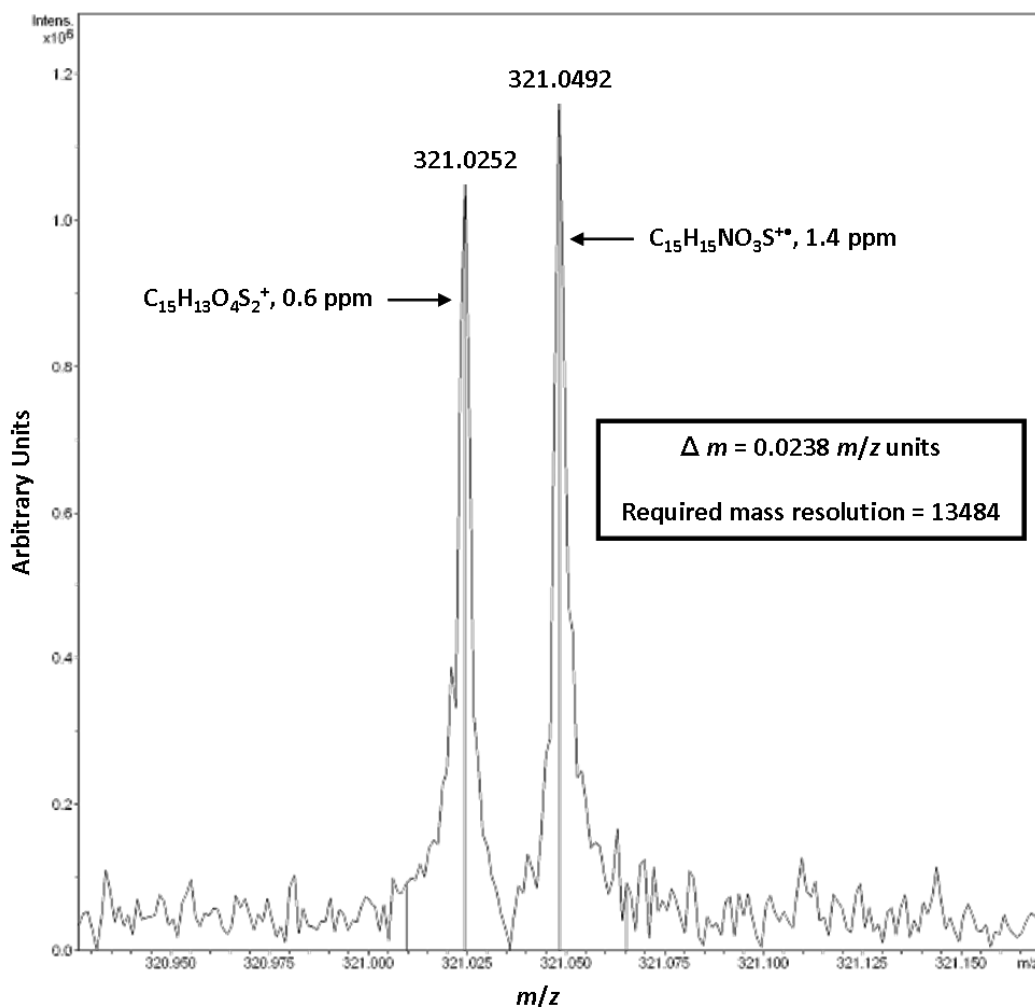
Figure 5.8   **First-generation low-energy SORI-CID product ion spectrum of protonated Compound 5.1 (*m/z* 383) acquired using an Apex III FT-ICR mass spectrometer**

electron ion.[249]   Because of the deficiency of this value by 0.5 due to the addition of a proton to the molecule,[250] it was deduced that the number of rings plus double bond equivalents in the product ion was 10. **Figure 5.9** shows a proposed mechanism leading to the formation of a product ion which satisfies this value; the double bonds of the sulfone group are discounted due to sulfur not being in its lowest valence state.[249]   Protonation is postulated on the primary amine to facilitate the loss of the two exchangeable hydrogen atoms as part of a molecule of ammonia.

The speculative product ion structure is predominately planar as evinced by the molecular model in **Figure 5.10**. This is likely to provide the driving force for the

energetic rearrangement that involves a high-energy proton shift and leads to the loss of dimethylamine.[237] The planar structure allows easy delocalisation of the charge, making the formation of the product ion thermodynamically favourable.
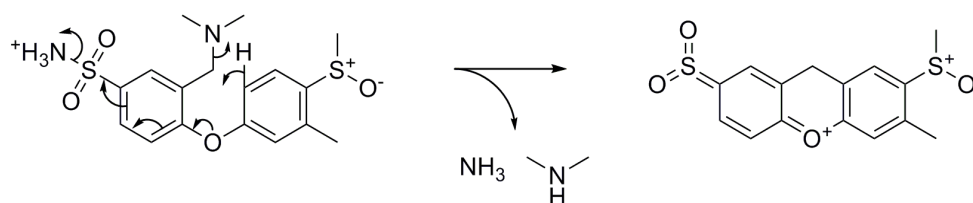
Figure 5.9   **Proposed mechanism for the formation of Compound 5.3 through the loss of $C_2H_{10}N_2$ as molecules of ammonia and dimethylamine from protonated Compound 5.1**
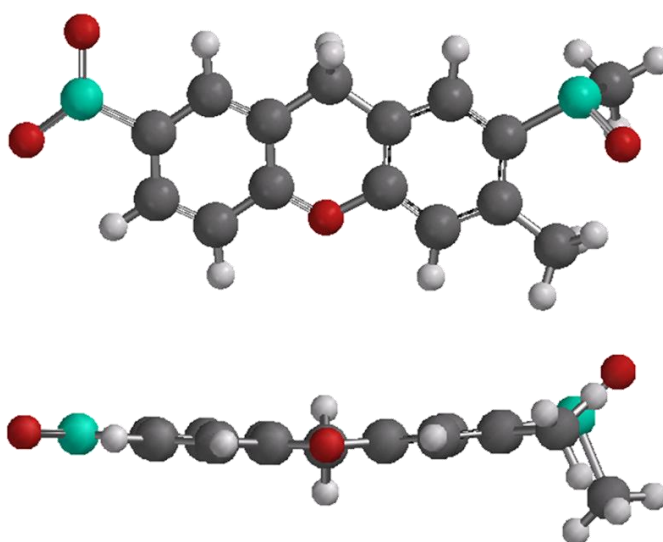
Figure 5.10   **Molecular models of Compound 5.3 demonstrating the predominately planar structure of the proposed product ion**

The product ion with an elemental formula of $C_{15}H_{15}NO_3S_2^{+\bullet}$ (**Compound 5.4**) has a ring plus double bond equivalents value of 10 *i.e.* an odd-electron species.[249] **Figure 5.11** shows a proposed mechanism to form a radical product ion structure that is consistent with this value. The speculative product ion structure is again predominately planar, (**Figure 5.12**), thus allowing facile delocalisation of both the charge and the radical site. This is particularly important due to the energetically unfavourable formation of a radical product

ion from an even-electron precursor.[264] However, the resonance stabilisation across the two aromatic rings, and the sulfone and sulfoxide functionalities, is likely to facilitate this dissociation.
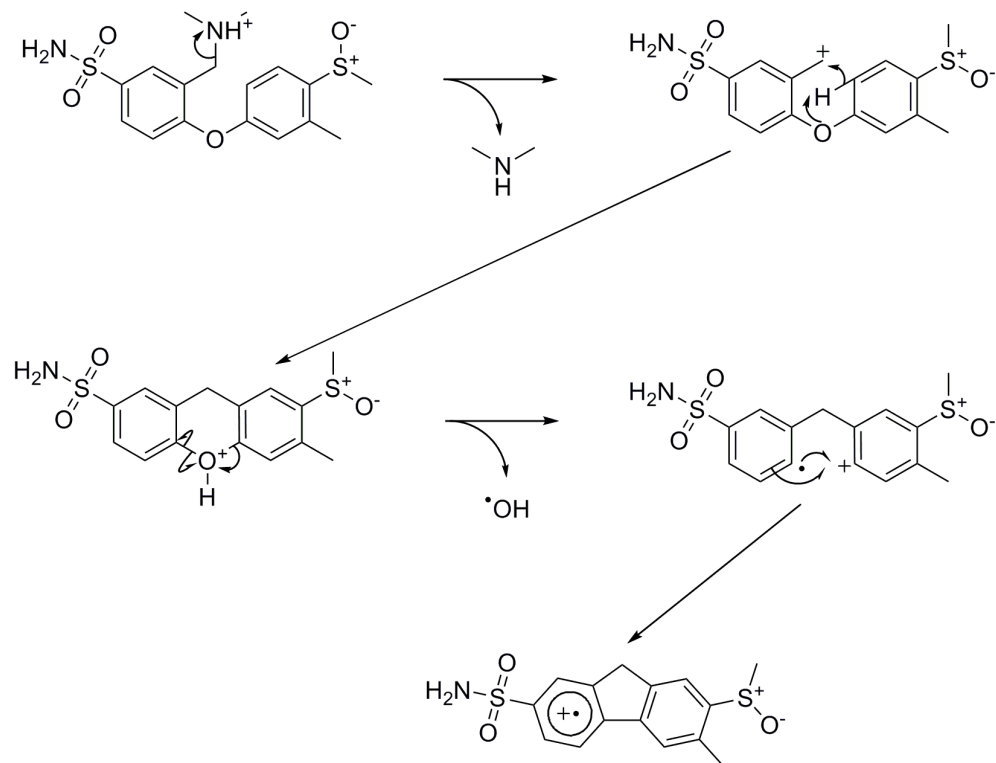
Figure 5.11 Proposed mechanism for the formation of Compound 5.4 through the loss of $C_2H_8NO^\bullet$ as a molecule of dimethylamine and a hydroxyl radical from protonated Compound 5.1
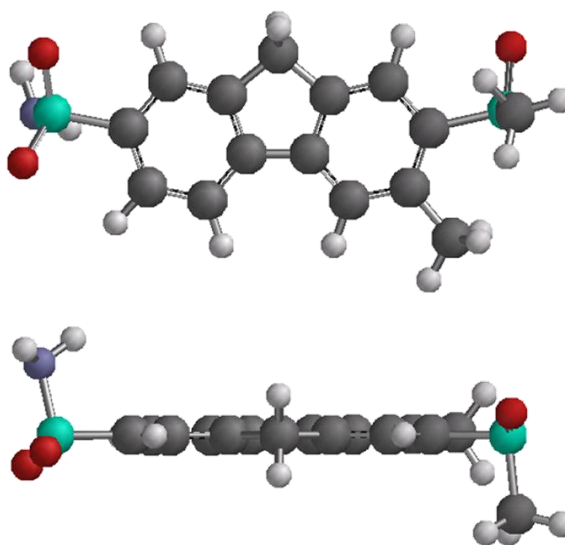
Figure 5.12 Molecular models of Compound 5.4 demonstrating the predominately planar structure of the proposed product ion

Both proposed dissociation mechanisms involve the loss of dimethylamine. However, the pathways leading to this loss differ for the two product ions. The formation of **Compound 5.3** is postulated to involve the loss of dimethylamine facilitated by the shift of a non-exchangeable hydrogen atom. Conversely, the formation of **Compound 5.4** proceeds *via* protonation of the tertiary amine followed by a charge-directed inductive cleavage of the carbon-nitrogen bond. Thus, an exchangeable hydrogen atom *i.e.* the ionising proton (deuteron) is proposed to facilitate the loss of dimethylamine in this instance. The loss of dimethylamine was also observed in the first-generation low-energy CID product ion spectrum of protonated **Compound 5.1** (**Figure 5.2**; product ion at *m/z* 338). The dissociation of the fully exchanged, deuterated species (**Figure 5.5**) showed that the loss increased by 1 *m/z* unit to produce a peak at *m/z* 340, demonstrating the involvement of a single exchangeable hydrogen atom in the dissociation. The protonated molecule can not be spatially arranged such that the two exchangeable hydrogen atoms on the primary amine can be in close proximity to the tertiary amine functionality to allow intra-ionic transfer. Thus, they can be excluded as being the source of the exchangeable hydrogen atom involved in the loss of dimethylamine. Hence, the exchangeable hydrogen atom must be the ionising proton (deuteron). From the two mechanisms postulated for the losses of 62 *m/z* units (**Figures 5.9 and 5.11**), only one involves protonation at the tertiary amine and the loss of dimethylamine facilitated by an exchangeable hydrogen atom *i.e.* the loss of $C_2H_8NO^•$. Protonation at the primary amine is inferred for the loss of $C_2H_{10}N_2$ to facilitate elimination of a molecule of ammonia from the precursor ion. This could not be confirmed using solution-phase H/D exchange experiments because the loss of ammonia is not observed in the first-generation low-energy CID product ion spectrum of protonated **Compound 5.1** (**Figure 5.2**). However, supportive evidence for the proposed mechanisms was obtained through the acquisition of the second-generation low-energy CID product ion spectrum of fully exchanged, deuterated **Compound 5.1** using the ion at *m/z* 340 as the precursor ion for the second stage of mass analysis (**Figure 5.13**). The dissociation of the fully exchanged, deuterated molecule, rather than the protonated molecule, was investigated so
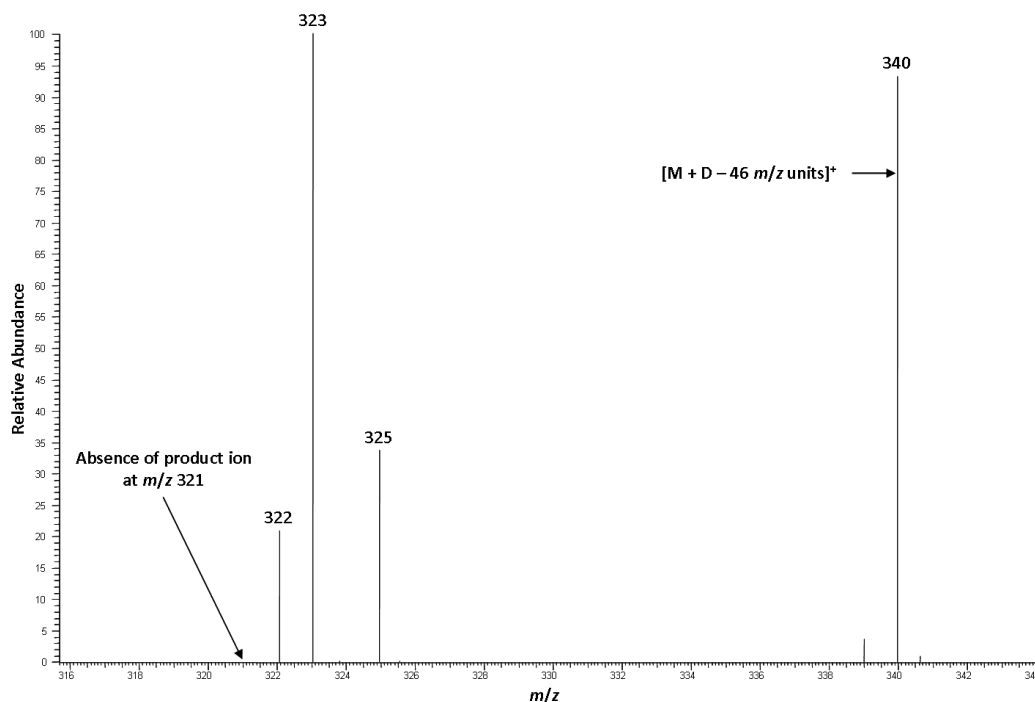
Figure 5.13   **Second-generation low-energy CID product ion spectrum of fully exchanged, deuterated Compound 5.1 (*m/z* 386) using the ion at *m/z* 340 as the precursor ion for the second stage of mass analysis acquired using a LCQ Classic QIT mass spectrometer with WideBand activation on**

that the product ions would be mass-resolved on the QIT mass spectrometer if they were both formed.   In the mass range of interest, a product ion was observed at *m/z* 323, which suggested that **Compound 5.4** is formed through protonation at the tertiary amine, followed by the loss of dimethylamine and then elimination of a hydroxyl radical.   The mass difference of 17 *m/z* units between the precursor ion for the second stage of mass analysis and the final product ion indicated that the loss of the hydroxyl radical involved a non-exchangeable hydrogen atom.   If an exchangeable hydrogen atom was involved, the loss would become a deuterohydroxyl radical, and thus the mass loss would increase to 18 *m/z* units, under deuterated conditions.   The observations were consistent with the proposed mechanism for the dissociation (**Figure 5.11**).   No peak was observed at *m/z* 321, which indicated that a second dissociation pathway existed for the loss of dimethylamine.   This provided supportive evidence for a loss of dimethylamine facilitated by the shift of a non-exchangeable hydrogen atom, which is consistent with the proposed

mechanism (**Figure 5.9**). The absence of the losses of ammonia and dimethylamine facilitated by a non-exchangeable hydrogen atom in the first-generation low-energy CID product ion spectrum of protonated **Compound 5.1** suggested that the dissociation is concerted, or at least that the intermediates undergo rapid decomposition to the final product ion. Further, the solution-phase H/D exchange experiments suggested that **Compound 5.1** had more than one site of protonation in the gas phase because the loss of the tertiary amine group was not *via* protonation at that site in the formation of **Compound 5.3**. Thus, it was plausible that the molecule could protonate at the primary amine, further supporting the mechanism proposal.

The discussed work has implications for structural elucidation using low-energy CID product ion spectra, particularly for metabolite identification studies. To identify the sites of metabolism on a NCE using MS, the structures of the metabolites must be deduced from their low-energy CID product ion spectra. From the low-resolution low-energy CID product ion spectrum of protonated **Compound 5.1**, *S*-oxidation is likely to be proposed based upon the initial assignment of the 62 *m/z* unit loss as methanethial, *S*-oxide *via* a four-centred rearrangement. In this case, the proposal of *S*-oxidation would be correct but the assignments of the product ions leading to it would be wrong. If this were an unknown metabolite, oxidation of the parent compound could have occurred, for example, through aromatic hydroxylation of the 1-methyl-2-methylsulfanylbenzene ring and potentially not affected either of the actual losses of 62 *m/z* units. Nevertheless, the attractive nature of *S*-oxidation facilitating the loss of methanethial, *S*-oxide *via* a four-centred rearrangement could lead to an incorrect assignment. Hence, time and money may be spent synthesising analogues and/or homologues to protect the methyl sulfide functionality of the parent compound only to discover that the hypothesised site of oxidation is incorrect. The discussed example highlights the possibility of unexpected rearrangements under low-energy CID conditions, which could easily lead to incorrect assignments of product ion structures, and hence sites of metabolism in drug discovery studies. A simple and cost-effective approach to

reduce the likelihood of this occurrence is the use of solution-phase H/D exchange experiments, which provide a straightforward method of introducing isotopic labels into the compound. Thus, dissociations proposed to involve exchangeable hydrogen atoms can be verified. Further, employment of mass spectrometers capable of high-resolution mass measurement, even when coupled to fast chromatography as utilised in metabolite identification studies, would also reduce the possibility of incorrect product ion structure assignment. The study has also been of relevance to the understanding of fragmentation under low-energy CID conditions. The dissociations involve more complex rearrangements than that initially proposed. Further, the formation of an energetically unfavourable radical product ion occurred. However, the final shapes of the product ions appear to have a bearing on the dissociation pathways followed. The initially proposed product ion structure formed through the loss of methanethial, *S*-oxide has free rotation about the ether linkage. The product ions actually formed are posited to be predominately planar, thus allowing easier delocalisation of the charge. This may suggest that rearrangements leading to the formation of planar product ion structures predominate under low-energy CID conditions. Furthermore, the study indicated that solution-phase H/D exchange experiments can be useful in determining sites of gas-phase protonation under ESI-low-energy CID-MS/MS conditions, as previously reported,[265] thus allowing rationalisation of dissociation mechanisms.

5.4   Conclusions

The experimental investigation of the dissociation of a model *S*-oxidised metabolite, **Compound 5.1**, has been presented. The product ion at *m/z* 321 in the low-resolution low-energy CID product ion spectrum was initially assigned as being formed through the loss of methanethial, *S*-oxide from the protonated molecule. It was thought that this loss could be used to assign the site of oxidation as the sulfur of the methyl sulfide group. Subsequent deuterium labelling experiments and AMMs acquired using a high-resolution low-energy

CID product ion spectrum proved that the initial assignment was incorrect. Instead, two unexpected rearrangements led to the formation of nominally isobaric product ions. Only through the use of solution-phase H/D exchange experiments and high-resolution MS was it possible to mass-resolve these species. Mechanisms consistent with the experimental findings were postulated. Supportive evidence for the proposals was obtained through the acquisition of a second-generation low-energy CID product ion spectrum. The speculative planar product ion structures were concluded to provide the driving force for the rearrangements, particularly in the formation of an energetically unfavourable radical cation. The study is of relevance to pharmaceutical drug metabolite identification because it demonstrated that a rigorous analytical approach is required to ensure that incorrect assignment of the sites of metabolism of NCEs is precluded. A greater understanding of fragmentation under low-energy CID conditions was also obtained, with the shape of the product ion apparently offsetting the complexity of the rearrangement required to form it. Further, the data verified the usefulness of solution-phase H/D exchange experiments in determining sites of protonation under ESI-low-energy CID-MS/MS conditions.

Chapter 6

A rapid methodology for the characterisation of dialkyl tertiary amine-*N*-oxide metabolites using structurally dependent dissociation pathways and reconstructed ion current chromatograms

6.1   Introduction

Many pharmaceutical compounds contain amine groups that act as hydrogen bond acceptors to affect the solubility and permeability of the molecule in biological organisms.[266] A particularly common substructure is a dialkyl tertiary amine group. The literature cites many examples of the loss of the nitrogen-containing group in this substructure under low-energy CID conditions.[267-277] However, only small libraries, or structurally similar compounds, were investigated in each case. Thus, there is no reported comprehensive understanding of the dissociation behaviour of this substructure, such as whether the loss of the group is always observed under low-energy CID conditions when it is present in structurally diverse compounds. Further, little knowledge is available as to whether the oxidised analogue of a dialkyl tertiary amine group, representative of an *N*-oxidised metabolite, also displays the corresponding loss mass shifted by 16 *m/z* units to account for the addition of the oxygen. Lay and co-workers utilised high-energy FAB-MS and FAB-CID-MS/MS to show that the losses of dimethylamine and *N,N*-dimethylhydroxylamine were observed for a series of ethylenediamine, ethanolamine and propylamine antihistamine drugs and their tertiary amine-*N*-oxides respectively.[229]   However, equivalent data under low-energy CID conditions has never been reported. To address these voids in knowledge, a library of structurally diverse commercially available pharmaceutical compounds containing dialkyl tertiary amine groups, as well as a number of model, synthetic *N*-oxides, were analysed by ESI-low-energy CID-MS/MS to gain

a greater understanding of the gas-phase ion chemistry. The acquired information allowed the development of a rapid and definitive approach for the characterisation of dialkyl tertiary amine-*N*-oxide metabolites using reconstructed ion current chromatograms (RICCs). The approach uses existing, readily available HPLC-MS/MS technology, thus allowing facile implementation. This approach could be of benefit in definitively characterising *N*-oxides early in the drug discovery process, which is important as this type of metabolite has long been recognised as being a potentially toxic species.[278]

6.2 Experimental

6.2.1 Chemicals

A library of seventy commercially available pharmaceutical compounds and model, synthetic *N*-oxides were provided by Pfizer Global Research and Development (Sandwich, UK) (The full library can be found in **Appendix 1**, **Tables A1-4**). Solutions were prepared for QqTOF-MS experiments as detailed in **Chapter 3**. The same solutions were used for the QIT-MS experiments. Solutions of amitriptyline, amitriptyline-*N*-oxide, sunitinib and sunitinib-*N*-oxide were prepared for FT-ICR-MS and solution-phase H/D exchange experiments as detailed in **Chapter 3**.

An incubation was performed in a shaking water bath at 37^oC. Tetracaine at a concentration of 10 micromolar (μM) was pre-incubated for 15 minutes with rat liver microsomes at a concentration of 0.5 μM in 50 millimolar (mM) phosphate buffer (pH 7.4). In addition, 5 mM magnesium chloride ($MgCl_2$), 5 mM isocitric acid and 1 unit mL^{-1} isocitric dehydrogenase were present in the incubation mixture. The incubation was initiated by adding 40 microlitres (μL) of 20 mM nicotinamide adenine dinucleotide phosphate ($NADP^+$). After 60 minutes, the incubation was terminated by the addition of 4 mL of cold acetonitrile. The incubate was centrifuged at 3000 revolutions per minute (rpm) for 40 minutes at 4^oC to precipitate the protein. The supernatant was removed and evaporated to dryness under nitrogen. The sample was then resuspended in

200 µL of LC-MS grade Chromasolv® acetonitrile and HPLC grade water (1:1) in preparation for analysis by QqTOF-MS.

6.2.2 Instrumental

QIT-MS experiments were performed as detailed in **Chapter 3** to acquire "in-time" low-energy CID product ion spectra. The source conditions were; sheath gas, 25 arbitrary units; auxiliary gas, 0 arbitrary units (45 arbitrary units for the solution-phase H/D exchange experiments); spray voltage, 4.5 kV; capillary voltage, 10 V; capillary temperature, 160°C; tube lens offset, - 5 V. The normalised collision energy was set to either 50% or 60% to cause complete dissociation of the precursor ion. Acquisitions were performed with WideBand activation both on and off.

QqTOF-MS experiments were performed as detailed in **Chapter 3** to acquire "in-space" low-energy CID product ion spectra. Further, full scan spectra of the tetracaine incubate were acquired by setting the collision energy to 4 eV. Low-energy CID product ion spectra were acquired at 20 eV.

FT-ICR-MS experiments were performed as detailed in **Chapter 3** to acquire AMM "in-time" low-energy SORI-CID product ion spectra of amitriptyline, amitriptyline-*N*-oxide, sunitinib and sunitinib-*N*-oxide. The ion source conditions were; capillary voltage, - 4.5 kV; end plate voltage, - 3.8 kV; capillary exit voltage, 85 V; skimmer 1, 15 V; skimmer 2, 8.5 V; Offset, 1.25; RF amplitude, 600 Hz; dry gas temperature, 250°C; dry gas flow rate, 30 arbitrary units; nebulising gas pressure, 50 psi. The excitation amplitude was 7.0 dB. Low-energy SORI-CID product ion spectra were acquired for thirty-two scans using 512K data points. The MS/MS parameters were; corr sweep pulse length, 1000 µs; corr sweep attenuation, 28.5 dB; ejection safety belt, 3000 Hz; user pulse length, 1000 µs; ion activation pulse length, 250000 µs; ion activation attenuation, 38.9 dB; frequency offset from activation mass, - 500 Hz; user delay length, 3 s.

6.3 Results and discussion

In an attempt to understand the dissociation of molecules containing dialkyl tertiary amine groups, and their corresponding *N*-oxidised analogues, a library of seventy structurally diverse commercially available pharmaceutical compounds were analysed by ESI-low-energy CID-MS/MS. **Figures 6.1a-d** show the composition of the library in terms of the nitrogen-containing groups present in the compounds analysed. The numbers of compounds containing each substructure are also shown.

a) 42   b) 16   c) 10   d) 2
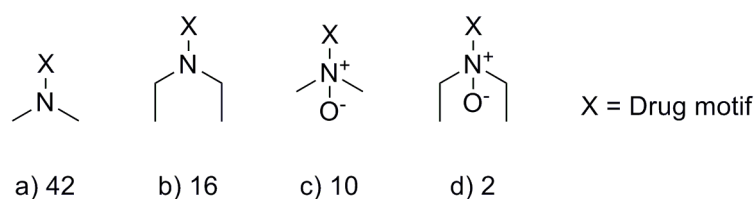
Figure 6.1   **Composition of the investigated library with respect to the nitrogen-containing groups represented. The number of each substructure type analysed are shown below the structures**

Two hypotheses were under scrutiny. The first was that the loss of the nitrogen-containing group was generic *i.e.* always observed in the low-energy CID product ion spectrum. The second was that oxidation of the dialkyl tertiary amine group did not change the dissociation behaviour of the compound *i.e.* if the loss of the nitrogen-containing group was observed for the protonated parent compound, the corresponding loss was also seen for the protonated *N*-oxidised metabolite, and *vice versa*. Low-energy CID product ion spectra were acquired using both QIT and QqTOF mass spectrometers to assess whether the dissociation was observed using both "in-time" and "in-space" MS/MS platforms. Spectra were acquired using QIT-MS with a sufficient collision energy value to fragment the entire population of protonated molecules for each compound. Using QqTOF-MS, low-energy CID product ion spectra were acquired over a range of collision energies to determine whether second-generation product ions were formed, thus allowing inferences to be drawn regarding the stability of the ions produced through the loss of the nitrogen-containing group. The results were collated and are represented in four pie

charts (**Figures 6.2a-d**; relatives abundances for the relevant loss from each compound under the various experimental conditions can be found in **Appendix 1**, **Tables A5-8**).
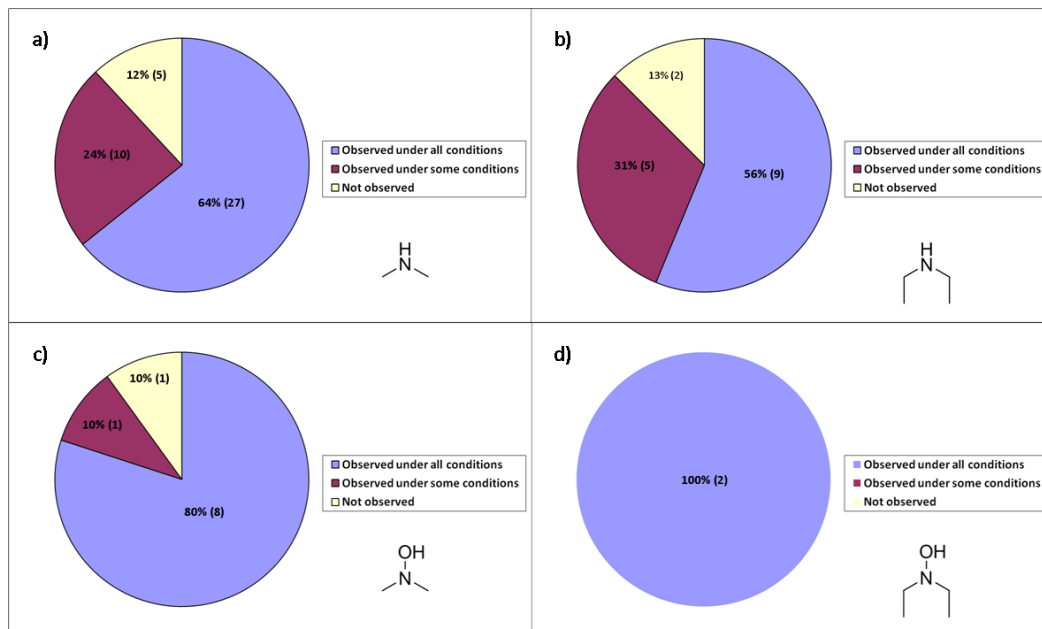
Figure 6.2   **Frequency of the losses of interest in percentage terms. Absolute numbers of compounds are shown in parentheses. The pie charts represent the following losses, as denoted by the molecular structures shown; a) dimethylamine; b) diethylamine; c) *N,N*-dimethylhydroxylamine; d) *N,N*-diethylhydroxylamine**

Figure 6.2a shows that 64% of the compounds containing a dimethylamine substructure showed the loss of this group at all collision energies utilised. Further, the loss of dimethylamine was observed at some of the collision energies, but not all, for 24% of the compounds. A smaller number of the compounds, 12%, did not display the loss of dimethylamine despite containing the necessary substructure to facilitate it. Similar percentages were observed for the equivalent bins for the compounds that could lose diethylamine and *N,N*-dimethylhydroxylamine (**Figures 6.2b-c**).   The loss of *N,N*-diethylhydroxylamine was observed at all collision energies utilised for both compounds containing this group (**Figure 6.2d**). Although not analytically rigorous due to the small size of the subset, the data gives an indication that the loss of *N,N*-diethylhydroxylamine can be observed for the *N*-oxides of

pharmaceutical compounds containing a diethylamine substituent. AMMs were acquired using FT-ICR-MS to confirm the identities of the losses. Amitriptyline, amitriptyline-*N*-oxide, sunitinib and sunitinib-*N*-oxide were selected as test analytes to represent each subsection of the library. The greatest MME recorded for the four losses was 0.6 ppm, giving confidence that they had been correctly assigned.

A number of conclusions can be drawn from the results of the library analysis. Combining the four subsets of data shows that the loss of the nitrogen-containing group is observed in 89% of the low-energy CID product ion spectra under all or some of the experimental conditions used. Thus, the loss of dialkyl tertiary amine groups and their *N*-oxidised analogues will be observed a vast majority of the time for compounds containing these substructures, and can thus be considered generic. Further, using the low-energy CID product ion spectra for the compounds for which a model, synthetic *N*-oxide was available, it was possible to determine that the dissociation was not altered by the oxidation. All of the pairs of compounds of this nature that were considered showed the loss of the dialkyl tertiary amine group as well as the corresponding oxidised substructure, with the exception of diphenhydramine and diphenhydramine-*N*-oxide. This compound did not show loss of either nitrogen-containing group. The coverage of pairs of compounds for which the losses of interest were observed for either both or neither of the compounds, but not only for one, lends support to the conclusion that oxidation does not change the dissociation behaviour. Finally, comparison of the "in-time" and "in-space" MS/MS datasets suggested that second-generation dissociation takes place. When the loss of interest was observed at only certain collision energies, the absence was generally at higher collision energies using the QqTOF mass spectrometer (see **Appendix 1**, **Tables A5-8**). Further, there was a general trend of decreasing relative abundance as the collision energy was increased, again using QqTOF-MS. These observations suggest that the product ions are formed, as evinced by their recording at lower collision energies, but are sufficiently unstable that an increase in collision energy causes their decomposition. This

conclusion is supported by the observation that the relative abundances of the product ions formed through the losses of interest were generally greater using QIT-MS compared to QqTOF-MS. As fragmentation is effected by resonant excitation using QIT-MS,[95] the product ions can not undergo second-generation dissociation, regardless of their susceptibility to further decomposition. Thus, they survive to detection. The higher relative abundances using QIT-MS are hence consistent with the explanation that the product ions of interest are formed *via* favourable fragmentation pathways under low-energy CID conditions, but a significant proportion of the ions undergo second-generation dissociation using QqTOF-MS.

To understand the dissociation further, a mechanism was proposed and tested using solution-phase H/D exchange experiments. **Figure 6.3** shows a generalised mechanism that covers the range of structures present in the library.
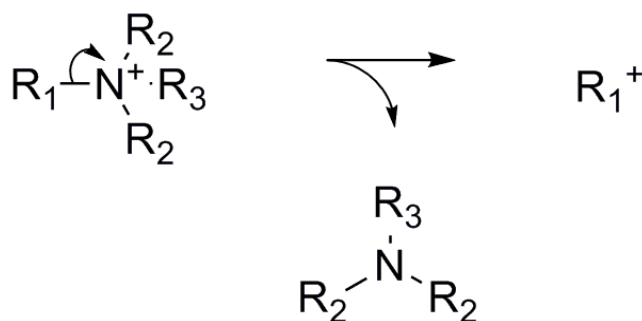
where: R_1 = Remainder of precursor ion
          R_2 = 2 x CH_3 or 2 x C_2H_5
          R_3 = H or OH

Figure 6.3   Generalised proposed mechanism for the loss of the nitrogen-containing group

The mechanism proposed protonation at the tertiary amine nitrogen or the oxygen atom of the *N*-oxide group. This is a reasonable assumption given the high solution-phase basicity of these atoms. Protonation at these sites was

proposed to lead to charge-directed inductive cleavage of the R-N bond, thus causing the loss of the nitrogen-containing group as a neutral molecule. Thus, involvement of a single exchangeable hydrogen atom would mean that if the mechanism were correct, the loss of interest should increase by 1 *m/z* unit under deuterated conditions. The proposed mechanism is also consistent with the observation of second-generation dissociation. For a large proportion of the library, the nitrogen-containing group was bonded initially to the rest of the molecule *via* a methylene group. Thus, cleavage of the C-N bond would produce a primary carbocation; an unstable species that would be susceptible to further dissociation. Amitriptyline, amitriptyline-*N*-oxide, sunitinib and sunitinib-*N*-oxide were selected as test analytes from each sub-section of the library to probe the hypothesised mechanism. The first-generation low-energy CID product ion spectra acquired using QIT-MS are shown in **Figure 6.4**.
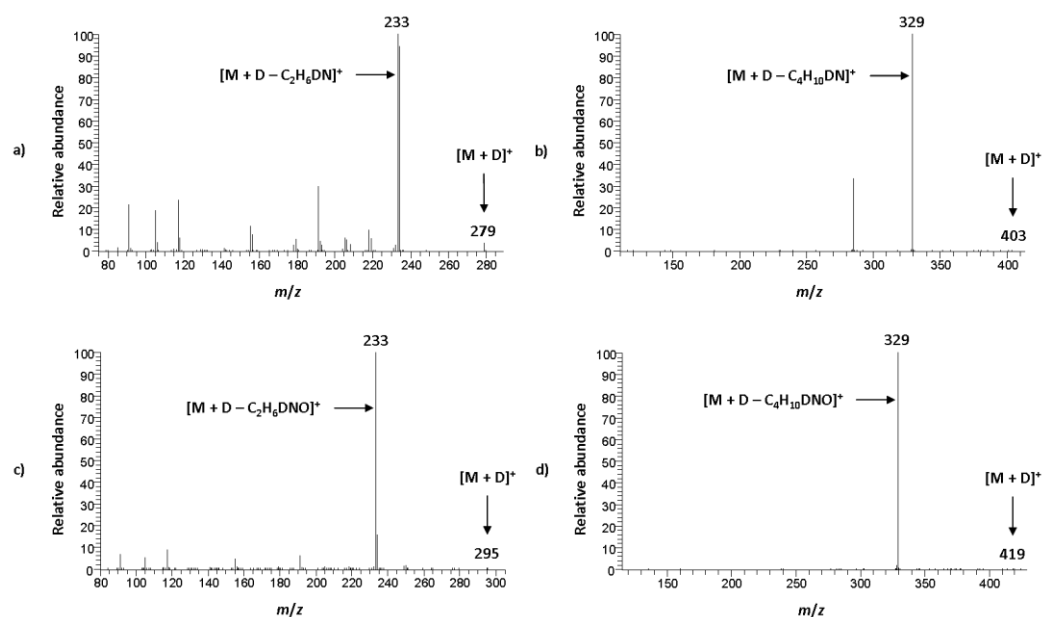
Figure 6.4   **First-generation low-energy CID product ion spectra of a) deuterated amitriptyline (*m/z* 279); b) fully exchanged, deuterated sunitinib (*m/z* 403); c) deuterated amitriptyline-*N*-oxide (*m/z* 295); d) fully exchanged, deuterated sunitinib-*N*-oxide (*m/z* 419) acquired using a LCQ Classic QIT mass spectrometer with WideBand activation on**

All four compounds demonstrated an increase in the mass of the neutral loss by 1 *m/z* unit compared to that observed in protic solvents. Thus, the low-energy

CID product ion spectra indicated that one exchangeable hydrogen atom is involved in the loss, and are hence supportive of the proposed mechanism. The understanding of the mechanism allows a rationalisation for the absence of the loss of the nitrogen-containing group for some of the compounds analysed to be postulated. The loss requires protonation at either the nitrogen or the oxygen atom, depending upon the character of the nitrogen-containing group, and does not appear to be facilitated by the shift of a non-exchangeable hydrogen atom. So, if the compound does not protonate at the nitrogen-containing group, its loss will not be observed in the resultant low-energy CID product ion spectrum. Thus, the compounds that did not show the loss of the nitrogen-containing group may preferentially protonate elsewhere on the molecule. Molecular modelling experiments would allow calculation of gas-phase proton affinities for the different sites of protonation on each compound not showing the loss of the nitrogen-containing group. This would determine the likelihood of protonation at the nitrogen or oxygen atom relative to other possible sites of ionisation. Thus, deductions could be made as to whether the necessary precursor ions exist in the population of protonated molecules to facilitate the loss of the nitrogen-containing group for each compound. Previous studies have shown that computational calculations at the DFT level can be a useful tool to determine the gas-phase proton affinities of analytes and rationalise fragmentation under low-energy CID conditions.[230, 265, 279] However, such an in-depth study is beyond the scope of the presented work.

At this juncture, an understanding of the fragmentation of pharmaceutical compounds containing dialkyl tertiary amine groups and their *N*-oxidised metabolites under low-energy CID conditions has been established. It appears that the losses of *N*,*N*-dimethylhydroxylamine and *N*,*N*-diethylhydroxylamine can be diagnostic for oxidised dialkyl tertiary amine groups. The losses are particularly useful in the context of characterising pharmaceutical drug metabolites because they are both of reasonably high mass (61 and 89 *m/z* units). Thus, the likelihood of a false positive result *i.e.* characterising a mono-oxidised metabolite as a dialkyl tertiary amine-*N*-oxide when the site of

oxidation is elsewhere on the molecule, is reduced compared to using a lower mass loss.

The diagnostic loss can be integrated into a data interpretation approach that allows rapid and definitive characterisation of dialkyl tertiary amine-*N*-oxides. This methodology could be of benefit to metabolite identification scientists, as data interpretation is a recognised bottleneck to high-throughput studies.[178] The approach is demonstrated below using the QqTOF mass spectrometer with tetracaine as a test analyte (**Figure 6.5**), which was incubated with rat liver microsomes to produce phase I metabolites. This compound was selected because it contains two possible sites for *N*-oxidation.
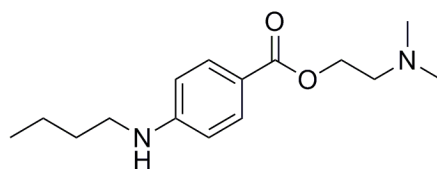
Figure 6.5   **Molecular structure of tetracaine**

Using the tools described in **Chapter 2**, an *N*-oxidised metabolite could be rapidly identified. However, none of the approaches, apart from the difficult to implement ion-molecule reactions, would determine whether the secondary or tertiary amine had been oxidised. Using the methodology described below, rapid and definitive characterisation is possible by incorporating the structurally dependent dissociation behaviour that is known to be diagnostic of dialkyl tertiary amine-*N*-oxides but not secondary amines. A positive result would indicate that the parent compound has been oxidised at the dialkyl tertiary amine. From a negative result, an analyst could infer that the site of oxidation is the secondary amine. Although the approach is described using an "in-space" MS/MS platform, it is equally applicable to a mass spectrometer that performs "in-time" MS/MS.

The approach requires a dual scan mass spectrometric experiment, which the instrument alternates between throughout the analysis. The first scan involves

the acquisition of a full scan mass spectrum. This will record all of the species produced from the ESI ion source at that time point within the mass range employed, including any protonated mono-oxidised metabolites of tetracaine in this example. Combination of all of the full scan mass spectra acquired throughout the analysis produces a total ion current chromatogram (TICC) (**Figure 6.6a**). The second scan is a product ion scan MS/MS experiment. This scan involves dissociating all or some of the precursor ions entering the mass spectrometer, either using an MS^E experiment[280] or data-dependent acquisition (DDA).[281] An MS^E experiment was performed to acquire the presented data. The second scan allows structural information about the precursor ions, such as the metabolites of tetracaine in the exemplar, to be derived. Thus, another TICC, this time of the low-energy CID product ion spectra, is produced (**Figure 6.6b**). The TICCs are used to characterise any dialkyl tertiary amine-*N*-oxides present by extracting the ion current related to specific *m/z* values of interest *i.e.* forming RICCs. From the full scan TICC, the *m/z* value related to the protonated molecule of the parent compound is extracted; *m/z* 265 in the case of tetracaine (**Figure 6.6c**). This RICC provides useful information about the retention time of the protonated parent compound. Another RICC is constructed from the full scan TICC by extracting the ion current related to the *m/z* value of [M + H + 16 *m/z* unit]$^+$, which for tetracaine is *m/z* 281. This trace (**Figure 6.6d**) shows peaks for all of the protonated mono-oxidised metabolites, plus any nominally isobaric species. The RICC in **Figure 6.6d** shows a peak eluting just after the protonated parent compound (**Figure 6.6c**) at 5.12 minutes. An analyst may assign this chromatographic peak as an *N*-oxide based upon its elution after the protonated parent compound. However, it is not possible to determine whether the secondary or tertiary amine has been oxidised using just the RICC in **Figure 6.6d**. To achieve this, the analyst would have to interrogate the low-energy CID product ion spectra related to the chromatographic peak; a potentially time-consuming process. A faster approach to determining the site of oxidation would be to use the product ion scan TICC to create an RICC. From the product ion scan TICC, the *m/z* value related to the diagnostic loss from the relevant dialkyl tertiary amine-*N*-oxide
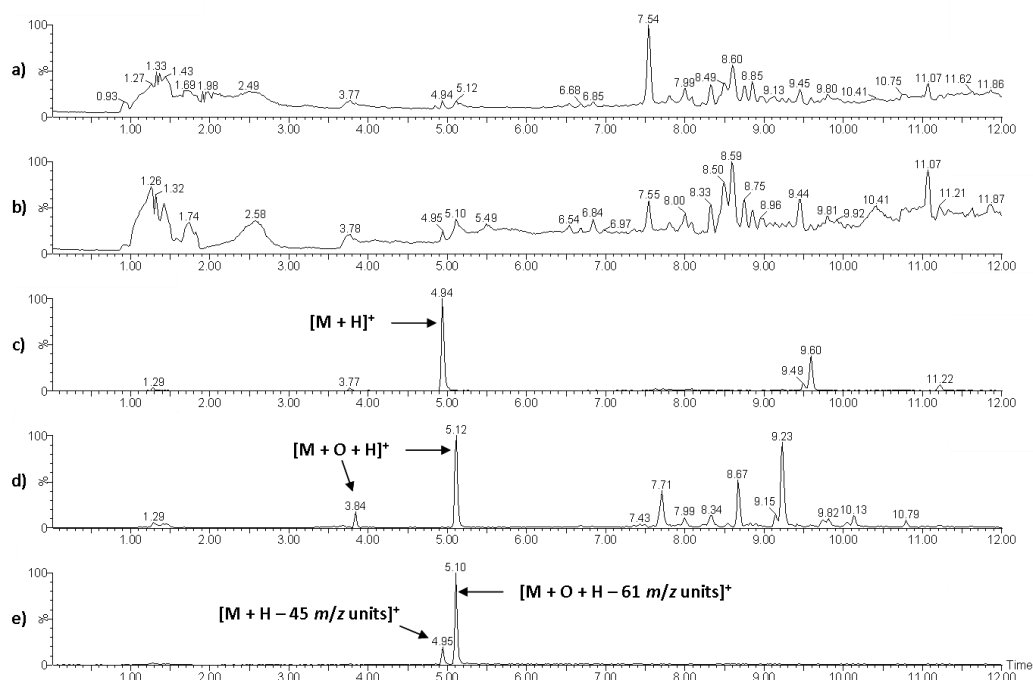
Figure 6.6 **Total ion current chromatograms (TICCs) and reconstructed ion current chromatograms (RICCs) acquired using a Premier QqTOF mass spectrometer; a) Full scan TICC; b) Product ion scan TICC; c) RICC of *m/z* 265 from full scan TICC; d) RICC of *m/z* 281 from full scan TICC; e) RICC of *m/z* 220 from product ion scan TICC**

for the compound under investigation is extracted. In the case of tetracaine, this is *m/z* 220 due to the loss of *N,N*-dimethylhydroxylamine from the oxidised dialkyl tertiary amine substructure. The resultant trace shows two chromatographic peaks (**Figure 6.6e**). The peak at 5.10 minutes aligns with that of the protonated mono-oxidised metabolite at 5.12 minutes. Because the *m/z* value selected is known to relate to diagnostic dissociation behaviour, this peak can be definitively assigned as a dialkyl tertiary amine-*N*-oxide. The second peak in the RICC is due to the same *m/z* value being observed in the low-energy CID product ion spectrum of the protonated parent compound. This signal is important because it confirms that the loss of the nitrogen-containing group is observed for the protonated parent compound. As detailed above, the data indicated that the loss or retention of the dialkyl tertiary amine group by the protonated parent compound is accompanied by equivalent dissociation behaviour for the nitrogen-containing group of the protonated dialkyl tertiary amine-*N*-oxide metabolite. Therefore, the presence of a chromatographic peak

for the protonated parent compound in the product ion scan RICC proves that the loss of the nitrogen-containing group will be observed for the dialkyl tertiary amine-*N*-oxide if it is present in the sample. Thus, if no chromatographic peak in the product ion scan RICC aligns with a chromatographic peak of a protonated mono-oxidised metabolite from the full scan RICC, an analyst can conclude that the metabolite is not formed. The alternative conclusion, that the dialkyl tertiary amine-*N*-oxide is formed but the diagnostic loss is not observed in its low-energy CID product ion spectrum, can be excluded if a chromatographic peak is observed in the product ion scan RICC for the protonated parent compound. In addition, the absence of a chromatographic peak that aligns with a protonated mono-oxidised metabolite, accompanied by the absence of a chromatographic peak for the protonated parent compound, would indicate that a dialkyl tertiary amine-*N*-oxide may have been formed but that it could not be characterised using the discussed approach. This would be the case for diphenhydramine because the loss of the nitrogen-containing group was observed for neither the parent compound nor the *N*-oxide metabolite.

6.4   Conclusions

A rapid and definitive methodology for the characterisation of dialkyl tertiary amine-*N*-oxides has been developed. The approach builds upon the understanding of the fragmentation behaviour under low-energy CID conditions of protonated dialkyl tertiary amines gained through the analysis of a structurally diverse library of commercially available pharmaceutical compounds. The analyses showed that the loss of the nitrogen-containing group occurred in 89% of the low-energy CID product ion spectra, suggesting that the dissociation behaviour was generic. Further, the product ions formed were demonstrated to be relatively unstable due to the observation of second-generation dissociation using QqTOF-MS. The increased understanding of low-energy CID and gas-phase ion chemistry could be of use to developers on *in silico* packages for fragmentation prediction by allowing them to create more robust algorithms and models upon which the programs work. Further, the

increased understanding of low-energy CID and gas-phase ion chemistry could be useful to mass spectrometrists interested in structural elucidation.

The methodology for the characterisation of dialkyl tertiary amine-*N*-oxides overcomes the limitation of other tools for *N*-oxide identification by utilising dissociation behaviour that was shown to be diagnostic for a particular structural motif. This allowed discrimination between potential sites of oxidation in different chemical environments in a mono-oxidised metabolite of tetracaine. The approach is a high-throughput method because it removes the need for the analyst to interrogate the low-energy CID product ion spectrum of the metabolite, which reduces the data interpretation time. The process could be automated, thus further decreasing the time taken. The methodology is better suited to trap-configured mass spectrometers due to the greater ion current observed for the product ions of interest using QIT-MS. However, with prudent selection of collision energy, it is amenable to collision cell-configured instruments, as evinced by the example of tetracaine on the QqTOF mass spectrometer. Thus, the approach is low-energy CID-MS/MS platform independent and hence has scope for wide employment.

The methodology is not applicable for the characterisation of all dialkyl tertiary amine-*N*-oxides because of the absence of the diagnostic loss in its low-energy CID product ion spectrum *e.g.* diphenhydramine-*N*-oxide. In this circumstance, full interpretation of the low-energy CID product ion spectrum would be required to localise the site of oxidation. However, attempting the RICC approach is not detrimental to throughput because full interpretation of the low-energy CID product ion spectrum is the method currently used for metabolite identification.

Chapter 7

Evidence for site-specific intra-ionic hydrogen/deuterium exchange in the low-energy collision-induced dissociation product ion spectra of protonated small molecules generated by electrospray ionisation

7.1 Introduction

The use of isotopic labelling in structural elucidation studies and the rationalisation of dissociation mechanisms is a well-established approach in MS.[282, 283] The use of solution-phase H/D exchange is particularly common due to the ease with which the number of exchangeable hydrogen atoms involved in a dissociation can be determined.[284]

It is known that isomerisation of activated ions in the gas phase, leading to "scrambling" of the isotopic labels, can occur *i.e.* transfer of the isotopic label from its original location in the ion to another position.[285] This observation has been documented extensively for ions formed by the highly energetic processes that take place in EI. Under these conditions, randomisation of alkyl and aromatic hydrogen and carbons atoms has been detailed.[286-295] However, very few reports of scrambling under low-energy CID conditions exist for protonated small molecules formed by ESI.[296-299] Herein, an example of site-specific intra-ionic H/D exchange in the gas phase for protonated molecules generated by ESI is detailed. This example of ion-chemistry could be used to introduce an isotopic label into the carbon skeleton of a molecule without the need to produce an analogue synthetically.

7.2 Experimental

7.2.1 Chemicals

Amiodarone, amitriptyline, amitriptyline-*N*-oxide, benzydamine, cinchocaine, cinchocaine-*N*-oxide, chlorphenamine, chlorpromazine, a tri-oxidised chlorpromazine metabolite, a di-oxidised fluorinated chlorpromazine analogue, chloroquine, dibenzepin, dicycloverine, doxepin, hydroxychloroquine, levomepromazine, metoclopramide, nordoxepin, promethazine, protriptyline, sunitinib and sunitinib-*N*-oxide were provided by Pfizer Global Research and Development (Sandwich, UK). Hexylamine was purchased from Sigma-Aldrich Company Ltd. (Gillingham, UK). Solutions were prepared for QIT-MS and solution-phase H/D exchange experiments as detailed in **Chapter 3**. A solution of amitriptyline was prepared for FT-ICR-MS experiments as detailed in **Chapter 3**. Further solutions of amitriptyline were prepared at 100 ng mL^{-1} in LC-MS grade methanol and analytical grade methanoic acid [99.9:0.1, v/v] for QqQ-MS experiments and at 10 mg mL^{-1} in both >99.5% deuterated methanol and 99.5% deuterated methanoic acid [99.9:0.1, v/v], and >99.9% deuterated acetone (Apollo Scientific Ltd., Stockport, UK) for NMR spectroscopy experiments.

7.2.2 Instrumental

QIT-MS experiments were performed as detailed in **Chapter 3** to acquire "in-time" low-energy CID product ion spectra. The ion source conditions were; sheath gas, 25 arbitrary units; auxiliary gas, 0 arbitrary units (45 arbitrary units for the solution-phase H/D exchange experiments); spray voltage, 4.5 kV; capillary voltage, 10 V; capillary temperature, 160°C; tube lens offset, - 5 V. Low-energy CID product ion spectra were acquired using an isolation width of 1 *m/z* unit and with WideBand activation on. The normalised collision energy was set to 50%, except for the analyses of amiodarone (60%) and hexylamine (45%).

"In-space" low-energy CID product ion spectra of amitriptyline were acquired using a Xevo TQMS QqQ mass spectrometer (Waters Ltd., Elstree, UK). Positive ion ESI-MS/MS was performed by infusing the solutions directly into the nano-

ESI ion source at a constant flow rate of 0.25 μL min^{-1}. Nitrogen was used as the cone, purge and nanoflow gas. The ion source conditions were as follows; cone gas flow; 0 L hr^{-1}; purge gas flow, 0 L hr^{-1}; nanoflow gas flow, 0.1 bar; capillary voltage, 1.5 kV; sampling cone, 30 V; extraction cone, 3 V; source temperature, 70 ^{o}C. Low-energy CID product ion spectra were acquired at a collision energy of 25 eV using argon as the collision gas. Acquisitions were performed for twenty scans. The scan time was 0.5 s and the interscan time was 0.005 s. Data acquisition was performed using MassLynx version 4.1 (Waters Ltd., Elstree, Herts., UK).

FT-ICR-MS experiments were performed as detailed in **Chapter 3** to acquire an AMM "in-time" low-energy SORI-CID product ion spectrum of amitriptyline. The ion source conditions were; capillary voltage, - 4.5 kV; end plate voltage, - 3.8 kV; capillary exit voltage, 85 V; skimmer 1, 15 V; skimmer 2, 8.5 V; Offset, 1.25; RF amplitude, 600 Hz; dry gas temperature, 250°C; dry gas flow rate, 30 arbitrary units; nebulising gas pressure, 50 psi. The excitation amplitude was 7.0 dB. A low-energy SORI-CID product ion spectrum was acquired for thirty-two scans using 512K data points. The MS/MS parameters were; corr sweep pulse length, 1000 μs; corr sweep attenuation, 28.5 dB; ejection safety belt, 3000 Hz; user pulse length, 1000 μs; ion activation pulse length, 250000 μs; ion activation attenuation, 38.9 dB; frequency offset from activation mass, - 500 Hz; user delay length, 3 s.

Proton (^{1}H) NMR spectra were recorded using a DPX-400 (Bruker, Coventry, UK) at 298 K. Chemical shifts for the ^{1}H spectra are reported on the δ scale in ppm and were referenced to residual solvent references. All coupling constants (*J* values) are reported in Hz. Amitriptyline in deuterated acetone; δH (400 MHz) 7.33-7.06 (m, 8H, aromatic H), 5.91 (t, 1H, *J* = 7.3), other peaks obscured by water signal at 3.13. Amitriptyline in deuterated methanol and deuterated methanoic acid; δH (400 MHz) 7.30-7.05 (m, 8H, aromatic H), 5.83 (t, 1H, *J* = 7.3), 3.25 (t, 2H, *J* = 7.8), 2.81 (s, 6H), 2.59 (dt, 2H, *J* = 7.3), other peaks obscured by background signal.

7.3   Results and discussion

The experimental data presented in **Chapter 6** showed that under low-energy CID conditions, dialkyl tertiary amine-containing compounds frequently display the loss of dimethylamine in their product ion spectra.   Solution-phase H/D exchange experiments were conducted to determine the number of exchangeable hydrogen atoms involved in this loss.   During these experiments, intra-ionic H/D exchange was noted upon comparison of the low-energy CID product ion spectra of protonated amitriptyline and deuterated amitriptyline acquired using QIT-MS (**Figure 7.1**).   Similar observations were made for the structurally similar compounds in **Compound set 1**; doxepin and nordoxepin (**Figures 7.2-7.4**).   Based upon the hypothesis that the deuteron is localised on the nitrogen atom in solution (a reasonable assumption given the high solution-phase basicity of the lone pair of electrons on the nitrogen atom relative to the delocalised π-electrons), it would be expected that the loss of dimethylamine would involve the deuteron *i.e.* a loss of deuterodimethylamine (46 *m/z* units) would be observed.   However, dissociation of the deuterated molecule of amitriptyline generates product ions formed through the losses of both dimethylamine (*m/z* 234) and deuterodimethylamine (*m/z* 233).   Further, the other annotated product ions in **Figure 7.1a** appeared to undergo intra-ionic H/D exchange.   This is indicated by the presence of pairs of peaks along the mass scale under deuterated conditions of similar abundance relative to one another as those observed at *m/z* 233 and 234.   These observations suggested that intra-ionic H/D exchange takes place prior to fragmentation when the precursor ion is activated under low-energy CID conditions. Low-energy CID product ion spectra of protonated and deuterated amitriptyline were also acquired using QqQ-MS.   The resultant spectra show the same dissociation patterns (**Figure 7.5**).   This demonstrated that there was no involvement from possible traces of water present in the helium buffer gas used in the QIT-MS, which would affect the dissociation of ions using these types of instrument.[300] Interferences from water could lead to some of the mass isolated deuterated molecules of amitriptyline being converted to protonated molecules prior to
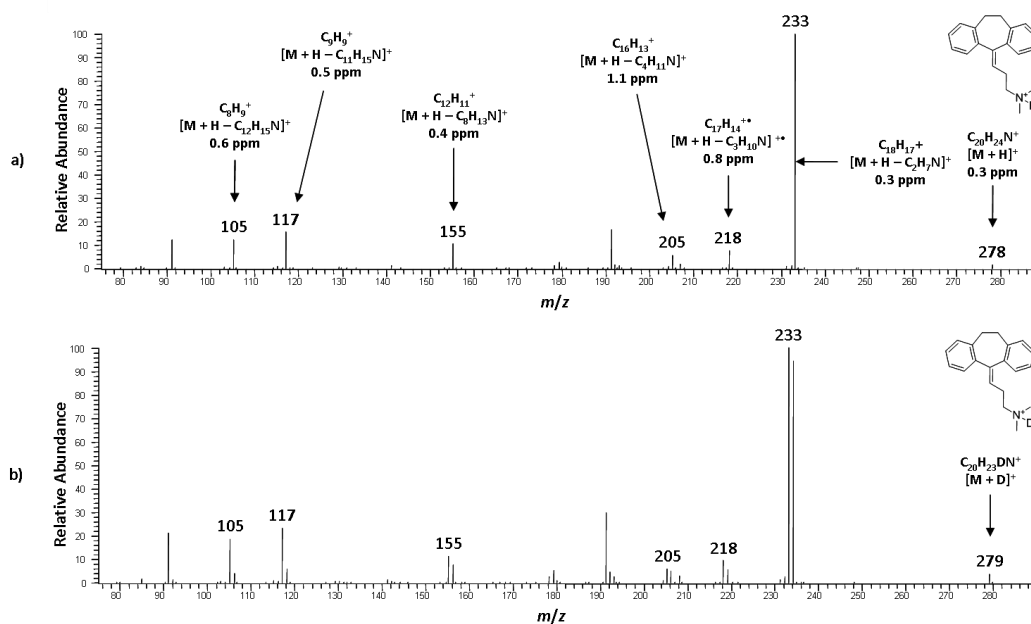
Figure 7.1 First-generation low-energy CID product ion spectra of a) protonated amitriptyline (*m/z* 278) and b) deuterated amitriptyline (*m/z* 279) acquired using a LCQ Classic QIT mass spectrometer with WideBand activation on. AMMs were acquired using an Apex III FT-ICR mass spectrometer

Doxepin   Nordoxepin
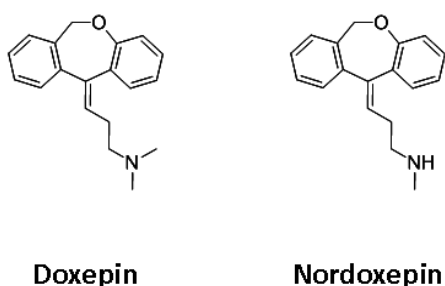
Figure 7.2 Molecular structures in Compound set 1

dissociation. This would explain the losses of both dimethylamine and deuterodimethylamine. However, the observation of the same losses using a beam-type instrument, where no interference from water is likely to occur, lends support to the hypothesis of intra-ionic H/D exchange. The observation of intra-ionic H/D exchange using QqQ-MS also ruled out the involvement of an ion-neutral complex in the transfer of the deuterium label. Extended time frames, such as those afforded by the millisecond activation times utilised during low-energy CID using QIT-MS, are required to facilitate the formation of ion-neutral complexes. Conversely, the microsecond time frame available for
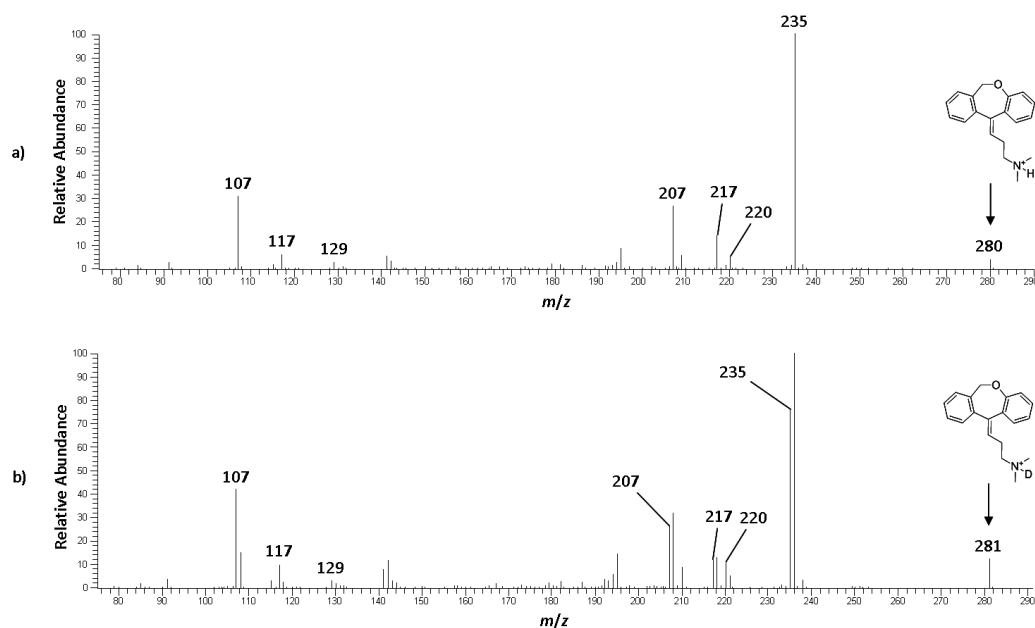
Figure 7.3 First-generation low-energy CID product ion spectra of a) protonated doxepin (*m/z* 280) and b) deuterated doxepin (*m/z* 281) acquired using a LCQ Classic QIT mass spectrometer with WideBand activation on
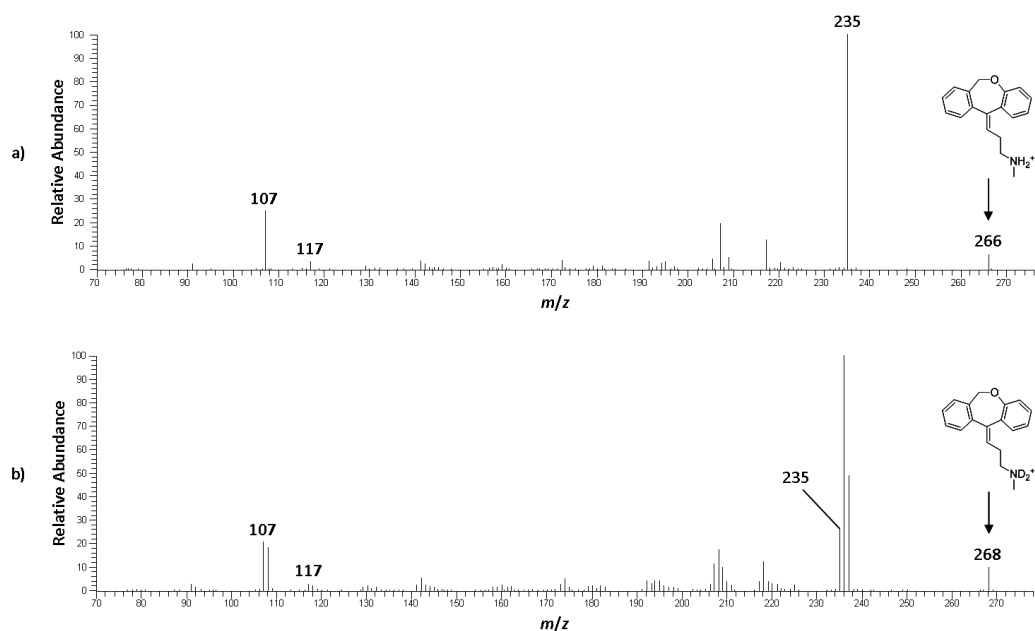
Figure 7.4 First-generation low-energy CID product ion spectra of a) protonated nordoxepin (*m/z* 266) and b) fully exchanged, deuterated nordoxepin (*m/z* 268) acquired using a LCQ Classic QIT mass spectrometer with WideBand activation on

ion activation during low-energy CID on QqQ mass spectrometers does not allow their formation.[301]   Therefore, as the intra-ionic H/D exchange is seen irrespective of the time available for ion activation, it can be concluded that an ion-neutral complex does not facilitate the isomerisation that is observed.
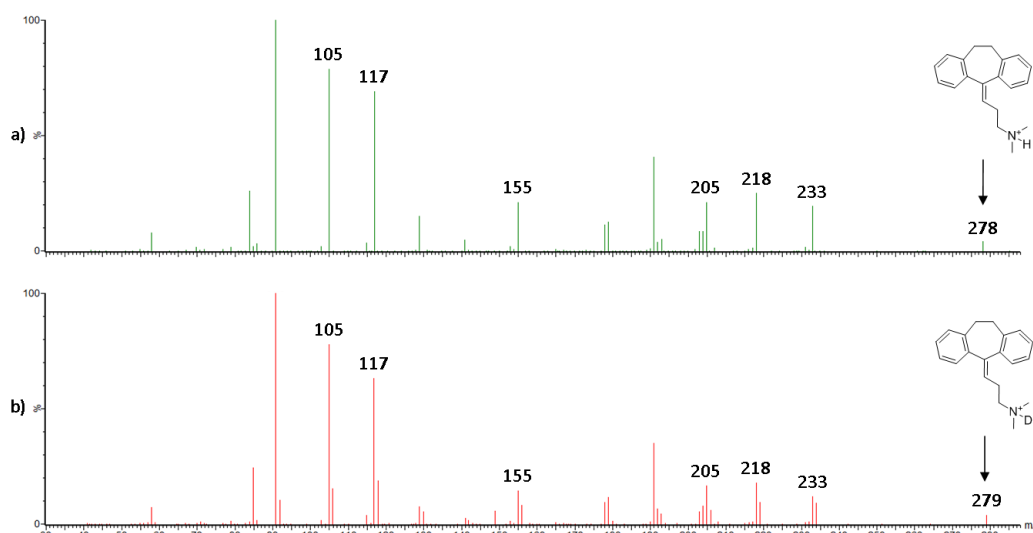
Figure 7.5   **Product ion spectra of a) protonated amitriptyline (*m/z* 278) and b) deuterated amitriptyline (*m/z* 279) acquired using a Xevo TQMS QqQ mass spectrometer**

Two alternative hypotheses were considered and excluded.   The first postulation was that the peak at *m/z* 234 was formed through the loss of dimethylamine from the ^{13}C-isotopologue of the protonated molecule of amitriptyline.   This hypothesis was discounted because a high auxiliary gas pressure (45 arbitrary units) was utilised to prevent back-exchange in the gas phase.[296]   This led to a low intensity of protonated amitriptyline relative to deuterated amitriptyline (9%:100%) being observed in the full scan mass spectrum (data not shown).   Thus, the contribution of the ^{13}C-isotopologue of protonated amitriptyline to the isolated precursor ion signal at *m/z* 279 was deemed negligible.   Further, it was concluded that any ^{13}C-isotopologue of protonated amitriptyline present would provide insufficient ion current to be exclusively responsible for the product ion intensity at *m/z* 234, particularly given that some of the ion current would be distributed through the other dissociation pathways that exist for amitriptyline.   The second hypothesis was

that two losses of dimethylamine took place; one facilitated by the ionising proton and one involving the shift of a non-exchangeable hydrogen atom. This postulation was consistent with the experimental observations under deuterated conditions. The loss involving the non-exchangeable hydrogen atom would remain as 45 *m/z* units whilst the ionising deuteron would cause the second loss to become 46 *m/z* units. This hypothesis would require a heterogeneous population of protonated molecules to be produced by the ESI ion source. Some of the members of the population would be protonated at the nitrogen atom to facilitate the loss involving an exchangeable hydrogen atom. Other members of the population would be ionised at a site other than the nitrogen atom to allow the loss involving a non-exchangeable hydrogen atom. Ion mobility spectrometry (IMS) experiments have shown that small molecules ionised by ESI can protonate at more than one site.[42] Thus, this hypothesis could not be completely excluded on the basis of the experimental data obtained through the analysis of amitriptyline. However, it was deemed less likely than the intra-ionic H/D exchange hypothesis due to the absence of a second heteroatom in the structure of amitriptyline to provide a plausible site of protonation under ESI conditions. Hence, the most logical rationalisation was intra-ionic H/D exchange in the gas phase prior to dissociation.

The hypothesis of intra-ionic H/D exchange was investigated further by conducting NMR spectroscopy measurements in deuterated solvents. The experiments were undertaken to determine whether intra-ionic H/D exchange took place in solution. Two samples were prepared; one in solvents with acidic deuterons *i.e.* deuterated methanol and deuterated methanoic acid, and one without *i.e.* deuterated acetone. Given that the *pK$_a$* of amitriptyline is 9.4,[302] the ionised form of the compound, by virtue of deuteration, would exist in the sample in deuterated methanol and deuterated methanoic acid. Thus, intra-ionic H/D exchange was feasible. The sample in deuterated acetone acted as a control because amitriptyline would not be ionised through deuteration due to the absence of acidic deuterons in the solvent. Thus, the amitriptyline would exist as the free base and no intra-ionic H/D exchange would be possible.

Comparison of the signals in the two ^{1}H NMR spectra suggested that all of the hydrogen atoms were localised on the carbon skeleton of amitriptyline in solution, regardless of whether the solvents contained acidic deuterons or not. This observation supports the hypothesis of intra-ionic H/D exchange taking place in the gas phase.

Further investigations were undertaken using FT-ICR-MS. AMMs were acquired and indicated that all of the product ions thought to undergo transfer of the deuterium label involve the loss of the nitrogen atom during their formation (**Figure 7.1a**). Concurrent loss of the deuterium atom would be expected if intra-ionic H/D exchange did not take place, assuming that the deuteron was localised on the nitrogen atom. However, the AMMs added confidence to the hypothesis that the deuterium atom was inserted into the carbon skeleton of the molecule *via* intra-ionic H/D exchange prior to dissociation.

A sample of amitriptyline-*N*-oxide was analysed to determine the effect that a different site of ionisation would have on the intra-ionic H/D exchange. For this compound, ionisation would be expected to take place at the oxygen of the *N*-oxide substructure *c.f.* the nitrogen atom of amitriptyline. The spectra in **Figure 7.6** show that intra-ionic H/D exchange of the deuterium atom does take place, although to a lesser extent than for amitriptyline.

The observation of intra-ionic H/D exchange for the compounds analysed led to the question of whether the proposed exchange is site-specific, or whether complete randomisation of all of the hydrogen and deuterium atoms takes place. It was hypothesised that the exchange involves the γ-hydrogen relative to the nitrogen atom. To determine whether the intra-ionic H/D exchange is facilitated by the γ-hydrogen relative to the nitrogen atom, and is thus site-specific, first-generation low-energy CID product ion spectra of dibenzepin and promethazine were acquired (**Compound set 2, Figure 7.7**). These compounds lack a γ-hydrogen relative to the nitrogen atom and do not exhibit intra-ionic H/D exchange (**Figures 7.8-7.9**). This suggested that the intra-ionic H/D
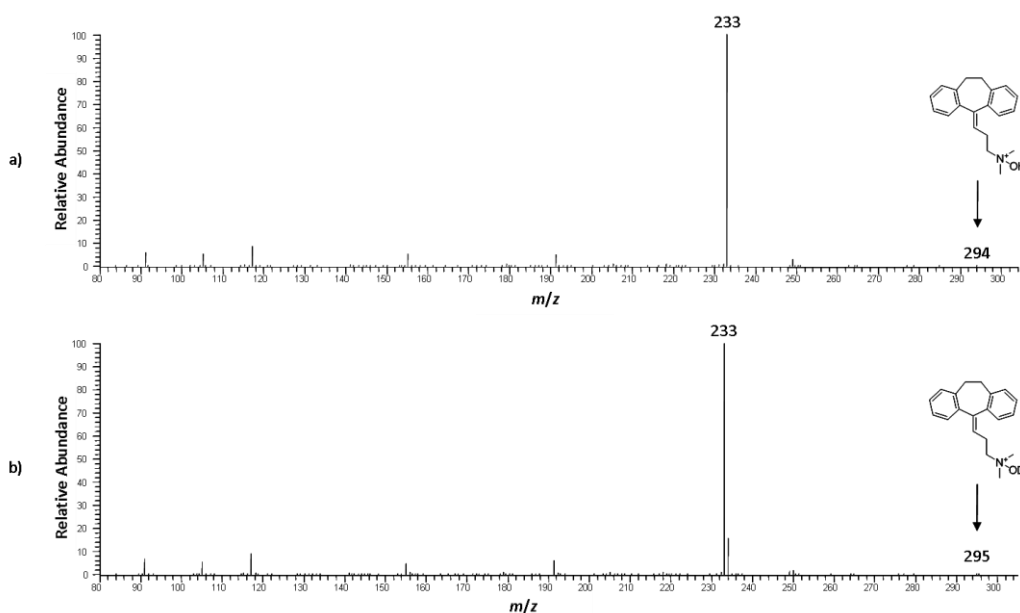
Figure 7.6 **First-generation low-energy CID product ion spectra of a) protonated amitriptyline-*N*-oxide (*m/z* 294) and b) deuterated amitriptyline-*N*-oxide (*m/z* 295) acquired using a LCQ Classic QIT mass spectrometer with WideBand activation on**

exchange is dependent upon the presence of a γ-hydrogen relative to the nitrogen atom, and thus is site-specific. By extension, this excluded the exchanged hydrogen atom in amitriptyline and amitriptyline-*N*-oxide from being originally located on the α, β or aromatic carbon atoms. If any of the hydrogen atoms at these sites were exchanged, analogous behaviour would be expected of dibenzepin and promethazine. The combination of observations thus far leads to the conclusions that the intra-ionic H/D exchange is site-specific, requiring a γ-hydrogen relative to the nitrogen atom, and takes place in the gas phase. The NMR spectroscopy measurements support the final conclusion by showing that the alkene hydrogen atom to aromatic hydrogen atom signal ratio
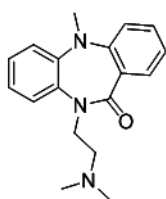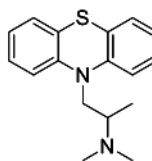
Dibenzepin   **Promethazine**

Figure 7.7   **Molecular structures in Compound set 2**
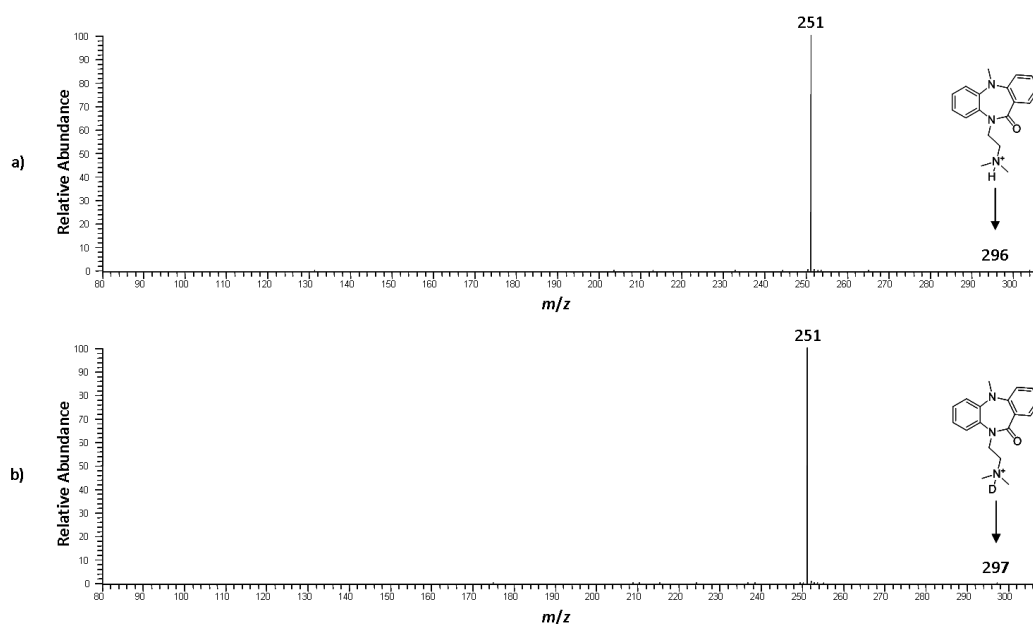
Figure 7.8 First-generation low-energy CID product ion spectra of a) protonated dibenzepin (*m/z* 296) and b) deuterated dibenzepin (*m/z* 297) acquired using a LCQ Classic QIT mass spectrometer with WideBand activation on
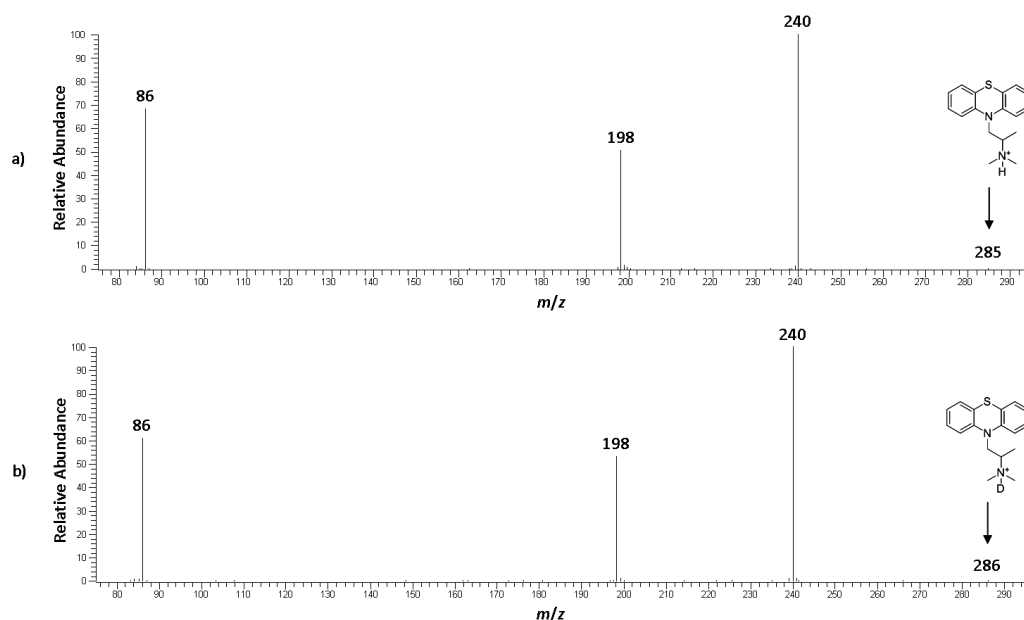
Figure 7.9 First-generation low-energy CID product ion spectra of a) protonated promethazine (*m/z* 285) and b) deuterated promethazine (*m/z* 286) acquired using a LCQ Classic QIT mass spectrometer with WideBand activation on

stays constant, regardless of the solvents used. This indicates that the γ-hydrogen relative to the nitrogen atom remains bonded to the carbon atom in solution. Thus, no intra-ionic H/D exchange takes place in solution, otherwise a decrease in the alkene hydrogen atom to aromatic hydrogen atom signal ratio would be observed.

Two sets of compounds were analysed to further confirm the site-specificity of the intra-ionic H/D exchange. **Compound set 3** contained amiodarone and dicycloverine (**Figure 7.10**). Instead of a γ-hydrogen relative to the nitrogen atom, both compounds have an oxygen atom at this position. Thus, no intra-ionic H/D exchange would be expected if the transfer were site-specific due to the absence of the relevant hydrogen atom. The comparison between the compound sets is like for like because the hybridisation states of an oxygen atom and a methylene group are identical *i.e.* sp^3. Thus, no significant change in the shape of the chain, nor its ability to rotate, should result from the modification in substructure. As a result, no difference in the likelihood of other hydrogen atoms exchanging with the deuterium label should result; an occurrence that could affect the interpretation of the data. The first-generation low-energy CID product ion spectra of amiodarone and dicycloverine in protic and deuterated solvents show no evidence of intra-ionic H/D exchange (**Figures 7.11-7.12**).

Amiodarone   Dicycloverine
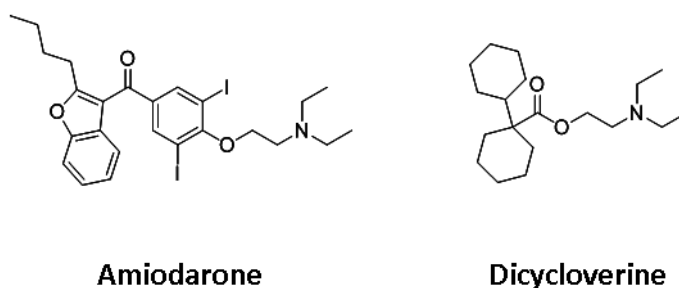
Figure 7.10   Molecular structures in Compound set 3

The second group of compounds, **Compound set 4**, contained cinchocaine, cinchocaine-*N*-oxide, metoclopramide, sunitinib and sunitinib-*N*-oxide (**Figure 7.13**). The molecules in **Compound set 4** contain a γ-hydrogen relative to the
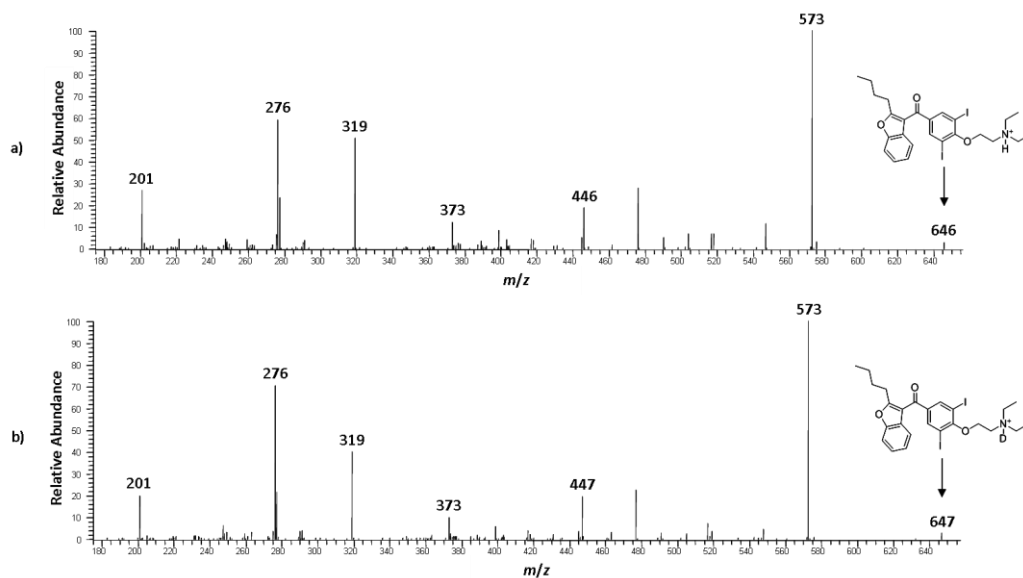
Figure 7.11   First-generation low-energy CID product ion spectra of a) protonated amiodarone (*m/z* 646) and b) deuterated amiodarone (*m/z* 647) acquired using a LCQ Classic QIT mass spectrometer with WideBand activation on
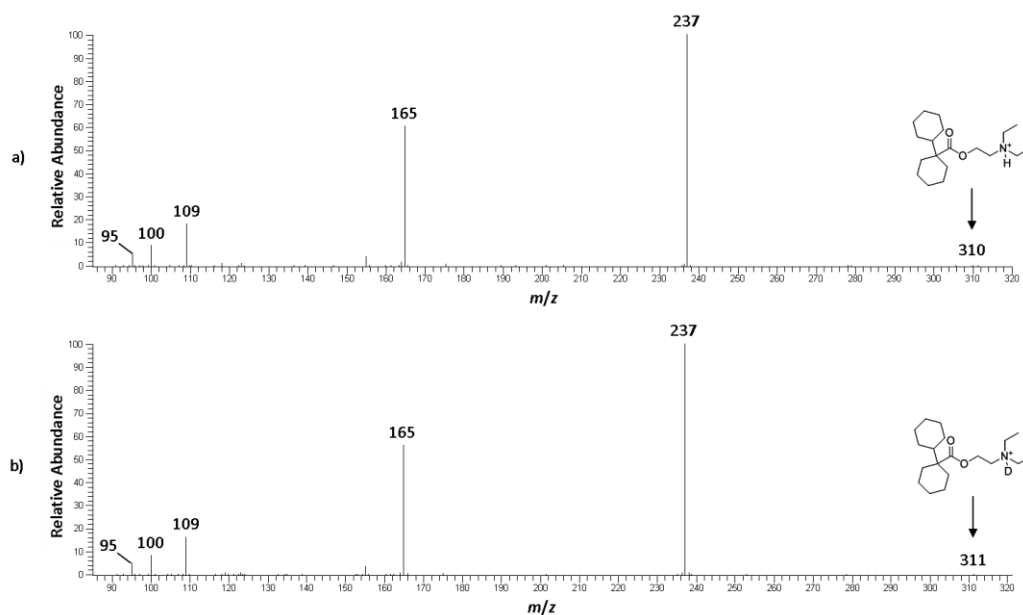
Figure 7.12   First-generation low-energy CID product ion spectra of a) protonated dicycloverine (*m/z* 310) and b) deuterated dicycloverine (*m/z* 311) acquired using a LCQ Classic QIT mass spectrometer with WideBand activation on

Cinchocaine   Cinchocaine-*N*-oxide   Metoclopramide

Sunitinib   Sunitinib-*N*-oxide
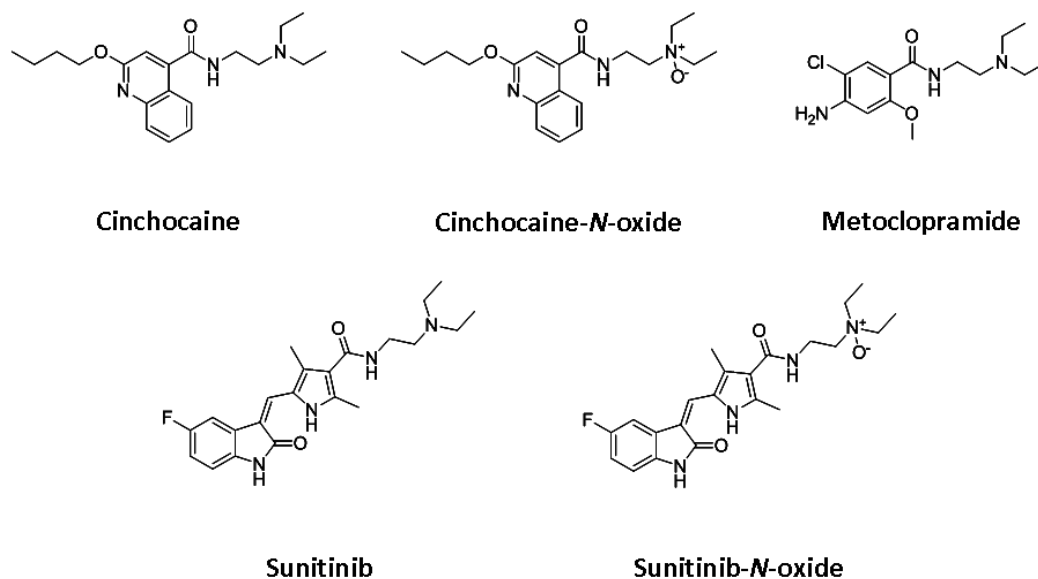
Figure 7.13   Molecular structures in Compound set 4

nitrogen atom, but in this case it is an exchangeable hydrogen atom. Thus, under deuterated conditions in solution, it exchanges for a deuterium atom. If the intra-ionic H/D exchange in the gas phase were indeed site-specific as postulated, the ionising deuteron localised at the tertiary amine group would exchange for another deuteron. Thus, subsequent loss of the tertiary amine group in the low-energy CID product ion spectrum would show no evidence of transfer of the deuterium label even if intra-ionic H/D exchange had taken place. **Figure 7.14** shows the first-generation low-energy CID product ion spectra of sunitinib in protic and deuterated solvents as an exemplar for the compound set. The first-generation low-energy CID product ion spectrum acquired under deuterated conditions only displays the loss of deuterodiethylamine, consistent with exchange of the deuteron at the tertiary amine group taking place with another deuterium atom. The first-generation low-energy CID product ion spectra of the other four compounds in the compound set also only show the losses of deuterodiethylamine and deuterodiethylhydroxylamine, depending upon whether the tertiary amine group is oxidised or not (**Figures 7.15-7.18**). The analysis of **Compound sets 3** and **4** provide supportive evidence for site-specific intra-ionic H/D exchange by showing that in the absence of a γ-hydrogen relative to the nitrogen atom, no evidence for the transfer of the deuterium label could be obtained.
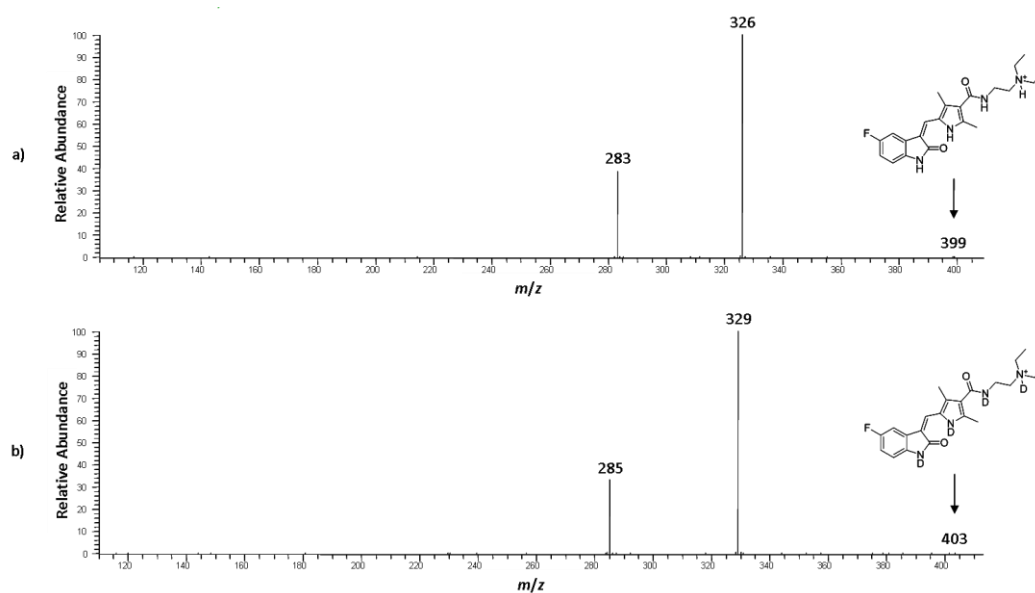
Figure 7.14 First-generation low-energy CID product ion spectra of a) protonated sunitinib (*m/z* 399) and b) fully exchanged, deuterated sunitinib (*m/z* 403) acquired using a LCQ Classic QIT mass spectrometer with WideBand activation on

Figure 7.15 First-generation low-energy CID product ion spectra of a) protonated cinchocaine (*m/z* 344) and b) fully exchanged, deuterated cinchocaine (*m/z* 346) acquired using a LCQ Classic QIT mass spectrometer with WideBand activation on
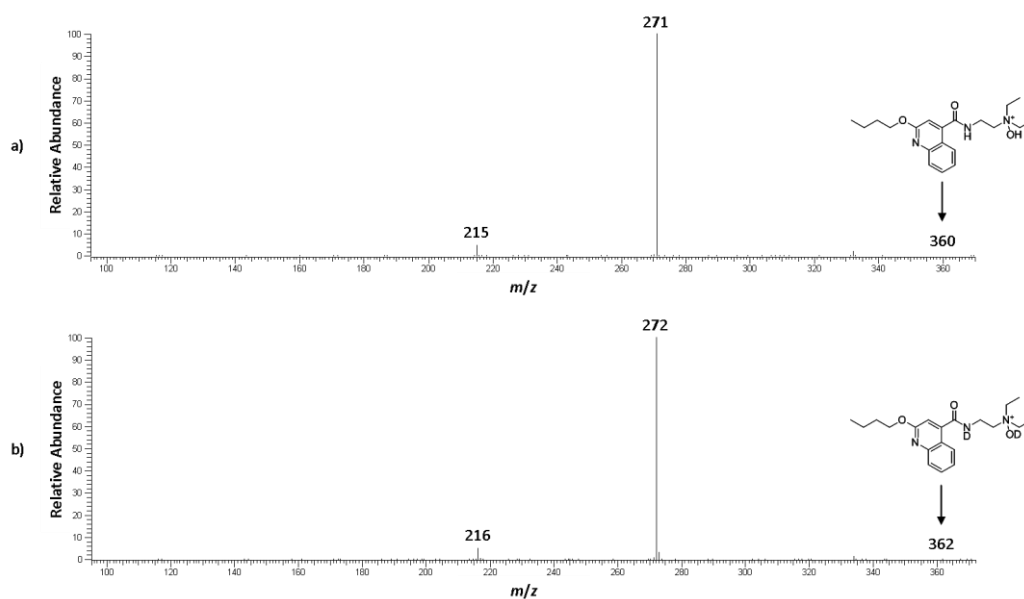
Figure 7.16 **First-generation low-energy CID product ion spectra of a) protonated cinchocaine-*N*-oxide (*m/z* 360) and b) fully exchanged, deuterated cinchocaine-*N*-oxide (*m/z* 362) acquired using a LCQ Classic QIT mass spectrometer with WideBand activation on**

Figure 7.17 **First-generation low-energy CID product ion spectra of a) protonated metoclopramide (*m/z* 300) and b) fully exchanged, deuterated metoclopramide (*m/z* 304) acquired using a LCQ Classic QIT mass spectrometer with WideBand activation on**
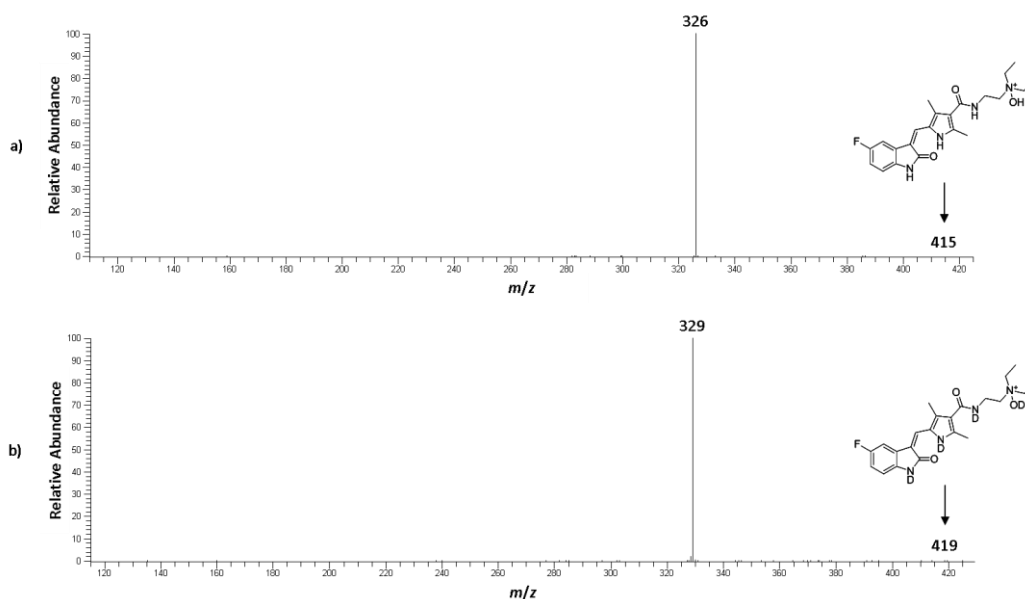
Figure 7.18 First-generation low-energy CID product ion spectra of a) protonated sunitinib-*N*-oxide (*m/z* 415) and b) fully exchanged, deuterated sunitinib-*N*-oxide (*m/z* 419) acquired using a LCQ Classic QIT mass spectrometer with WideBand activation on

Thus far, the intra-ionic H/D exchange has been observed for compounds with the exchanged hydrogen atom bonded to an alkene carbon. To determine whether the exchange is dependent upon the hybridisation state of the carbon atom, a fifth set of compounds was analysed; chlorpromazine, a tri-oxidised chlorpromazine metabolite, a di-oxidised chlorpromazine analogue, chloroquine, hydroxychloroquine, levomepromazine and protriptyline (**Figure 7.19**). All of these compounds contain a γ-hydrogen, relative to the nitrogen atom, which is bonded to a sp^3 hybridised carbon atom. The first-generation low-energy CID product ion spectra of chlorpromazine (**Figure 7.20**) show evidence of intra-ionic H/D exchange for the three most abundant product ions. The other compounds in the set also display intra-ionic H/D exchange (**Figures 7.21-7.26**). This suggests that the intra-ionic H/D exchange can take place with a γ-hydrogen relative to a nitrogen atom, irrespective of whether the hydrogen is bonded to an sp^2 or sp^3 hybridised carbon atom.
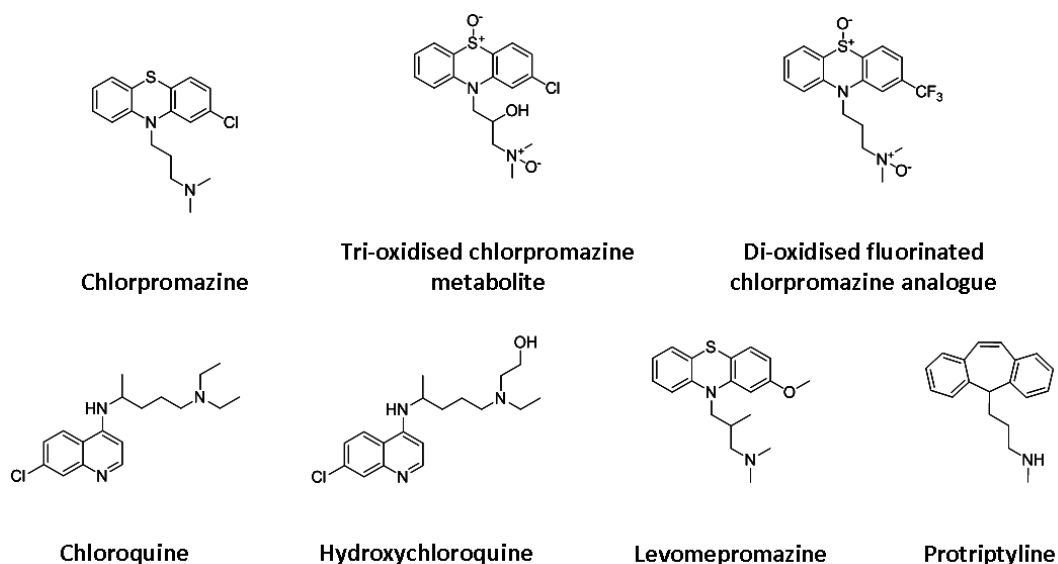
Figure 7.19   Molecular structures in Compound set 5
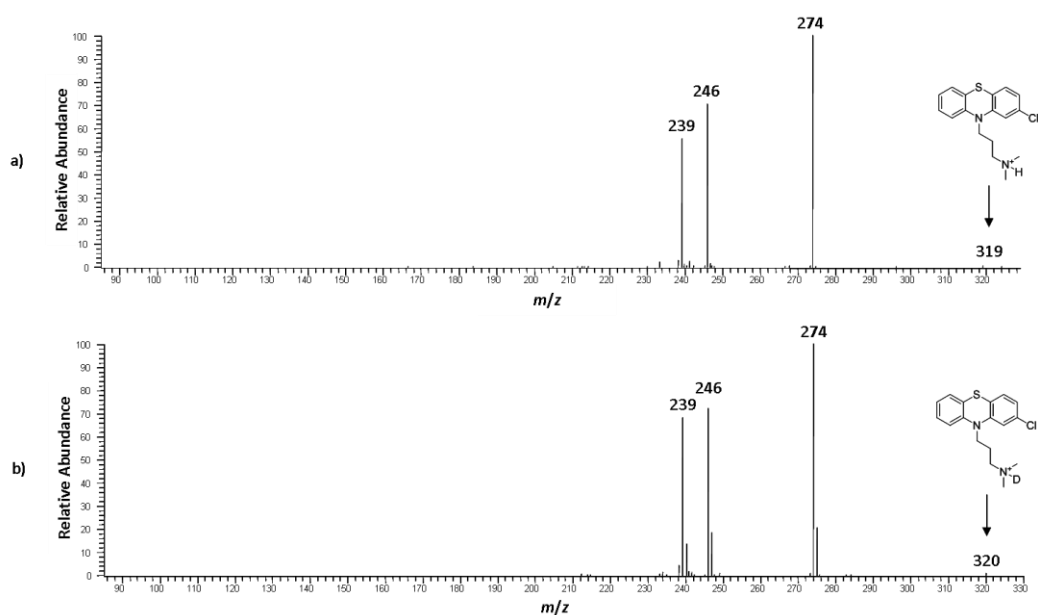
Figure 7.20   First-generation low-energy CID product ion spectra of a) protonated chlorpromazine (*m/z* 319) and b) deuterated chlorpromazine (*m/z* 320) acquired using a LCQ Classic QIT mass spectrometer with WideBand activation on
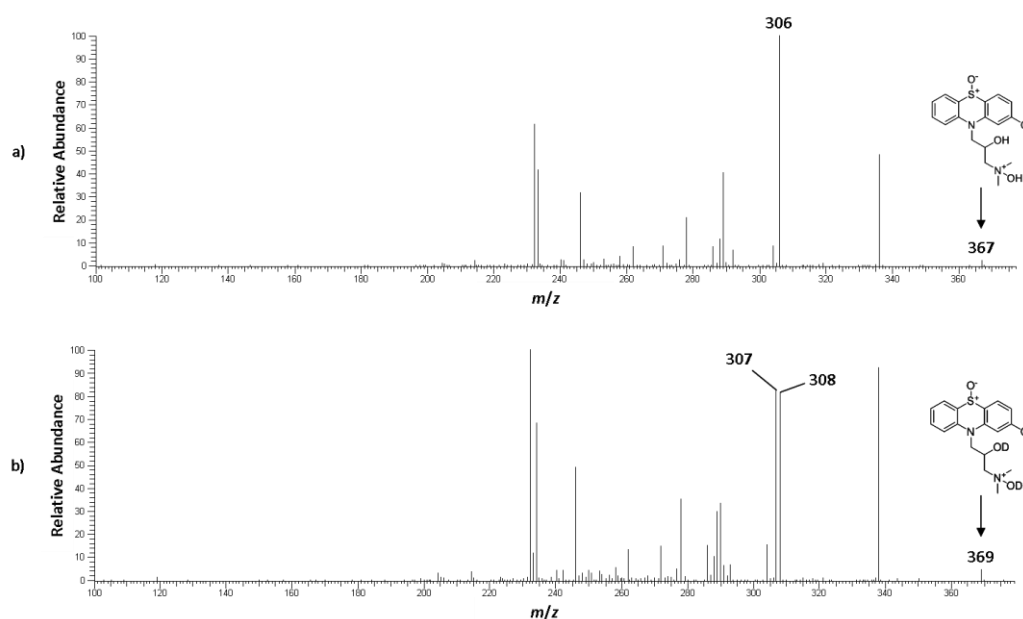
Figure 7.21 First-generation low-energy CID product ion spectra of a) a protonated tri-oxidised chlorpromazine metabolite (*m/z* 367) and b) fully exchanged, deuterated tri-oxidised chlorpromazine metabolite (*m/z* 369) acquired using a LCQ Classic QIT mass spectrometer with WideBand activation on
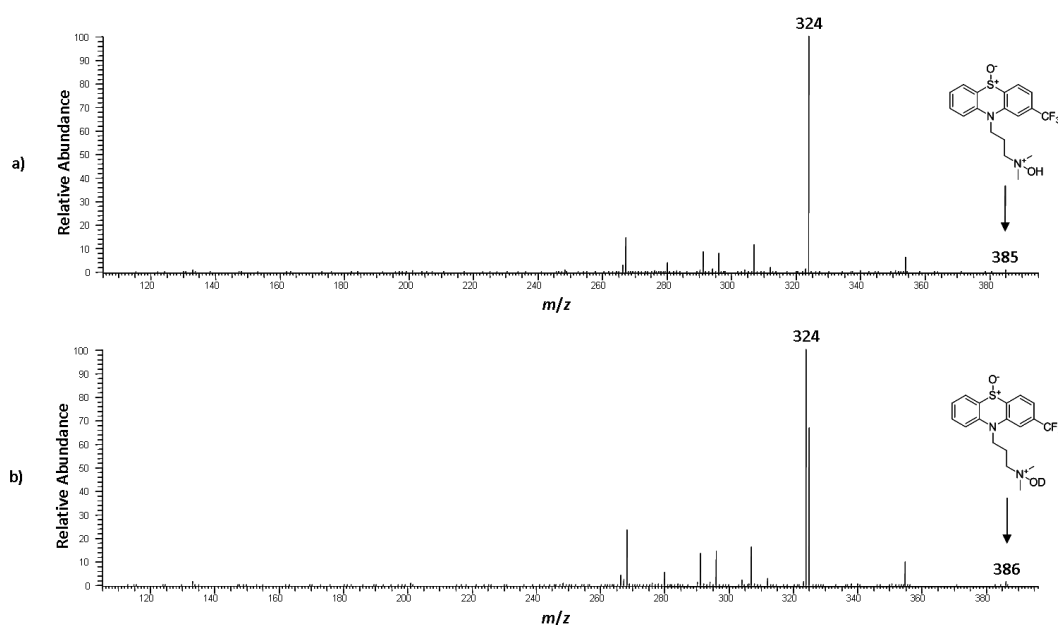
Figure 7.22 First-generation low-energy CID product ion spectra of a) a protonated di-oxidised chlorpromazine analogue (*m/z* 385) and b) deuterated di-oxidised chlorpromazine analogue (*m/z* 386) acquired using a LCQ Classic QIT mass spectrometer with WideBand activation on
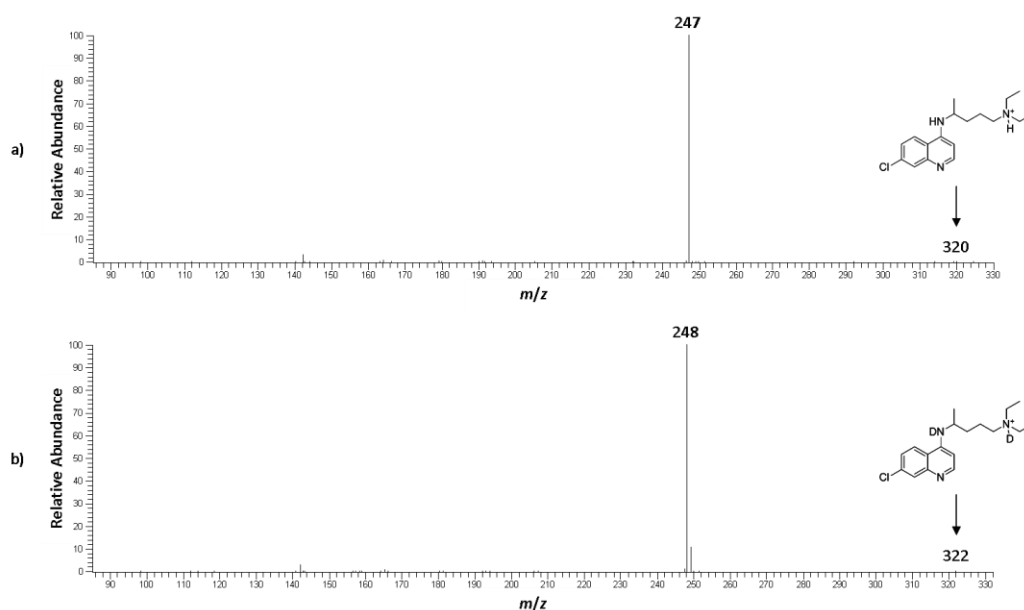
Figure 7.23 First-generation low-energy CID product ion spectra of a) protonated chloroquine (*m/z* 320) and b) fully exchanged, deuterated chloroquine (*m/z* 322) acquired using a LCQ Classic QIT mass spectrometer with WideBand activation on
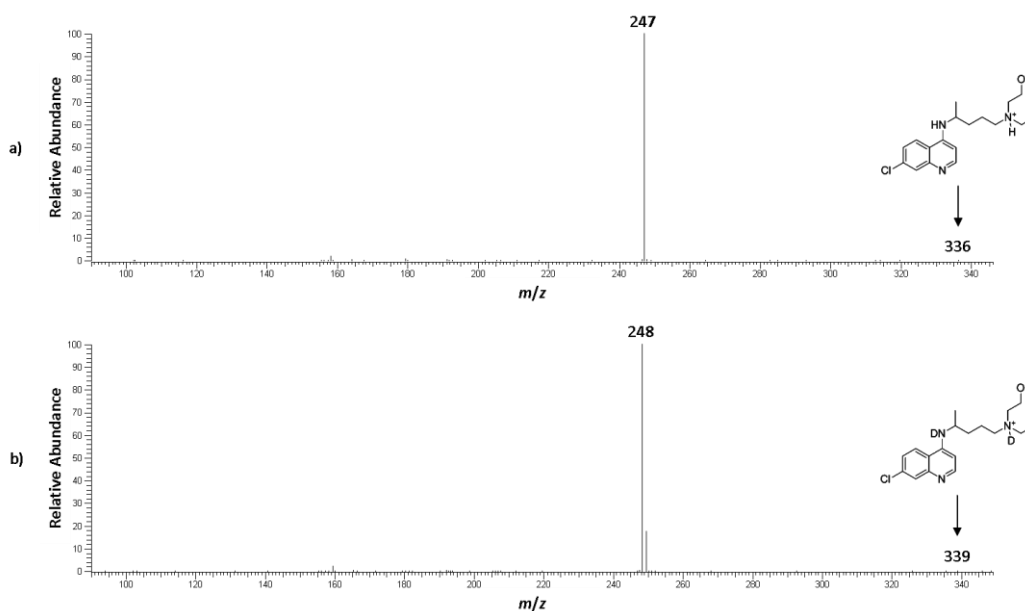
Figure 7.24 First-generation low-energy CID product ion spectra of a) protonated hydroxychloroquine (*m/z* 336) and b) fully exchanged, deuterated hydroxychloroquine (*m/z* 339) acquired using a LCQ Classic QIT mass spectrometer with WideBand activation on
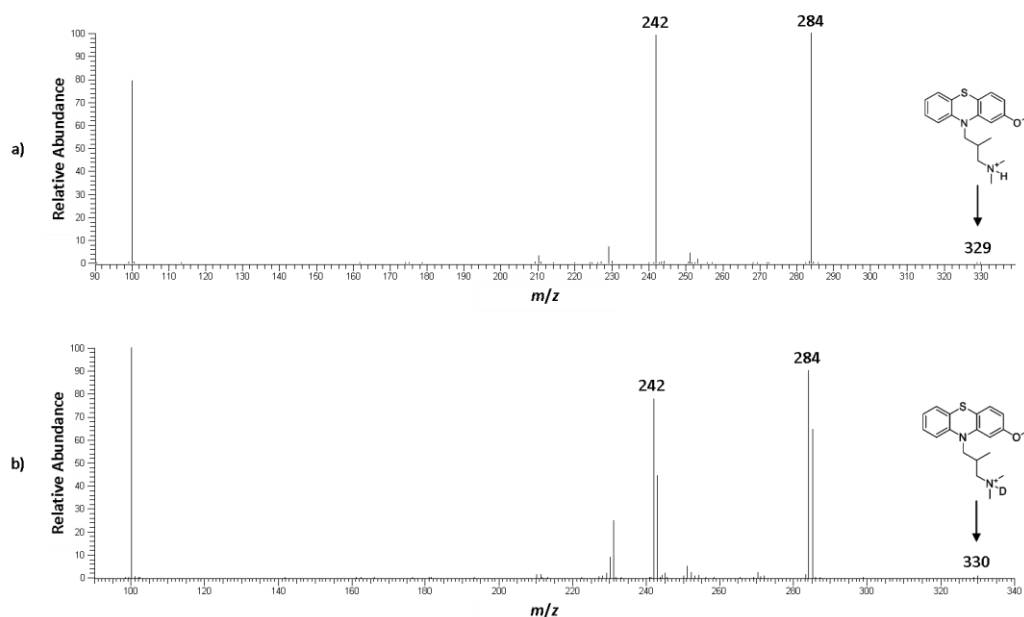
Figure 7.25 **First-generation low-energy CID product ion spectra of a) protonated levomepromazine (*m/z* 329) and b) deuterated levomepromazine (*m/z* 330) acquired using a LCQ Classic QIT mass spectrometer with WideBand activation on**
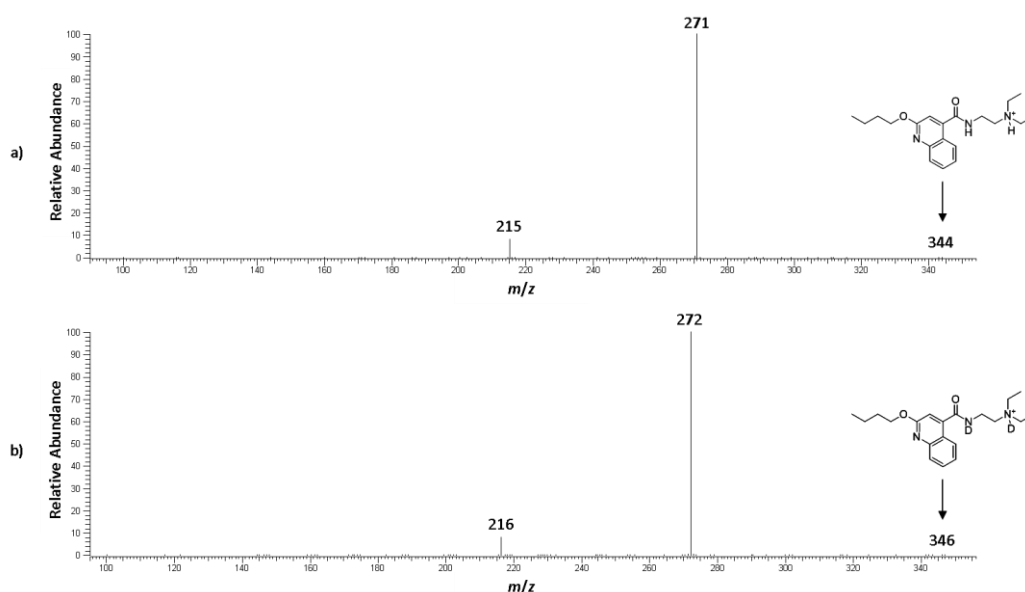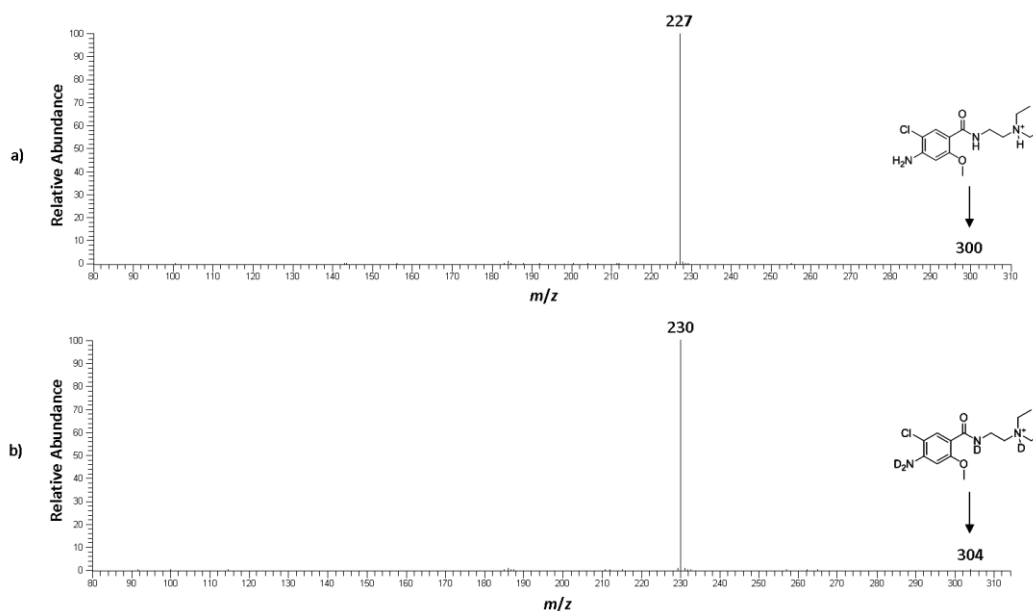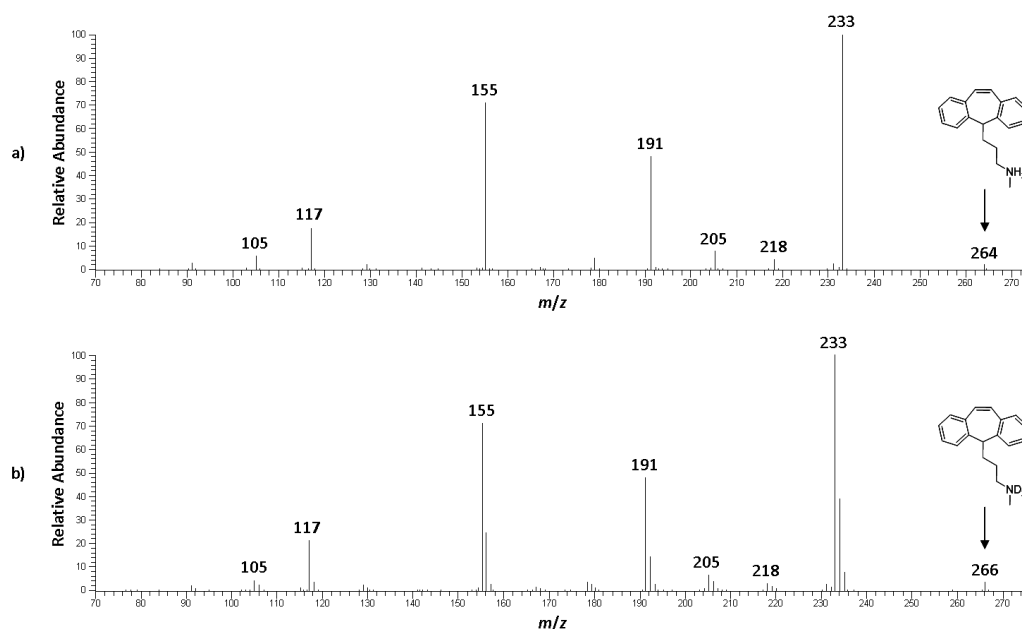

Figure 7.26 **First-generation low-energy CID product ion spectra of a) protonated protriptyline (*m/z* 264) and b) fully exchanged, deuterated protriptyline (*m/z* 266) acquired using a LCQ Classic QIT mass spectrometer with WideBand activation on**

A further set of compounds was analysed to investigate the intra-ionic H/D exchange. This set contained benzydamine and chlorphenamine (**Compound set 6**, **Figure 7.27**), both of which contain a γ-hydrogen relative to a nitrogen atom. However, the carbon bearing the γ-hydrogen is also bonded to an electron-withdrawing group; an oxygen atom and a chlorinated phenyl ring for benzydamine and chlorphenamine respectively. Neither of these compounds display intra-ionic H/D exchange in their first generation low-energy CID product ion spectra (**Figures 7.28-7.29**). The absence of intra-ionic H/D exchange suggests that the presence of an electron-withdrawing group adjacent to the carbon atom bearing the γ-hydrogen can prevent exchange from taking place. However, the properties of the electron-withdrawing group appear to determine whether the intra-ionic H/D exchange is precluded. This is because the presence of the nitrogen atom bonded to the γ-carbon in chlorpromazine, the tri-oxidised chlorpromazine metabolite, the di-oxidised fluorinated chlorpromazine analogue and levomepromazine (**Figure 7.19**) does not prevent intra-ionic H/D exchange in these compounds (**Figures 7.20-7.22 and Figure 7.25**). This observation may be consistent with the fact that nitrogen has a lower electronegativity than oxygen or a chlorinated phenyl ring. However, the compounds available in this study did not provide an extensive enough dataset on which to draw any robust conclusions.

Benzydamine   Chlorphenamine
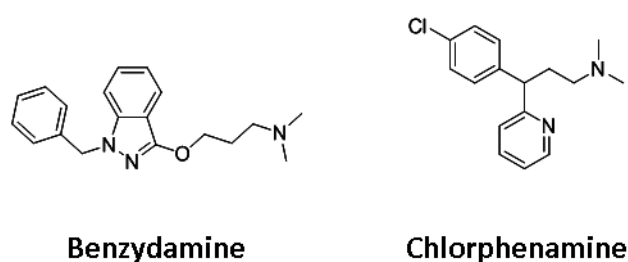
Figure 7.27   Molecular structures in Compound set 6

Finally, to address whether the chemical environment of the alkyl chain affects the observation of intra-ionic H/D exchange, first-generation low-energy CID product ion spectra of a "linear" tertiary amine with a γ-hydrogen, hexylamine, were acquired (**Figure 7.30**). Comparison of the product ion spectra shows that
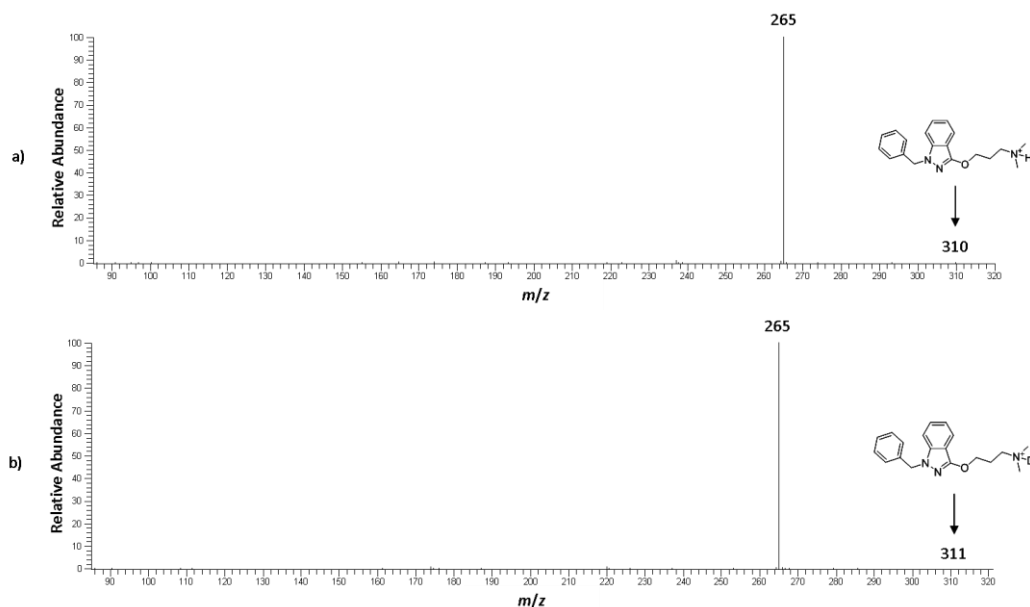
Figure 7.28 **First-generation low-energy CID product ion spectra of a) protonated benzydamine (*m/z* 310) and b) deuterated benzydamine (*m/z* 311) acquired using a LCQ Classic QIT mass spectrometer with WideBand activation on**
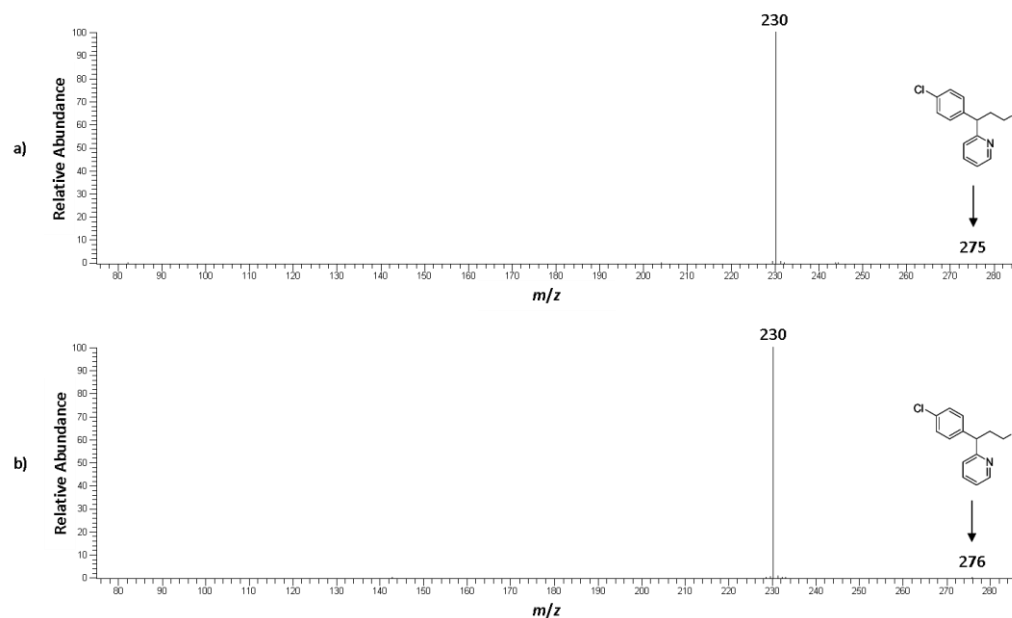
Figure 7.29 **First-generation low-energy CID product ion spectra of a) protonated chlorphenamine (*m/z* 275) and b) deuterated chlorphenamine (*m/z* 276) acquired using a LCQ Classic QIT mass spectrometer with WideBand activation on**

no intra-ionic H/D exchange takes place (**Figure 7.31**). The additional peaks observed under deuterated conditions that are not observed under protonated conditions are due to noise *i.e.* the peaks were not seen repeatably. The absence of intra-ionic H/D exchange suggests that the chemical environment provided by the molecule influences whether the deuterium label is transferred. Specifically, the molecules for which intra-ionic H/D exchange was observed were all pharmaceutical compounds containing substructures such as aromatic rings. These more complex molecules may provide chemical environments that facilitate intra-ionic H/D exchange. However, the exact substructures that assist the intra-ionic H/D exchange could not be determined from the compounds that were available. Additional experiments are being conducted to further investigate the facilitating substructures.
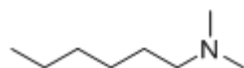
Figure 7.30   Molecular structure of hexylamine
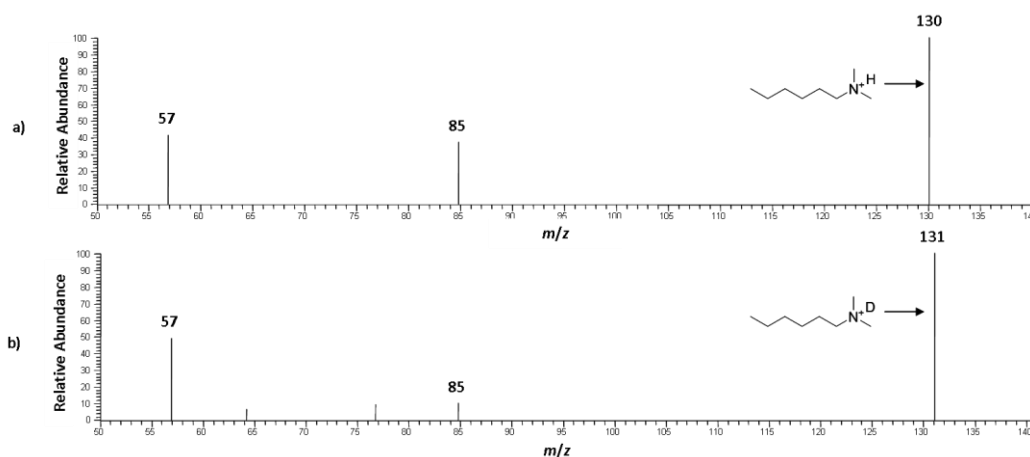
Figure 7.31   First-generation low-energy CID product ion spectra of a) protonated hexylamine (*m/z* 130) and b) deuterated hexylamine (*m/z* 131) acquired using a LCQ Classic QIT mass spectrometer with WideBand activation on

The experimental investigation has demonstrated the conditions under which the site-specific intra-ionic H/D exchange is observed. The observations have relevance to structural elucidation studies by providing a simple, non-synthetic

means of introducing a deuterium label into the carbon skeleton of a molecule. If an analyst has a compound containing a tertiary amine or tertiary amine-*N*-oxide with a γ-hydrogen, analysis in deuterated solvents will cause exchange of this hydrogen atom for the ionising deuteron under low-energy CID conditions. Thus, the product ions known to lose the nitrogen-containing group, but which display intra-ionic H/D exchange, must retain the γ-carbon relative to the nitrogen atom. The γ-carbon can be either sp^2 or sp^3 hybridised but adjacent electron-withdrawing groups can preclude the occurrence of intra-ionic H/D exchange. Further, if an analyst is working with an unknown compound in deuterated solvents, the observation of intra-ionic H/D exchange under low-energy CID conditions, which is rare, may indicate that a tertiary amine or tertiary amine-*N*-oxide with a γ-hydrogen not adjacent to specific electron-withdrawing groups is present in the molecule.

7.4   Conclusions

Site-specific intra-ionic H/D exchange under low-energy CID conditions in a series of protonated small molecules has been observed. Experiments have shown that the exchange takes place between the deuteron that ionises either a tertiary amine or tertiary amine-*N*-oxide group and a γ-hydrogen relative to the nitrogen atom. The presence of an electron-withdrawing group bonded to the carbon atom bearing the γ-hydrogen can prevent the site-specific intra-ionic H/D exchange in some circumstances. Further, the chemical environment in which the γ-hydrogen relative to the nitrogen atom structural motif is present appears to influence the ion's propensity to undergo site-specific intra-ionic H/D exchange. The observations could aid structural elucidation studies by providing a simple, non-synthetic means of introducing an isotopic label into the carbon skeleton of a molecule in a site-specific manner when a particular structural motif is present in the compound. This is of practical benefit because it would enable faster completion of structural elucidation studies, as well as reducing costs because a deuterium-labelled analogue would not have to be produced synthetically.

Chapter 8

Concluding remarks

8.1   Summary and conclusions

The aim of the presented study was to elucidate structurally dependent dissociation pathways that could be used to rapidly and definitively identify and characterise pharmaceutical drug metabolites using low-energy CID-MS/MS. The work was initiated as a result of promising data from the study by Wright and co-workers.[230] Their work demonstrated that distinctive fragmentation behaviour under low-energy CID conditions could be used to characterise *S*-oxidised metabolites. Very few other groups had demonstrated this approach to definitively identify oxidised metabolites *i.e.* through the understanding of the dissociation behaviour of the substructure containing the site of oxidation. Therefore, the lack of existing literature, in combination with the recognition of the potential of the approach to shift the accepted bottleneck in modern pharmaceutical drug metabolite identification studies *i.e.* data interpretation and the associated time-commitment of skilled analysts,[303] meant that further investigation was desirable.

The study has been successful in identifying two potentially useful dissociation pathways that could allow definitive characterisation of certain *S*- and *N*-oxidised metabolites (see **Chapters 4** and **6**). These pathways were elucidated by understanding, through both experimental and computational approaches, the dissociation of the substructure containing the site of oxidation in a similar manner to Wright and co-workers. It was recognised early in the study that the marginal change to a drug's structure that occurs when oxidation takes place would rarely alter the dissociation behaviour significantly enough to cause distinctly different product ions or losses for the metabolite compared to the

parent compound. Thus, diagnostic product ions and losses arising solely from the S^+-O$^-$, N^+-O$^-$ and *C*-OH moieties is unlikely because the structural change is almost certainly insufficient to create a substructure that will drive the dissociation differently. Therefore, it is the author's opinion that completely generic dissociation behaviour *i.e.* the same product ion or loss being formed due to the presence of S^+-O$^-$, N^+-O$^-$ or *C*-OH bond in the metabolite regardless of the overall molecular structure, is not possible under low-energy CID conditions. However, by understanding how the dissociation is driven by the chemical environment in which the oxidised group is positioned, it is possible to elucidate structurally dependent dissociation pathways that can be used to definitively characterise pharmaceutical drug metabolites using low-energy CID-MS/MS, as evinced by the presented study. As dissociation is known to be driven by the structure of the molecule, it should be possible to determine further substructures that drive particular fragmentation pathways. Thus, further work in the area of understanding fragmentation under low-energy CID conditions is required due to the current lack of knowledge. The potential benefit to the area of structural elucidation, including metabolite identification, and the likelihood of success is demonstrated by the presented study. Furthermore, the investigation of the dissociation of pharmaceutical drug metabolites using other ion activation techniques should be conducted. In particular, electron capture dissociation (ECD) is garnering interest as a method to dissociate small molecules.[304] Recent work has shown that, contrary to widespread belief, singly charged molecules can be dissociated using ECD.[305] The study demonstrated that the product ions formed are complementary to those observed under low-energy CID conditions. Most interestingly, the work reports cleavages across benzene rings, which are resistant to fragmentation under low-energy CID conditions. ECD may therefore enable definitive assignment of the site of hydroxylation on a benzene ring, which is a challenging proposition using the current technology and approaches. A related ion activation technique, electron transfer dissociation (ETD),[306] has yet to be applied to the area of small molecule structural elucidation. It is therefore the author's opinion that investigation of the application of both types of radical-induced dissociation

techniques should be performed, as they could provide useful additions to the small molecule structural elucidation approaches. Further studies of MS/MS dissociation, regardless of the employed ion activation technique, will also be of use to developers of *in silico* packages for fragmentation prediction. These software packages generally use rules derived from EI mass spectra for small molecule fragmentation prediction,[234] which are not necessarily directly applicable to CID, ECD or ETD product ion spectra, or are based on case-specific information derived from compiled MS/MS databases.[307] Therefore, increased knowledge and understanding of MS/MS dissociation would be useful to make these packages more accurate and robust, and hence more useful.

In addition to the original aim of the study, extensive interrogation and interpretation of product ion spectra has enabled an increased understanding of ion-chemistry under low-energy CID conditions. Each chapter has made a contribution to the body of knowledge in this area. **Chapter 4** showed that sequential radical losses can take place from an even-electron precursor ion under low-energy CID conditions. This would not be expected on energetic grounds based upon the even-electron rule.[251] Further, the experimental observations suggested a preference for the formation of planar product ion structures under low-energy CID conditions. This proposal was supported by the observations detailed in **Chapter 5**, which again suggested that planar product ion structures are preferentially formed over those that have a greater number of bonds which have free rotation. **Chapter 5** also showed that unexpected rearrangements take place under low-energy CID conditions. This highlighted the need for an analytically rigorous experimental methodology when performing structural elucidation studies to prevent incorrect ion structure assignments. **Chapter 6** demonstrated that dialkyl tertiary amines and their *N*-oxides generally dissociate in a predictable way, with the neutral loss of this group observed in the low-energy CID product ion spectrum. The loss appeared to be governed by ionisation taking place at this substructure and is likely to only occur when this prerequisite is fulfilled. The data also suggested that the product ions formed through the loss of the dialkyl tertiary amine

group or its *N*-oxidised analogue are relatively unstable and thus susceptible to further dissociation. Finally, **Chapter 7** illustrated that site-specific intra-ionic H/D exchange can take place such that the ionising deuteron can be swapped with a non-exchangeable γ-hydrogen and thus be inserted into the carbon skeleton of the compound. This is a rare observation, and the site-specificity of the exchange also allows it to be a useful tool for structural elucidation studies.

Appendix 1

Table A1   **Molecular structures of compounds containing a dimethylamine substructure**

Compound	Molecular structure
Alimemazine	
Almotriptan	
Amitriptyline	
Amlodipine structural analogue 1	
Amlodipine structural analogue 2	

Amlodipine structural analogue 3	
Amlodipine structural analogue 4	
Benzydamine	
Chlorphenamine	
Chlorpromazine	
Chlorpromazine structural analogue 1	
Chlorpromazine structural analogue 2	

Chlorprothixene	
Citalopram	
Clomipramine	
Cyclopentolate	
Demeclocycline	
Dibenzepin	
Diltiazem	

Diphenhydramine	
Doxepin	
Doxycycline	
Imipramine	
Iprindole	
Levomepromazine	
Metformin	
Moxisylyte	

Olopatadine	
Orphenadrine	
Promazine	
Promethazine	
Ranitidine	
Rivastigmine	
Sibutramine	
Sumatriptan	

Sunitinib structural analogue	
Tamoxifen	
Tetracaine	
Tramadol	
Trimipramin	
Venlafaxine	
Zimelidine	

Table A2   **Molecular structures of compounds containing a diethylamine substructure**

Compound	Molecular structure
Amiodarone	
Amlodipine structural analogue 5	
Chloroquine	
Cinchocaine	
Clomifene	
Dicycloverine	
Disulfiram	

Lidocaine	
Macrogol	
Metoclopramide	
Naftidrofuryl	
Oxybuprocaine	
Oxybutynin	
Procainamide	
Procaine	
Sunitinib	

Table A3   Molecular structures of compounds containing an *N,N*-dimethylhydroxylamine substructure

Compound	Molecular structure
Amitriptyline-*N*-oxide	
Chlorpromazine-*N*-oxide 1	
Chlorpromazine-*N*-oxide 2	
Chlorpromazine structural analogue-*N*-oxide 1	
Chlorpromazine structural analogue-*N*-oxide 2	
Diphenhydramine-*N*-oxide	
Ephedrine structural analogue-*N*-oxide	

Tamoxifen structural analogue-*N*-oxide 1	
Tamoxifen structural analogue-*N*-oxide 2	
Tetracaine-*N*-oxide	

Table A4   **Molecular structures of compounds containing an *N,N*-diethylhydroxylamine substructure**

Compound	Molecular structure
Cinchocaine-*N*-oxide	
Sunitinib-*N*-oxide	

Table A5 **Relative abundances (RA) for the product ion formed through the loss of dimethylamine from a series of pharmaceutical compounds using QqTOF-MS and QIT-MS at various collision energies**

Compound	RA using QqTOF-MS at 15 eV / %	RA using QqTOF-MS at 20 eV / %	RA using QqTOF-MS at 25 eV / %	RA using QIT-MS at 50%, WideBand activation on / %	RA using QIT-MS at 50%, WideBand activation off / %
Alimemazine	6	4	1	41	37
Almotriptan	52	100	31	17	16
Amitriptyline	76	64	20	100	100
Amlodipine structural analogue 1	11	4	1	94	89
Amlodipine structural analogue 2	23	18	-	100	100
Amlodipine structural analogue 3	2	1	-	63	71
Amlodipine structural analogue 4	5	4	2	100	100
Benzydamine	11	5	1	100	100
Chlorphenamine	100	100	100	100	100
Chlorpromazine	4	3	2	100	100
Chlorpromazine structural analogue 1	-	-	-	7	7
Chlorpromazine structural analogue 2	1	8	3	21	21
Chlorprothixene	100	100	66	100	42
Citalopram	8	2	-	12	16
Clomipramine	6	4	3	100	100
Cyclopentolate	-	-	-	-	-
Demeclocycline	-	-	-	-	-
Dibenzepin	100	100	100	100	100
Diltiazem	19	3	-	18	33
Diphenhydramine	-	-	-	-	-
Doxepin	39	18	9	100	100
Doxycycline	-	-	2	3	-
Imipramine	4	3	2	21	15

Iprindole	2	4	5	1	1
Levomepromazine	8	4	4	100	99
Metformin	33	23	14	15	14
Moxisylyte	9	5	1	100	100
Olopatadine	8	13	6	16	19
Orphenadrine	-	-	-	-	-
Promazine	7	4	3	55	47
Promethazine	15	12	5	100	100
Ranitidine	7	2	-	71	100
Rivastigmine	100	49	11	100	100
Sibutramine	-	-	-	-	-
Sumatriptan	100	71	12	100	81
Sunitinib structural analogue	100	63	33	89	100
Tamoxifen	2	1	-	100	100
Tetracaine	11	10	5	16	17
Tramadol	-	2	-	16	-
Trimipramin	4	4	2	21	18
Venlafaxine	-	-	-	-	-
Zimelidine	14	6	3	79	80

Table A6 **Relative abundances (RA) for the product ion formed through the loss of diethylamine from a series of pharmaceutical compounds using QqTOF-MS and QIT-MS at various collision energies**

Compound	RA using QqTOF-MS at 15 eV / %	RA using QqTOF-MS at 20 eV / %	RA using QqTOF-MS at 25 eV / %	RA using QIT-MS at 50%, WideBand activation on / %	RA using QIT-MS at 50%, WideBand activation off / %
Amiodarone	-	-	2	100	100
Amlodipine structural analogue 5	3	1	-	59	61
Chloroquine	100	100	100	100	100
Cinchocaine	100	100	81	100	100
Clomifene	-	1	-	7	7
Dicycloverine	41	59	24	100	100
Disulfiram	-	-	-	18	13
Lidocaine	-	-	-	-	-
Macrogol	100	100	64	100	100
Metoclopramide	100	100	100	100	100
Naftidrofuryl	8	3	-	38	55
Oxybuprocaine	28	28	26	46	53
Oxybutynin	-	-	-	-	-
Procainamide	100	100	51	100	100
Procaine	50	46	21	100	100
Sunitinib	100	100	80	100	100

Table A7 **Relative abundances (RA) for the product ion formed through the loss of *N,N*-dimethylhydroxylamine from a series of pharmaceutical compounds using QqTOF-MS and QIT-MS at various collision energies**

Compound	RA using QqTOF-MS at 15 eV / %	RA using QqTOF-MS at 20 eV / %	RA using QqTOF-MS at 25 eV / %	RA using QIT-MS at 50%, WideBand activation on / %	RA using QIT-MS at 50%, WideBand activation off / %
Amitriptyline-*N*-oxide	100	65	22	100	100
Chlorpromazine-*N*-oxide 1	2	5	3	6	5
Chlorpromazine-*N*-oxide 2	13	52	13	100	100
Chlorpromazine structural analogue-*N*-oxide 1	79	100	26	100	100
Chlorpromazine structural analogue-*N*-oxide 2	32	100	73	100	100
Diphenhydramine-*N*-oxide	-	-	-	-	-
Ephedrine structural analogue-*N*-oxide	97	30	9	21	19
Tamoxifen structural analogue-*N*-oxide 1	-	2	1	31	43
Tamoxifen structural analogue-*N*-oxide 2	1	2	1	29	35
Tetracaine-*N*-oxide	100	100	44	100	100

Table A8 **Relative abundances (RA) for the product ion formed through the loss of *N,N*-diethylhydroxylamine from a series of pharmaceutical compounds using QqTOF-MS and QIT-MS at various collision energies**

Compound	RA using QqTOF-MS at 15 eV / %	RA using QqTOF-MS at 20 eV / %	RA using QqTOF-MS at 25 eV / %	RA using QIT-MS at 50%, WideBand activation on / %	RA using QIT-MS at 50%, WideBand activation off / %
Cinchocaine-*N*-oxide	100	100	96	100	100
Sunitinib-*N*-oxide	100	100	100	100	100

References

1.   E. de Hoffmann and V. Stroobant, *Mass Spectrometry: Principles and Applications*, 2nd Edn., John Wiley & Sons Ltd., Chichester, 2001.
2.   A. J. Dempster, *Phys. Rev.*, 1918, **11**, 316-325.
3.   M. Yamashita and J. B. Fenn, *J. Phys. Chem.*, 1984, **88**, 4451-4459.
4.   Z. Takáts, J. M. Wiseman, B. Gologan and R. G. Cooks, *Science*, 2004, **306**, 471-473.
5.   M. S. B. Munson and F. H. Field, *J. Am. Chem. Soc.*, 1966, **88**, 2621-2630.
6.   E. C. Horning, M. G. Horning, D. I. Carroll, I. Dzidic and R. N. Stillwell, *Anal. Chem.*, 1973, **45**, 936-943.
7.   R. B. Cody, J. A. Larame and H. D. Durst, *Anal. Chem.*, 2005, **77**, 2297-2302.
8.   M. Karas, D. Bachmann, U. Bahr and F. Hillenkamp, *Int. J. Mass Spectrom. Ion Proc.*, 1987, **78**, 53-68.
9.   D. B. Robb, T. R. Covey and A. P. Bruins, *Anal. Chem.*, 2000, **72**, 3653-3659.
10.   C. N. McEwen, R. G. McKay and B. S. Larsen, *Anal. Chem.*, 2005, **77**, 7826-7831.
11.   M. Dole, L. L. Mack, R. L. Hines, R. C. Mobley, L. D. Ferguson and M. B. Alice, *J. Chem. Phys.*, 1968, **49**, 2240-2249.
12.   M. Yamashita and J. B. Fenn, *J. Phys. Chem.*, 1984, **88**, 4671-4675.
13.   J. B. Fenn, *Angew. Chem. Int. Ed.*, 2003, **42**, 3871-3894.
14.   S. J. Gaskell, *J. Mass Spectrom.*, 1997, **32**, 677-688.
15.   N. B. Cech and C. G. Enke, *Mass Spectrom. Rev.*, 2001, **20**, 362-387.
16.   W. J. Griffiths, A. P. Jonsson, S. Liu, D. K. Rai and Y. Wang, *Biochem. J.*, 2001, **355**, 545-561.
17.   A. S. Fang, X. Miao, P. W. Tidswell, M. H. Towle, W. K. Goetzinger and J. N. Kyranos, *Mass Spectrom. Rev.*, 2008, **27**, 20-34.
18.   A. N. R. Nedderman, *Biopharm. Drug Dispos.*, 2009, **30**, 153-162.
19.   Y. Wu, *Biomed. Chromatogr.*, 2000, **14**, 384-396.
20.   F. Qiu and D. L. Norwood, *J. Liq. Chromatogr. R. T.*, 2007, **30**, 877-935.
21.   B. L. Ackermann, M. J. Berna, J. A. Eckstein, L. W. Ott and A. K. Chaudhary, *Annu. Rev. Anal. Chem.*, 2008, **1**, 357-396.
22.   T. Liu, M. E. Belov, N. Jaitly, W.-J. Qian and R. D. Smith, *Chem. Rev.*, 2007, **107**, 3621-3653.
23.   J. Tost and I. G. Gut, *J. Mass Spectrom.*, 2006, **41**, 981-995.
24.   J. Zaia, *Mass Spectrom. Rev.*, 2004, **23**, 161-227.
25.   J. L. P. Benesch, B. T. Ruotolo, D. A. Simmons and C. V. Robinson, *Chem. Rev.*, 2007, **107**, 3544-3567.
26.   M. Barber, R. S. Bordoli, R. D. Sedgwick and A. N. Tyler, *J. Chem. Soc. Chem. Commun.*, 1981, 325-327.
27.   H. D. Beckey, *Int. J. Mass Spectrom. Ion Phys.*, 1969, **2**, 500-503.
28.   M. G. Inghram and R. Gomer, *J. Chem. Phys.*, 1954, **22**, 1279-1280.
29.   C. R. Blakley and M. L. Vestal, *Anal. Chem.*, 1983, **55**, 750-754.

30. V. Matamoros, E. Jover and J. M. Bayona, *Anal. Bioanal. Chem.*, 2009, **393**, 847-860.
31. T. A. Brettell, J. M. Butler and J. R. Almirall, *Anal. Chem.*, 2009, **81**, 4695-4711.
32. W. J. Griffiths and Y. Wang, *Chem. Soc. Rev.*, 2009, **38**, 1882-1896.
33. H. H. Maurer, *Anal. Bioanal. Chem.*, 2007, **388**, 1315-1325.
34. V. Gabelica and E. De Pauw, *Mass Spectrom. Rev.*, 2005, **24**, 566-587.
35. A. P. Bruins, *J. Chromatogr. A*, 1998, **794**, 345-357.
36. A. W. T. Bristow, *Mass Spectrom. Rev.*, 2006, **25**, 99-111.
37. J. G. Stroh, C. J. Petucci, S. J. Brecker, N. Huang and J. M. Lau, *J. Am. Soc. Mass Spectrom.*, 2007, **18**, 1612-1616.
38. S. F. Wong, C. K. Meng and J. B. Fenn, *J. Phys. Chem.*, 1988, **92**, 546-550.
39. J. B. Fenn, M. Mann, C. K. Meng, S. F. Wong and C. M. Whitehouse, *Science*, 1989, **246**, 64-71.
40. T. Dülcks and R. Juraschek, *J. Aerosol. Sci.*, 1999, **30**, 927-943.
41. K. Downard, *Mass Spectrometry: A Foundation Course*, Royal Society of Chemistry, Cambridge, 2004.
42. A. Kaufmann, P. Butcher, K. Maden, M. Widmer, K. Giles and D. Uría, *Rapid Commun. Mass Spectrom.*, 2009, **23**, 985-998.
43. C. M. Whitehouse, R. N. Dreyer, M. Yamashita and J. B. Fenn, *Anal. Chem.*, 1985, **57**, 675-679.
44. J. A. Olivares, N. T. Nguyen, C. R. Yonker and R. D. Smith, *Anal. Chem.*, 1987, **59**, 1230-1232.
45. J. Abian, *J. Mass Spectrom.*, 1999, **34**, 157-168.
46. R. M. Caprioli, T. Fan and J. S. Cottrell, *Anal. Chem.*, 1986, **58**, 2949-2954.
47. W. M. A. Niessen, *J. Chromatogr. A*, 1998, **794**, 407-435.
48. G. Siuzdak and J. K. Lewis, *Biotechnol. Bioeng.*, 1998, **61**, 127-134.
49. M. Holčapek, L. Kolářová and M. Nobilis, *Anal. Bioanal. Chem.*, 2008, **391**, 59-78.
50. G. Siuzdak, *Mass Spectrometry in Biotechnology*, 2nd Edn., MCC Press, San Diego, 2006.
51. P. Kebarle and U. H. Verkerk, *Mass Spectrom. Rev.*, 2009, **28**, 898-917.
52. T. C. Rohner, N. Lion and H. H. Girault, *Phys. Chem. Chem. Phys.*, 2004, **6**, 3056-3068.
53. P. Kebarle and M. Peschke, *Anal. Chim. Acta*, 2000, **406**, 11-35.
54. M. H. Amad, N. B. Cech, G. S. Jackson and C. G. Enke, *J. Mass Spectrom.*, 2000, **35**, 784-789.
55. T. R. Covey, B. A. Thomson and B. B. Schneider, *Mass Spectrom. Rev.*, 2009, **28**, 870-897.
56. A. P. Bruins, T. R. Covey and J. D. Henion, *Anal. Chem.*, 1987, **59**, 2642-2646.
57. S. K. Chowdhury, V. Katta and B. T. Chait, *Rapid Commun. Mass Spectrom.*, 1990, **4**, 81-87.
58. M. H. Allen and M. L. Vestal, *J. Am. Soc. Mass Spectrom.*, 1992, **3**, 18-26.
59. J. B. Fenn, *J. Biomol. Tech.*, 2002, **13**, 101-118.
60. L. L. Mack, P. Kralik, A. Rheude and M. Dole, *J. Chem. Phys.*, 1970, **52**, 4977-4986.

61. J. B. Fenn, *J. Am. Soc. Mass Spectrom.*, 1993, **4**, 524-535.
62. J. V. Iribarne and B. A. Thomson, *J. Chem. Phys.*, 1976, **64**, 2287-2294.
63. B. A. Thomson and J. V. Iribarne, *J. Chem. Phys.*, 1979, **71**, 4451-4463.
64. J. Fernández de la Mora, *Anal. Chim. Acta*, 2000, **406**, 93-104.
65. I. G. Loscertales and J. Fernández de la Mora, *J. Chem. Phys.*, 1995, **103**, 5041-5060.
66. M. Gamero-Castano and J. Fernández de la Mora, *Anal. Chim. Acta*, 2000, **406**, 67-91.
67. M. Gamero-Castano and J. Fernández de la Mora, *J. Mass Spectrom.*, 2000, **35**, 790-803.
68. G. Wang and R. B. Cole, *Anal. Chem.*, 1998, **70**, 873-881.
69. G. Wang and R. B. Cole, *Anal. Chim. Acta*, 2000, **406**, 53-65.
70. P. Kebarle, *J. Mass Spectrom.*, 2000, **35**, 804-817.
71. R. B. Cole, *J. Mass Spectrom.*, 2000, **35**, 763-772.
72. J. B. Fenn, M. Mann, C. K. Meng, S. F. Wong and C. M. Whitehouse, *Mass Spectrom. Rev.*, 1990, **9**, 37-70.
73. I. Manisali, D. D. Y. Chen and B. B. Schneider, *TrAC, Trends Anal. Chem.*, 2006, **25**, 243-256.
74. R. D. Voyksner and H. Lee, *Anal. Chem.*, 1999, **71**, 1441-1447.
75. R. D. Smith, J. A. Loo, R. R. Ogorzalek Loo, M. Busman and H. R. Udseth, *Mass Spectrom. Rev.*, 1991, **10**, 359-451.
76. J. T. Watson and O. D. Sparkman, *Introduction to Mass Spectrometry: Instrumentation, Applications and Strategies for Data Interpretation*, 4th Edn., John Wiley & Sons Ltd., Chichester, 2007.
77. R. T. Kelly, A. V. Tolmachev, J. S. Page, K. Tang and R. D. Smith, *Mass Spectrom. Rev.*, 2009, DOI 10.1002/mas.20232.
78. V. D. Berkout and V. M. Doroshenko, *J. Am. Soc. Mass Spectrom.*, 2006, **17**, 335-340.
79. S. A. Shaffer, K. Tang, G. A. Anderson, D. C. Prior, H. R. Udseth and R. D. Smith, *Rapid Commun. Mass Spectrom.*, 1997, **11**, 1813-1817.
80. E. de Hoffmann, *J. Mass Spectrom.*, 1996, **31**, 129-137.
81. L. Sleno and D. A. Volmer, *J. Mass Spectrom.*, 2004, **39**, 1091-1112.
82. J. V. Johnson, R. A. Yost, P. E. Kelley and D. C. Bradford, *Anal. Chem.*, 1990, **62**, 2162-2172.
83. A. K. Shukla and J. H. Futrell, *J. Mass Spectrom.*, 2000, **35**, 1069-1090.
84. M. S. Rashed, P. T. Ozand, M. E. Harrison, P. J. F. Watkins and S. Evans, *Rapid Commun. Mass Spectrom.*, 1994, **8**, 129-133.
85. D. H. Chace, *J. Mass Spectrom.*, 2008, **44**, 163-170.
86. E. E. Bessette, A. K. Goodenough, S. Langouët, I. Yasa, I. D. Kozekov, S. D. Spivack and R. J. Turesky, *Anal. Chem.*, 2009, **81**, 809-819.
87. V. Lange, P. Picotti, B. Domon and R. Aebersold, *Mol. Syst. Biol.*, 2008, **4**, 1-14.
88. S. A. McLuckey, *J. Am. Soc. Mass Spectrom.*, 1992, **3**, 599-614.
89. P. M. Mayer and C. Poon, *Mass Spectrom. Rev.*, 2009, **39**, 608-639.
90. S. A. McLuckey and J. M. Wells, *Chem. Rev.*, 2001, **101**, 571-606.
91. K. Vékey, *J. Mass Spectrom.*, 1996, **31**, 445-463.

92. M. Claeys, H. Van den Heuvel, S. Chen, P. J. Derrick, F. A. Mellon and K. R. Price, *J. Am. Soc. Mass Spectrom.*, 1996, **7**, 173-181.

93. R. E. March, H. Li, O. Belgacem and D. Papanastasiou, *Int. J. Mass Spectrom.*, 2007, **262**, 51-66.

94. G. C. Stafford, P. E. Kelley, J. E. P. Syka, W. E. Reynolds and J. F. J. Todd, *Int. J. Mass Spectrom. Ion Proc.*, 1984, **60**, 85-98.

95. K. R. Jonscher and J. R. Yates III, *Anal. Biochem.*, 1997, **244**, 1-15.

96. L. E. Matamoros Fernández, *Carbohyd. Polymers*, 2007, **68**, 797-807.

97. J. N. Louris, R. G. Cooks, J. E. P. Syka, P. E. Kelley, G. C. Stafford and J. F. J. Todd, *Anal. Chem.*, 1987, **59**, 1677-1685.

98. J. Allison and R. M. Stepnowski, *Anal. Chem.*, 1987, **59**, 1072A-1088A.

99. R. E. March, *Mass Spectrom. Rev.*, 2009, **28**, 961-989.

100. G. Stafford, *J. Am. Soc. Mass Spectrom.*, 2002, **13**, 589-596.

101. R. G. Cooks and R. E. Kaiser, *Acc. Chem. Res.*, 1990, **23**, 213-219.

102. L.-K. Zhang, D. Rempel, B. N. Pramanik and M. L. Gross, *Mass Spectrom. Rev.*, 2005, **24**, 286-309.

103. S. A. McLuckey, G. J. Van Berkel, D. E. Goeringer and G. L. Glish, *Anal. Chem.*, 1994, **66**, 689A-696A.

104. J. N. Louris, J. S. Brodbelt-Lustig, R. G. Cooks, G. L. Glish, G. J. Van Berkel and S. A. McLuckey, *Int. J. Mass Spectrom. Ion Proc.*, 1990, **96**, 117-137.

105. R. E. March, *J. Mass Spectrom.*, 1997, **32**, 351-369.

106. D. J. Douglas, A. J. Frank and D. Mao, *Mass Spectrom. Rev.*, 2005, **13**, 1-29.

107. S. A. McLuckey and D. E. Goeringer, *J. Mass Spectrom.*, 1997, **32**, 461-474.

108. M.-Y. Zhang, N. Pace, E. H. Kerns, T. Kleintop, N. Kagan and T. Sakuma, *J. Mass Spectrom.*, 2005, **40**, 1017-1029.

109. C. Baumann, M. Cintora, M. Eichler, E. Lifante, M. Cooke, A. Przyborowska and J. M. Halket, *Rapid Commun. Mass Spectrom.*, 2000, **14**, 349-356.

110. L. L. Lopez, P. R. Tiller, M. W. Senko and J. C. Schwartz, *Rapid Commun. Mass Spectrom.*, 1999, **13**, 663-668.

111. J. W. Hager, *Anal. Bioanal. Chem.*, 2004, **378**, 845-850.

112. G. L. Glish and D. E. Goeringer, *Anal. Chem.*, 1984, **56**, 2291-2295.

113. J. H. J. Dawson and M. Guilhaus, *Rapid Commun. Mass Spectrom.*, 1989, **3**, 155-159.

114. M. Guilhaus, D. Selby and V. Mlynski, *Mass Spectrom. Rev.*, 2000, **19**, 65-107.

115. M. Guilhaus, *Spectrochim. Acta B*, 2000, **55**, 1511-1525.

116. H. R. Morris, T. Paxton, A. Dell, J. Langhorne, M. Berg, R. S. Bordoli, J. Hoyes and R. H. Bateman, *Rapid Commun. Mass Spectrom.*, 1996, **10**, 889-896.

117. D. J. Douglas, *Mass Spectrom. Rev.*, 2009, **28**, 937-960.

118. P. H. Dawson, *Mass Spectrom. Rev.*, 1986, **5**, 1-37.

119. C. Weickhardt, F. Moritz and J. Grotemeyer, *Mass Spectrom. Rev.*, 1996, **15**, 139-162.

120. W. C. Wiley and I. H. McLaren, *Rev. Sci. Instrum.*, 1955, **26**, 1150-1157.

121. M. Guilhaus, *J. Mass Spectrom.*, 1995, **30**, 1519-1532.
122. N. Mirsaleh-Kohan, W. D. Robertson and R. N. Compton, *Mass Spectrom. Rev.*, 2008, **27**, 237-285.
123. I. V. Chernushevich, A. V. Loboda and B. A. Thomson, *J. Mass Spectrom.*, 2001, **36**, 849-865.
124. R. S. Brown and J. J. Lennon, *Anal. Chem.*, 1995, **67**, 1998-2003.
125. M. L. Vestal, P. Juhasz and S. A. Martin, *Rapid Commun. Mass Spectrom.*, 1995, **9**, 1044-1050.
126. A. Staub, J. Schappler, S. Rudaz and J.-L. Veuthey, *Electrophoresis*, 2009, **30**, 1610-1623.
127. M. Balcerzak, *Anal. Sci.*, 2003, **19**, 979-989.
128. A. Shevchenko, I. Chernushevich, W. Ens, K. G. Standing, B. Thomson, M. Wilm and M. Mann, *Rapid Commun. Mass Spectrom.*, 1997, **11**, 1015-1024.
129. A. M. McKenna, J. M. Purcell, R. P. Rodgers and A. G. Marshall, *Energ. Fuel.*, 2009, **23**, 2122-2128.
130. J. Zhang, G. McCombie, C. Guenat and R. Knochenmuss, *Drug Discov. Today*, 2005, **10**, 635-642.
131. D. G. Schmid, P. Grosche, H. Bandel and G. Jung, *Biotechnol. Bioeng.*, 2001, **71**, 149-161.
132. A. G. Marshall and S. Guan, *Rapid Commun. Mass Spectrom.*, 1996, **10**, 1819-1823.
133. I. J. Amster, *J. Mass Spectrom.*, 1996, **31**, 1325-1337.
134. A. G. Marshall, C. L. Hendrickson and G. S. Jackson, *Mass Spectrom. Rev.*, 1998, **17**, 1-35.
135. C. L. Hendrickson and M. R. Emmett, *Annu. Rev. Phys. Chem.*, 1999, **50**, 517-536.
136. R. M. A. Heeren, A. J. Kleinnijenhuis, L. A. McDonnell and T. H. Mize, *Anal. Bioanal. Chem.*, 2004, **378**, 1048-1058.
137. A. G. Marshall and C. L. Hendrickson, *Int. J. Mass Spectrom.*, 2002, **215**, 59-75.
138. S. C. Brown, G. Kruppa and J.-L. Dasseux, *Mass Spectrom. Rev.*, 2005, **24**, 223-231.
139. A. G. Marshall, *Int. J. Mass Spectrom.*, 2000, **200**, 331-356.
140. A. G. Marshall, T.-C. L. Wang and T. L. Ricca, *J. Am. Chem. Soc.*, 1985, **107**, 7893-7897.
141. J. W. Gauthier, T. R. Trautman and D. B. Jacobson, *Anal. Chim. Acta*, 1991, **246**, 211-225.
142. J. M. Berg, J. L. Tymoczko and L. Stryer, *Biochemistry*, 6th Edn., W. H. Freeman and Company, New York, 2006.
143. M. S. Lee and E. H. Kerns, *Mass Spectrom. Rev.*, 1999, **18**, 187-279.
144. B. Testa and S. D. Krämer, *Chem. Biodivers.*, 2006, **3**, 1053-1101.
145. R. Kostiainen, T. Kotiaho, T. Kuuranne and S. Auriola, *J. Mass Spectrom.*, 2003, **38**, 357-372.
146. M. Pirmohamed, *Medicine*, 2008, **36**, 355-359.
147. A. Fura, *Drug Discov. Today*, 2006, **11**, 133-142.

148. C. Prakash, C. L. Shaffer and A. Nedderman, *Mass Spectrom. Rev.*, 2007, **26**, 340-369.

149. C. Sauer, F. T. Peters, A. E. Schwaninger, M. R. Meyer and H. H. Maurer, *Biochem. Pharmacol.*, 2009, **77**, 444-450.

150. T. Omura, *Biochem. Bioph. Res. Co.*, 1999, **266**, 690-698.

151. P. Anzenbacher and E. Anzenbacherová, *Cell. Mol. Life. Sci.*, 2001, **58**, 737-747.

152. C. Seibert, B. R. Davidson, B. J. Fuller, L. H. Patterson, W. J. Griffiths and Y. Wang, *J. Proteome Res.*, 2009, **8**, 1672-1681.

153. T. Johansson, L. Weidolf and U. Jurva, *Rapid Commun. Mass Spectrom.*, 2007, **21**, 2323-2331.

154. F. P. Guengerich, *Chem. Res. Toxicol.*, 2001, **14**, 611-650.

155. V. V. Shumyantseva, Y. D. Ivanov, N. Bistolas, F. W. Scheller, A. I. Archakov and U. Wollenberger, *Anal. Chem.*, 2004, **76**, 6046-6052.

156. J. H. Ansede and D. R. Thakker, *J. Pharm. Sci.*, 2004, **93**, 239-255.

157. M. D. Coleman, *Human Drug Metabolism*, John Wiley & Sons Ltd., Chichester, 2005.

158. J. Ayrton, R. Plumb, W. J. Leavens, D. Mallett, M. Dickins and G. J. Dear, *Rapid Commun. Mass Spectrom.*, 1998, **12**, 217-224.

159. J. E. Laine, S. Auriola, M. Pasanen and R. O. Juvonen, *Xenobiotica*, 2009, **39**, 11-21.

160. K. Mizuno, M. Katoh, H. Okumura, N. Nakagawa, T. Negishi, T. Hashizume, M. Nakajima and Y. Tsuyoshi, *Drug Metab. Dispos.*, 2009, **37**, 345-351.

161. P. Eddershaw and M. Dickins, *"Phase I Metabolism"* in *A Handbook of Bioanalysis and Drug Metabolism*, ed. G. Evans, CRC Press, Boca Raton, 2004.

162. C. K. Svensson, *Drug Metab. Dispos.*, 2009, **37**, 247-253.

163. R. F. Staack and G. Hopfgartner, *Anal. Bioanal. Chem.*, 2007, **388**, 1365-1380.

164. S. Ma, S. K. Chowdhury and K. B. Alton, *Curr. Drug Metab.*, 2006, **7**, 503-523.

165. S.-W. Myung, H.-Y. Kim, H.-K. Kim, D.-H. Kim, M. Kim, H.-W. Cho, H. S. Lee, J.-K. Kim and C. I. Hong, *Rapid Commun. Mass Spectrom.*, 2002, **16**, 2048-2053.

166. S. Ma and R. Subramanian, *J. Mass Spectrom.*, 2006, **41**, 1121-1139.

167. Y.-Z. Shu, B. M. Johnson and T. J. Yang, *The AAPS Journal*, 2008, **10**, 178-192.

168. FDA, *Guidance for Industry: Safety Testing of Drug Metabolites*, http://www.fda.gov/downloads/Drugs/GuidanceComplianceRegulatoryInformation/Guidances/ucm079266.pdf, Accessed 21 September, 2009.

169. L. Leclercq, F. Cuyckens, G. S. J. Mannens, R. de Vries, P. Timmerman and D. C. Evans, *Chem. Res. Toxicol.*, 2009, **22**, 280-293.

170. A.-E. F. Nassar, A. M. Kamel and C. Clarimont, *Drug Discov. Today*, 2004, **9**, 1020-1028.

171. P. Baranczewski, A. Stańczak, A. Kautiainen, P. Sandin and P.-O. Edlund, *Pharmacol. Reports*, 2006, **58**, 341-352.

172. G. G. Gibson and P. Skett, *Introduction to Drug Metabolism*, 3rd Edn., Nelson Thornes Publishers, Cheltenham, 2001.

173. A. Tolonen, M. Turpeinen and O. Pelkonen, *Drug Discov. Today*, 2009, **14**, 120-133.

174. S. Ekins, B. J. Ring, J. Grace, D. J. McRobie-Belle and S. A. Wrighton, *Pharmacol. Toxicol. Methods*, 2000, **44**, 313-324.

175. K. S. Hakala, M. Link, B. Szotakova, L. Skalova, R. Kostiainen and R. A. Ketola, *Anal. Bioanal. Chem.*, 2009, **393**, 1327-1336.

176. Y. Chen, M. Monshouwer and W. L. Fitch, *Pharmaceut. Res.*, 2007, **24**, 248-257.

177. M. Kiffe, D. G. Schmid and G. J. M. Bruin, *J. Liq. Chromatogr. R. T.*, 2008, **31**, 1593-1619.

178. J. M. Castro-Perez, *Drug Discov. Today*, 2007, **12**, 249-256.

179. R. N. Xu, L. Fan, M. J. Rieser and T. A. El-Shourbagy, *J. Pharmaceut. Biomed.*, 2007, **44**, 342-355.

180. R. King, R. Bonfiglio, C. Fernandez-Metzler, C. Miller-Stein and T. Olah, *J. Am. Soc. Mass Spectrom.*, 2000, **11**, 942-950.

181. B. K. Matuszewski, M. L. Constanzer and C. M. Chavez-Eng, *Anal. Chem.*, 2003, **75**, 3019-3030.

182. R. Dams, M. A. Huestis, W. E. Lambert and C. M. Murphy, *J. Am. Soc. Mass Spectrom.*, 2003, **14**, 1290-1294.

183. S. Souverain, S. Rudaz and J.-L. Veuthey, *J. Chromatogr. A*, 2004, **1058**, 61-66.

184. C. Apostolou, Y. Dotsikas, C. Kousoulos and Y. L. Loukas, *J. Pharmaceut. Biomed.*, 2008, **48**, 853-859.

185. T. Sangster, M. Spence, P. Sinclair, R. Payne and C. Smith, *Rapid Commun. Mass Spectrom.*, 2004, **18**, 1361-1364.

186. P. Songsermsakul, G. Sontag, M. Cichna-Markl, J. Zentek and E. Razzazi-Fazeli, *J. Chromatogr. B*, 2006, **843**, 252-261.

187. M. S. Chang, Q. Ji, J. Zhang and T. A. El-Shourbagy, *Drug Develop. Res.*, 2007, **68**, 107-133.

188. A. Van Eeckhaut, K. Lanckmans, S. Sarre, I. Smolders and Y. Michotte, *J. Chromatogr. B*, 2009, **877**, 2198-2201.

189. L. L. Jessome and D. A. Volmer, *LC GC N. Am.*, 2006, **24**, 83-89.

190. J.-P. Antignac, K. de Wasch, F. Monteau, H. De Brabander, F. Andre and B. Le Bizec, *Anal. Chim. Acta*, 2005, **529**, 129-136.

191. J. X. Shen, R. J. Motyka, J. P. Roach and R. N. Hayes, *J. Pharmaceut. Biomed.*, 2005, **37**, 359-367.

192. H. Mei, Y. Hsieh, C. Nardo, X. Xu, S. Wang, K. Ng and W. A. Korfmacher, *Rapid Commun. Mass Spectrom.*, 2003, **17**, 97-103.

193. C. G. Enke, *Anal. Chem.*, 1997, **69**, 4885-4893.

194. P. Kebarle and L. Tang, *Anal. Chem.*, 1993, **65**, 972A-986A.

195. R. Bonfiglio, R. C. King, T. V. Olah and K. Merkle, *Rapid Commun. Mass Spectrom.*, 1999, **13**, 1175-1185.

196. N. B. Cech and C. G. Enke, *Anal. Chem.*, 2000, **72**, 2717-2723.

197. C. H. P. Bruins, C. M. Jeronimus-Stratingh, K. Ensing, W. D. van Dongen and G. J. de Jong, *J. Chromatogr. A*, 1999, **863**, 115-122.

198. K. Biemann, *J. Am. Soc. Mass Spectrom.*, 2002, **13**, 1254-1272.

199. L. J. Christopher, D. Cui, W. Li, A. Barros, V. K. Arora, H. Zhang, L. Wang, D. Zhang, J. A. Manning, K. He, A. M. Fletcher, M. Ogan, M. Lago, S. J. Bonacorsi, W. G. Humphreys and R. A. Iyer, *Drug Metab. Dispos.*, 2008, **36**, 1341-1356.

200. Y. Wang, X. Chen, Q. Li and D. Zhong, *Rapid Commun. Mass Spectrom.*, 2008, **22**, 1843-1852.

201. Y. Liu, M. Wang, M. Xue, Y. Li, X. Li, J. Ruan and K. Liu, *J. Chromatogr. B*, 2008, **873**, 41-50.

202. G. Chen, I. Daaro, B. N. Pramanik and J. J. Piwinski, *J. Mass Spectrom.*, 2009, **44**, 203-213.

203. X.-S. Miao, C. Zhong, Y. Wang, R. E. Savage, R.-Y. Yang, D. Kizer, E. Volckova, M. A. Ashwell and T. C. K. Chan, *Rapid Commun. Mass Spectrom.*, 2009, **23**, 12-22.

204. L. Gianelli, G. G. Mellerio, E. Siviero, A. Rossi, W. Cabri and L. Sogli, *Rapid Commun. Mass Spectrom.*, 2000, **14**, 1260-1265.

205. D. Q. Liu, C. E. C. A. Hop, M. G. Beconi, A. Mao and S.-H. L. Chiu, *Rapid Commun. Mass Spectrom.*, 2001, **15**, 1832-1839.

206. D. Q. Liu, L. Wu, M. Sun and P. A. MacGregor, *J. Pharmaceut. Biomed.*, 2007, **44**, 320-329.

207. M. E. Hemling, J. J. Conboy, M. F. Bean, M. Mentzer and S. A. Carr, *J. Am. Soc. Mass Spectrom.*, 1994, **5**, 434-442.

208. J. E. Chipuk and J. Brodbelt, *Int. J. Mass Spectrom.*, 2007, **267**, 98-108.

209. D. Q. Liu and C. E. C. A. Hop, *J. Pharmaceut. Biomed.*, 2005, **37**, 1-18.

210. J. Clayden, N. Greeves, S. Warren and P. Wothers, *Organic Chemistry*, Oxford University Press, Oxford, 2001.

211. Z. Shen, J. R. Reed, M. Creighton, D. Q. Liu, Y. S. Tang, D. F. Hora, W. Feeney, J. Szewczyk, R. Bakhtiar, R. B. Franklin and S. H. Vincent, *Xenobiotica*, 2003, **33**, 499-509.

212. A.-E. F. Nassar and R. E. Talaat, *Drug Discov. Today*, 2004, **9**, 317-327.

213. M. A. Watkins, J. M. Price, B. E. Winger and H. I. Kenttämaa, *Anal. Chem.*, 2004, **76**, 964-976.

214. M. A. Watkins, B. E. Winger, R. C. Shea and H. I. Kenttämaa, *Anal. Chem.*, 2005, **77**, 1385-1392.

215. J. Somuramasami, P. Duan, M. A. Watkins, B. E. Winger and H. I. Kenttämaa, *Int. J. Mass Spectrom.*, 2007, **265**, 359-371.

216. R. Ramanathan, A.-D. Su, N. Alvarez, N. Blumenkrantz, S. K. Chowdhury, K. Alton and J. Patrick, *Anal. Chem.*, 2000, **72**, 1352-1359.

217. W. Tong, S. K. Chowdhury, J.-C. Chen, R. Zhong, K. B. Alton and J. E. Patrick, *Rapid Commun. Mass Spectrom.*, 2001, **15**, 2085-2090.

218. D. M. Peiris, W. Lam, S. Michael and R. Ramanathan, *J. Mass Spectrom.*, 2004, **39**, 600-606.

219. S. Ma, S. K. Chowdhury and K. B. Alton, *Anal. Chem.*, 2005, **77**, 3676-3682.

220. R. Singh Tomar, T. J. Joseph, A. S. R. Murthy, D. V. Yadav, G. Subbaiah and K. V. S. R. Krishna Reddy, *J. Pharmaceut. Biomed.*, 2004, **36**, 231-235.

221. M. C. Dumasia and P. Teale, *J. Pharmaceut. Biomed.*, 2005, **36**, 1085-1091.
222. X. Sun, L. Niu, X. Li, X. Lu and F. Li, *J. Pharmaceut. Biomed.*, 2009, **50**, 27-34.
223. H. Chen, Y. Chen, P. Du, F. Han, H. Wang and H. Zhang, *J. Pharmaceut. Biomed.*, 2006, **40**, 142-150.
224. P. Kulanthaivel, R. J. Barbuch, R. S. Davidson, P. Yi, G. A. Rener, E. L. Mattiuz, C. E. Hadden, L. A. Goodwin and W. J. Ehlhardt, *Drug Metab. Dispos.*, 2004, **32**, 966-972.
225. M. A. Watkins, D. V. WeWora, S. Li, B. E. Winger and H. I. Kenttämaa, *Anal. Chem.*, 2005, **77**, 5311-5316.
226. P. Duan, T. A. Gillespie, B. E. Winger and H. I. Kenttämaa, *J. Org. Chem.*, 2008, **73**, 4888-4894.
227. P. Duan, M. Fu, T. A. Gillespie, B. E. Winger and H. I. Kenttämaa, *J. Org. Chem.*, 2009, **74**, 1114-1123.
228. S. C. Habicht, N. R. Vinueza, E. F. Archibold, P. Duan and H. I. Kenttämaa, *Anal. Chem.*, 2008, **80**, 3416-3421.
229. J. O. Lay, C. L. Holder and W. M. Cooper, *Biomed. Environ. Mass Spectrom.*, 1989, **18**, 157-167.
230. P. Wright, A. Alex, D. Gibson, R. Jones and P. Macrae, *Rapid Commun. Mass Spectrom.*, 2005, **19**, 2005-2014.
231. M. L. Bandu, K. R. Watkins, M. L. Bretthauer, C. A. Moore and H. Desaire, *Anal. Chem.*, 2004, **76**, 1746-1753.
232. L. Yi, M. L. Bandu and H. Desaire, *Anal. Chem.*, 2005, **77**, 6655-6663.
233. L. Yi, J. Dratter, C. Wang, J. A. Tunge and H. Desaire, *Anal. Bioanal. Chem.*, 2006, **386**, 666-674.
234. K. Klagkou, F. Pullen, M. Harrison, A. Organ, A. Firth and G. J. Langley, *Rapid Commun. Mass Spectrom.*, 2003, **17**, 1163-1168.
235. K. Klagkou, F. Pullen, M. Harrison, A. Organ, A. Firth and G. J. Langley, *Rapid Commun. Mass Spectrom.*, 2003, **17**, 2373-2379.
236. F. W. McLafferty and R. S. Gohlke, *Anal. Chem.*, 1959, **31**, 2076-2082.
237. J. T. Bursey, M. M. Bursey and D. G. I. Kingston, *Chem. Rev.*, 1973, **73**, 191-234.
238. H. Schwarz, *Top. Curr. Chem.*, 1978, **73**, 231-263.
239. A. Barkow, S. Pilotek and H.-F. Grutzmacher, *Eur. Mass Spectrom.*, 1995, **1**, 525-537.
240. P. N. Reddy, R. Srikanth, N. Venkateswarlu, R. N. Rao and R. Srinivas, *Rapid Commun. Mass Spectrom.*, 2005, **19**, 72-76.
241. T. Donovan and J. Brodbelt, *Org. Mass Spectrom.*, 1992, **27**, 9-16.
242. T. Reemtsma, *J. Chromatogr. A*, 2001, **919**, 289-297.
243. A. Attygalle, J. Ruzicka, D. Varughese and J. Sayed, *Tetrahedron Lett.*, 2006, **47**, 4601-4603.
244. A. B. Attygalle, J. B. Bialecki, U. Nishshanka, C. S. Weisbecker and J. Ruzicka, *J. Mass Spectrom.*, 2008, **43**, 1224-1234.
245. Z. Li, F. Song and S. Liu, *Rapid Commun. Mass Spectrom.*, 2001, **15**, 1893-1898.

246. M. A. Mendes, R. Rittner, M. N. Eberlin, J. Suwinski and W. Szczepankiewicz, *Eur. J. Mass Spectrom.*, 2002, **8**, 27-33.

247. I. P. Nnane and L. A. Damani, *Biomed. Chromatogr.*, 2005, **19**, 87-98.

248. F. Jensen, *Introduction to Computational Chemistry*, John Wiley & Sons Ltd., Chichester, 1999.

249. F. W. McLafferty and F. Tureček, *Interpretation of Mass Spectra*, 4th Edn., University Science Books, Sausalito, 1993.

250. V. Pellegrin, *J. Chem. Educ.*, 1983, **60**, 626-633.

251. M. Karni and A. Mandelbaum, *Org. Mass Spectrom.*, 1980, **15**, 53-64.

252. F. W. McLafferty, *Org. Mass Spectrom.*, 1980, **15**, 114-121.

253. R. V. Vachet, B. M. Bishop, B. W. Erickson and G. L. Glish, *J. Am. Chem. Soc.*, 1997, **119**, 5481-5488.

254. A. G. Craig and S. W. Taylor, *J. Am. Soc. Mass Spectrom.*, 2001, **12**, 470-474.

255. P. R. Tiller, C. Raab and C. E. C. A. Hop, *J. Mass Spectrom.*, 2001, **36**, 344-345.

256. A. Cartoni, M. Altamura, F. Animati, G. Balacco, R. Cosi, A. Ettorre, A. Madami and A. Triolo, *J. Mass Spectrom.*, 2002, **37**, 1258-1265.

257. G. Hopfgartner, C. Husser and M. Zell, *J. Mass Spectrom.*, 2003, **38**, 138-150.

258. M. Jemal, Z. Ouyang, W. Zhao, M. Zhu and W. W. Wu, *Rapid Commun. Mass Spectrom.*, 2003, **17**, 2732-2740.

259. H. J. Yoo, H. Liu and K. Hakansson, *Anal. Chem.*, 2007, **79**, 7858-7866.

260. Q. Ruan, S. Peterman, M. A. Szewc, L. Ma, D. Cui, W. G. Humphreys and M. Zhu, *J. Mass Spectrom.*, 2008, **43**, 251-261.

261. P. R. Tiller, S. Yu, J. Castro-Perez, K. L. Fillgrove and T. A. Baillie, *Rapid Commun. Mass Spectrom.*, 2008, **22**, 1053-1061.

262. C. Cheng and M. L. Gross, *Mass Spectrom. Rev.*, 2000, **19**, 398-420.

263. C. E. Hudson and D. J. McAdoo, *J. Am. Soc. Mass Spectrom.*, 2004, **15**, 972-981.

264. R. G. Cooks, *Org. Mass Spectrom.*, 1969, **2**, 481-519.

265. S. W. Holman, P. Wright and G. J. Langley, *Rapid Commun. Mass Spectrom.*, 2008, **22**, 2355-2365.

266. C. A. Lipinski, F. Lombardo, B. W. Dominy and P. J. Feeney, *Adv. Drug Deliver. Rev*, 1997, **23**, 3-25.

267. S. McClean, E. J. O'Kane and W. F. Smyth, *J. Chromatogr. B*, 2000, **740**, 141-157.

268. W. F. Smyth, S. McClean and V. N. Ramachandran, *Rapid Commun. Mass Spectrom.*, 2000, **14**, 2061-2069.

269. S. McClean, R. C. Robinson, C. Shaw and W. F. Smyth, *Rapid Commun. Mass Spectrom.*, 2002, **16**, 346-354.

270. W. F. Smyth, *Anal. Chim. Acta*, 2003, **492**, 1-16.

271. W. F. Smyth, C. Joyce, V. N. Ramachandran, E. O'Kane and D. Coulter, *Anal. Chim. Acta*, 2004, **506**, 203-214.

272. C. Joyce, W. F. Smyth, V. N. Ramachandran, E. O'Kane and D. J. Coulter, *J. Pharmaceut. Biomed.*, 2004, **36**, 465-476.

273. W. F. Smyth, *J. Chromatogr. B*, 2005, **824**, 1-20.

274. W. F. Smyth, *Electrophoresis*, 2005, **26**, 1334-1357.
275. W. F. Smyth, J. C. Leslie, S. McClean, B. Hannigan, H. P. McKenna, B. Doherty, C. Joyce and E. O'Kane, *Rapid Commun. Mass Spectrom.*, 2006, **20**, 1637-1642.
276. W. F. Smyth and V. Rodriguez, *J. Chromatogr. A*, 2007, **1159**, 159-174.
277. Y. Wang, X. Chen, Q. Li and D. Zhong, *J. Mass Spectrom.*, 2008, **43**, 1099-1109.
278. M. H. Bickel, *Pharmacol. Rev.*, 1969, **21**, 325-355.
279. A. Alex, S. Harvey, T. Parsons, F. S. Pullen, P. Wright and J.-A. Riley, *Rapid Commun. Mass Spectrom.*, 2009, **23**, 2619-2627.
280. R. S. Plumb, K. A. Johnson, P. Rainville, B. W. Smith, I. D. Wilson, J. M. Castro-Perez and J. K. Nicholson, *Rapid Commun. Mass Spectrom.*, 2006, **20**, 1989-1994.
281. R. L. Fitzgerald, J. D. Rivera and D. A. Herold, *Clin. Chem.*, 1999, **45**, 1224-1234.
282. R. G. Cooks, J. H. Beynon, R. M. Caprioli and G. R. Lester, *Metastable ions*, Elsevier Scientific Publishing Company, Amsterdam, 1973.
283. J. L. Holmes, K. J. Jobst and J. K. Terlouw, *J. Labelled Compd. Rad.*, 2007, **50**, 1115-1123.
284. R. A. W. Johnstone, *Mass spectrometry for Organic Chemistry*, Cambridge University Press, London, 1972.
285. J. L. Holmes, C. Aubry and P. M. Mayer, *Assigning Structure to Ions in Mass Spectrometry*, CRC Press, Boca Raton, 2007.
286. D. H. Williams and J. Ronayne, *Chem. Commun.*, 1967, 1129-1130.
287. W. Carpenter, A. M. Duffield and C. Djerassi, *J. Am. Chem. Soc.*, 1968, **90**, 160-164.
288. D. H. Williams, S. W. Tam and R. G. Cooks, *J. Am. Chem. Soc.*, 1968, **90**, 2150-2155.
289. A. N. H. Yeo, R. G. Cooks and D. H. Williams, *Chem. Commun.*, 1968, 1269-1270.
290. R. G. Cooks, I. Howe and D. H. Williams, *Org. Mass Spectrom.*, 1969, **2**, 137-156.
291. B. Davies, D. H. Williams and A. N. H. Yeo, *J. Chem. Soc. B*, 1970, 81-87.
292. R. G. Cooks and S. L. Bernasek, *J. Am. Chem. Soc.*, 1970, **92**, 2129-2131.
293. I. Horman, A. N. H. Yeo and D. H. Williams, *J. Am. Chem. Soc.*, 1970, **92**, 2131-2132.
294. P. Wolkoff and J. L. Holmes, *Can. J. Chem.*, 1979, **57**, 348-354.
295. D. Kuck, *Int. J. Mass Spectrom.*, 2002, **213**, 101-144.
296. H. Lioe, R. A. J. O'Hair and G. E. Reid, *J. Am. Soc. Mass Spectrom.*, 2004, **15**, 65-76.
297. H. El Aribi, G. Orlova, A. C. Hopkinson and K. W. M. Siu, *J. Phys. Chem. A*, 2004, **108**, 3844-3853.
298. J. B. Bialecki, J. Ruzicka and A. B. Attygalle, *J. Mass Spectrom.*, 2006, **41**, 1195-1204.
299. J. Sultan, *Int. J. Mass Spectrom.*, 2008, **273**, 58-68.
300. S. Beuck, T. Schwabe, S. Grimme, N. Schlörer, M. Kamber, W. Schänzer and M. Thevis, *J. Am. Soc. Mass Spectrom.*, 2009, **20**, 2034-2048.

301. M. L. Bandu, T. Grubbs, M. Kater and H. Desaire, *Int. J. Mass Spectrom.*, 2006, **251**, 40-46.

302. K. Croes, P. T. McCarthy and R. J. Flanagan, *J. Chromatogr. A*, 1995, **693**, 289-306.

303. N. J. Clarke, D. Rindgen, W. A. Korfmacher and K. A. Cox, *Anal. Chem.*, 2001, **73**, 430A-439A.

304. R. A. Zubarev, N. L. Kelleher and F. W. McLafferty, *J. Am. Chem. Soc.*, 1998, **120**, 3265-3266.

305. J. A. Mosely, M. J. P. Smith, L. M. Turner, M. Jones, M. Sims and A. W. T. Bristow, in *Proceedings of the 18th International Mass Spectrometry Conference*, Bremen, 2009.

306. J. E. P. Syka, J. J. Coon, M. J. Schroeder, J. Shabanowitz and D. F. Hunt, *Proc. Natl. Acad. Sci. U.S.A.*, 2004, **101**, 9528-9533.

307. M. Heinonen, A. Rantanen, T. Mielikäinen, J. Kokkonen, J. Kiuru, R. A. Ketola and J. Rousu, *Rapid Commun. Mass Spectrom.*, 2008, **22**, 3043-3052.